NASA TECHNICAL NOTE

NASA TN D-2230

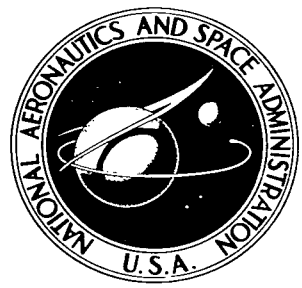

NASA TN D-2230

MEASUREMENT OF HEAT TRANSFER AND RECOVERY FACTOR OF A COMPRESSIBLE TURBULENT BOUNDARY LAYER ON A SHARP CONE WITH FOREIGN GAS INJECTION

by C. C. Pappas and Arthur F. Okuno

Ames Research Center
Moffett Field, Calif.

NATIONAL AERONAUTICS AND SPACE ADMINISTRATION • WASHINGTON, D. C. • APRIL 1964

MEASUREMENT OF HEAT TRANSFER AND RECOVERY FACTOR OF A COMPRESSIBLE TURBULENT BOUNDARY LAYER ON A SHARP CONE WITH FOREIGN GAS INJECTION

By C. C. Pappas and Arthur F. Okuno

Ames Research Center
Moffett Field, Calif.

NATIONAL AERONAUTICS AND SPACE ADMINISTRATION

For sale by the Office of Technical Services, Department of Commerce,
Washington, D.C. 20230 -- Price $2.25

MEASUREMENT OF HEAT TRANSFER AND RECOVERY FACTOR OF A COMPRESSIBLE TURBULENT BOUNDARY LAYER ON A SHARP CONE WITH FOREIGN GAS INJECTION

SUMMARY

Local heat-transfer and recovery temperatures of the turbulent boundary layer with foreign-gas injection of helium, air, and Freon-12 (CCl_2F_2) were measured on a porous cone at cone Mach numbers 0.7, 3.67, and 4.35 and in a Reynolds number range of 1 to 5 million. The heat-transfer coefficients generally show a substantial decrease of up to 80 percent from the zero-injection value for all injection gases and the relative effectiveness of the gases is in accord with theory. The recovery temperature (wall temperature for zero heat transfer to the wall) at $M = 0.7$, for helium injection, increases with injection to a value greater than the total stream temperature and then decreases with increased injection. At the two higher Mach numbers, for all the injection gases tested, the recovery temperature first decreases with injection then increases to values which can be greater than the total temperature of the stream. For the highest injection rates at Mach number 4.35 the heat transferred to the wall can increase with increased injection. The concept of a Stanton number and accompanying recovery factor cannot be used at the highest test injection rates to calculate the heat transfer to the wall because a recovery temperature cannot be defined. The effect of Mach number on the reduction of the heat-transfer coefficient from the zero-injection value with increase in injection rate, is less than the reduction in skin friction with air injection. The heat-transfer coefficient ratios are in general agreement with the Rubesin theory heat-transfer predictions for Mach numbers from 0 to 4.35.

INTRODUCTION

Transpiration cooling systems are an effective means of reducing the temperature of an aerodynamically heated surface. These systems have the advantage of an efficient heat exchange between the porous wall and the cooling transpiration gases, and further, the gases injected into the surrounding boundary layer can block a substantial part of the aerodynamically generated heat from entering the wall. One of the current motivations for an understanding of the effect of the transpiration process on the boundary layer is the wide and successful application of ablative cooling systems to high-speed reentry vehicles. The gases which emanate from an ablating surface act on the boundary layer similarly to the injection gases of a transpiration system, but the ablative gas may be of mixed molecular weight; therefore, the effects on heat transfer of the individual gases must be known, as well as the mixtures of different molecular weights, in order to evaluate an ablative cooling system. One purpose of the present tests was to determine the effectiveness of gases of different molecular weights, the light

gas helium, air, and the heavy gas Freon-12 (CCl_2F_2) on the local heat transfer from a compressible turbulent boundary layer to a porous wall. Injection of mixtures of gases will not be considered in this report.

The effects of transpiration of foreign gases into the compressible turbulent boundary layer were studied in reference 1. The effectiveness of the injected gas in reducing skin friction was found to be markedly influenced by the Mach number over the range from 0 to 4.3 when the data were represented as the skin-friction ratio, C_F/C_{F_o}, a function of the injection rate, $2F/C_{F_o}$. This result did not agree with theoretical predictions of Rubesin (ref. 2) for air injection, which show little dependence on Mach number. A second objective in the present study was to determine the effect of Mach number on the heat-transfer coefficient ratio, St/St_o, as a function of the local injection rate, F/St_o.

Of equal importance in the interpretation of the heat transfer to a wall with gas injection is the knowledge of the heat-transfer coefficient or Stanton number and its attendant recovery temperature or recovery factor. As an example of the unexpected behavior of the recovery factor with injection, Tewfik, Eckert, and Shirtliffe (ref. 3) recently reported that the recovery temperature of the low-speed (100 fps) turbulent boundary layer with helium injection rises continuously with increased injection to 40° F above the free-stream temperature. For air injection, they found the expected behavior that the recovery temperature equalled the free-stream temperature. A third objective was to examine the behavior of the recovery factor with foreign gas injection over the range of these tests.

The present tests cover such a wide range of variables that there are numerous related experimental and theoretical reports available in the literature. Fairly comprehensive reviews, up to about mid-year of 1960, of the effects of gas injection on skin friction and on the skin friction and heat transfer of the compressible turbulent boundary layer are presented in references 1, 4, and 5. Some of the more recent pertinent experimental heat-transfer and recovery factor data of the turbulent boundary layer will be discussed briefly here. Consider now some recently available heat-transfer measurements of Tewfik, Eckert, and Jurewicz (ref. 6) obtained on a circular cylinder with axis parallel to a low-speed stream ($U_\infty \approx 110$ fps) with uniform air injection, and the heat-transfer measurements of Bartle and Leadon (ref. 7) obtained on a side-wall porous plate of a supersonic wind tunnel ($M_\infty = 2$ and 3.2) with distributed injection to maintain a constant wall temperature. The heat transfer when presented as the ratio of heat-transfer coefficient, St, to the zero injection value, St_o, as a function of the local injection value F/St_o showed good agreement with the theory of Rubesin (ref. 2) for distributed air injection. Bartle and Leadon used as the zero injection Stanton numbers the values obtained by local skin-friction measurements converted to local Stanton number by the modified Renolds analogy of Rubesin (ref. 8). They also extrapolated the values of low-injection heat-transfer Stanton number to zero injection values, and these agree to within about 10 percent of the previous St_o values. In spite of this agreement, the effective St_o value, with high rates of injection, certainly is not either of these but one based on a lower effective length Reynolds number. Their results of St/St_o thus would be expected to trend above the theoretical predictions with increasing F/St_o values, and this concave upward curve shape is observed in

both sets of their data. This argument applies to any porous surface which is preceded by a considerable length of boundary-layer flow over a nonporous area. Some early heat-transfer measurements of Rubesin, Pappas, and Okuno (ref. 9) obtained with air injection on a flat plate at $M = 2.7$ also agree with the Rubesin theory predictions at the lower injection rates but trend above the theory at the highest injection rates. For air injection then, the heat-transfer measurements in the Mach number range from 0 to 3.2 are in good agreement with the theory of Rubesin and the skin-friction shows decidedly more variation with Mach number than the theoretical predictions.

There are some heat-transfer data available with other gases injected into the turbulent boundary layer. Tewfik, Eckert, and Shirtliffe (ref. 3) injected helium into the turbulent boundary layer of a cylinder with the axis parallel to the main stream flow and found that the heat-transfer coefficient ratio St/St_o was below the low-speed theoretical predictions of Rubesin and Pappas (ref. 10). Leadon and Scott (ref. 11) measured heat transfer at $M = 3.0$ on a small porous plate mounted flush in a wall of a supersonic wind tunnel. The evaluation of Leadon and Scott's results is influenced by a long run of the boundary layer along the wall preceding the porous plate, and there is some uncertainty as to the correct St_o value to use. The reduction of the St/St_o ratio with helium injection at $M = 3.0$ almost agrees with the low-speed results of Tewfik, Eckert, and Shirtliffe, showing little effect of Mach number on the heat-transfer coefficient reduction.

The present tests were proposed to help clarify the effects of Mach number on the reduction in heat transfer with foreign gas injection and to provide heat-transfer measurements for a compressible turbulent boundary layer over a wider range in molecular weights of the injection gases.

NOMENCLATURE

A	circumferential area corresponding to unit cone ray length at each exterior thermocouple location
$\frac{A}{A_n}$	equivalent cylinder area ratio, peripheral cone area to nozzle area at thermocouple location
b	gas constant for molecular weight, M
B_i	ratio of local interior mass-flow rate, $\frac{(\rho u)_i}{(\rho v)_w}$
c_p	specific heat
C_F	total skin-friction coefficient
D	diameter
E	temperature effectiveness ratio, $\frac{T_w - T_g}{T_{r_o} - T_g}$

F	injection mass flow normal to surface; $\frac{\rho_w v_w}{\rho_c u_c}$ for supersonic flow, $\frac{\rho_w v_w}{\rho_\infty u_\infty}$ for subsonic flow
G	mass-flow rate per unit area through porous wall
h	local heat-transfer coefficient, $q = h(T_r - T_w)$
k	thermal conductivity
M	Mach number
M_c	cone Mach number, inviscid cone surface value for supersonic flow, free-stream value for subsonic flow
Δp^2	difference of the square of the pressures across a porous cone wall
Pr	Prandtl number, $\frac{\mu c_p}{k}$
q	local heat transfer to the wall
r	temperature recovery factor, $\frac{T_r - T_c}{T_t - T_c}$
R_c	local Reynolds number of cone, $\frac{u_c \rho_c s}{\mu_c}$ for supersonic flow, $\frac{u_\infty \rho_\infty s}{\mu_\infty}$ for subsonic flow
R_x	local Reynolds number of flat plate, $\frac{u_\infty \rho_\infty x}{\mu_\infty}$
s	distance along cone ray from tip
s_o	effective nonporous ray length of cone tip
St	local heat-transfer Stanton number; $\frac{h}{(\rho u c_p)_c}$ for supersonic flow, $\frac{h}{(\rho u c_p)_\infty}$ for subsonic flow
t	thickness of porous cone wall
T	temperature
T'	reference temperature, defined in equation (3)
u	velocity component parallel to cone surface or in stream direction
v	velocity component normal to cone surface
x	distance along flat plate from leading edge
α, β	viscous and inertial resistance coefficients (eq. (A1))

ϵ total hemispherical emissivity

θ cone semivertex angle

μ viscosity of gas

ρ density of gas

$\rho_i u_i$ mass flow of coolant past internal coolant thermocouples corresponding to ith thermocouple

σ Stefan-Boltzmann radiation constant

Subscripts

a refers to air value

c cone condition; inviscid cone surface value for supersonic flow, free-stream value for subsonic flow

f evaluated at internal film temperature

g true value for internal coolant

i indicated value for internal coolant

n surface condition of wind-tunnel nozzle

o zero injection condition

r adiabatic recovery condition

t stagnation condition of stream

w cone surface condition

∞ free-stream condition

DESCRIPTION OF EQUIPMENT

Wind Tunnels

The tests were conducted in the Ames 2- by 2-foot transonic wind tunnel and in the Ames 10-inch heat transfer wind tunnel. Both tunnels may be continuously operated at a given test condition, thereby allowing steady-state heat-transfer measurements.

Cone Model

The heat-transfer model is shown in figure 1. Important dimensions and thermocouple locations are indicated on the figure. The model consists essentially of an outer porous stainless steel cone and an inner porous glass fiber cone. The outer seamless cone was formed of sintered type 316 stainless steel by the Mott Metallurgical Corp. The density of the cone material is approximately 263 pounds per cubic foot. The porous surface area of the cone is 0.290 square feet with an average surface thickness of 0.053 inch. Relative porosity indicated by the mass-flow distribution is shown in figure 2 along four rays of the cone. The technique of the porosity calibration is indicated in figure 3 and some results are presented in figure 4. For more details see appendix A. The surface of the outer cone was aerodynamically smooth throughout the test period and the average roughness height measured was ±200 microinches.

The inner cone was made of three glass fiber conical segments glued together. Each segment is a molded and cured mat of glass fibers treated with uncured phenolic resin. The density of the glass fiber cone is about 17 lb/cu ft and the thickness is 0.1 inch.

The main ray, A, of the outer cone has eight thermocouples numbered 1 through 8 and positioned 1 inch apart on the outer surface; each of the other three equidistant rays B, C, and D has four thermocouples positioned 2 inches apart. Thirty-six gage (0.005-inch diameter) chromel-constantan thermocouple wire was forced through two holes drilled in a 0.043-inch-diameter nylon 101 plug. The plug was then force-fitted into a hole drilled in the cone and the ends of the thermocouple wires were spot-welded flush with the surface as shown in figure 1.

Coolant thermocouples (36 gage chromel-constantan) were mounted on the surface of the inner glass fiber cone and extension. The extension was made of 0.026-inch-thick glass fiber material. There are eight internal thermocouples corresponding to the main cone ray A. They are located in the plane defined by the main ray and the cone axis and are on lines normal to the main cone ray at each of the eight external thermocouple locations. The last two thermocouples of the other rays have correspondingly located internal coolant thermocouples. These are approximately 0.425 inch inside the inner surface of the steel cone. In addition, along the main ray, there are three coolant thermocouples 1/8 inch outside the surface of the glass fiber cone on the lines normal to the fifth, sixth, and seventh external thermocouples and two coolant thermocouples 1/4 inch outside the surface on the lines normal to the fifth and seventh external thermocouples

Grade A helium, dry air, and commercial Freon-12 were injected through the porous surface. Prior to entering the model, the gases were metered with a rotameter and were filtered through a fibrous glass filter twice the thickness of the inner cone and denser. It is believed that no significant porosity variations were introduced in the outer cone as a result of accumulation of matter within the porous surface. The temperature of the injection gases was controlled by a parallel system of hot and cold heat exchangers. The hot side consisted of

a copper coil immersed in an electrically heated water bath, and the cold side consisted of a copper coil immersed in dry ice and acetone mixture (-110° F) or an ice bath for Freon-12.

To obtain turbulent flow over the model, a boundary layer trip was used. A double trip made from two 3/4-inch bands of 2/0 garnet paper with most of the backing removed was used for tests at free-stream Mach numbers of 4.0 and 0.7. The first trip was located about 1/4 inch back from the cone tip and the second trip 1/16 inch back of the first. A quadruple trip made from four 3/16-inch bands of 1/2 garnet paper was used for tests at a free-stream Mach number of 4.8. The first trip was located about 1/8 inch back from the cone tip and the other three trips were spaced 1/16 inch apart.

For the supersonic flow tests, shadowgraph pictures were taken of the boundary layer to confirm that the flow was turbulent. For the subsonic test at Reynolds numbers of 4 million per foot, one would expect the boundary layer to trip quite easily, but since shadowgraph pictures did not have sufficient definition to show whether or not the boundary layer was turbulent, a technique of subliming solids was used. A small conical-shaped waxed protuberance (about 1/16 inch high) was stuck on the black painted surface of a solid aluminum cone model. Naphthalene suspended in petroleum ether was sprayed on the model surface and the tunnel was run at test conditions. The parallel pattern of sublimation behind the protuberance indicated that the flow was turbulent.

TEST CONDITIONS AND CALCULATION PROCEDURES

Local heat-transfer measurements were made on the test cone at the following nominal test conditions.

M_∞	M_c	T_t	R_c/ft
0.7	0.7	522° R	3.96×10^6
4.00	3.67	648° R	6.94×10^6
4.80	4.35	750° R	3.79×10^6

The measurements required to determine the local heat-transfer coefficients with foreign gas injection were the foreign gas inlet temperature, the cone wall temperature (or foreign gas exit temperature), the local mass injection rates at each surface thermocouple, the standard wind-tunnel conditions of stagnation pressure and temperature, and the test section static pressure. Free-stream Mach number was determined from the ratio of free-stream static to tunnel stagnation pressures for all tests. The cone Mach number for supersonic flow was obtained from the conical flow tables of reference 12.

The electromotive force of the chromel-constantan thermocouple wire versus temperature was measured over the temperature range of interest for these tests. The calibration deviated very slightly from the standard calibration (maximum of

1° F over the range). The thermocouple outputs were measured and recorded. Accuracy of temperature measurement was ±0.2° F. Total time to obtain one readout of steady-state temperatures and pressures was 1 minute. Temperatures, foreign-gas, flow rate, and pressures were monitored during the course of the experiment until steady-state conditions were realized. Some 5 to 10 readouts were obtained at each test condition during the steady-state period.

Along with the necessity of maintaining accuracy of the individual measurements of temperature and pressure, the interpretation of the measurements rests on a knowledge of the basic heat balance on the surface element of the cone. The net heat convected into the surface is:

$$q \equiv h(T_r - T_w) = -kt\left(\frac{1}{s}\frac{\partial T_w}{\partial s} + \frac{\partial^2 T_w}{\partial s^2}\right) + \frac{\epsilon\sigma(T_w^4 - T_n^4)}{1 + \frac{\epsilon A}{A_n}\left(\frac{1}{\epsilon_n} - 1\right)}$$

$$+ (\rho v)_w c_{p_g}(T_w - T_g) \qquad (1)$$

The first term on the right is the heat transferred out of the cone surface element by conduction only in the cone ray direction; the second term is the heat radiated out of the surface assuming a concentric cylinder geometric arrangement; and the last term is heat absorbed by the foreign gas coolant where the final temperature of the coolant is considered as the outside wall temperature. For thermocouples 1 through 7, inclusive, $\partial T_w/\partial s$ and $\partial^2 T_w/\partial s^2$ were obtained directly from a smooth curve through the surface-temperature distribution. In the second term, T_w is directly measured and T_n is the nozzle wall temperature which is considered to be the recovery temperature for turbulent flow. The total hemispherical emissivity of the cone surface was measured ($\epsilon = 0.49$) and the nozzle wall emissivity, ϵ_n, was estimated to be 0.1 for a polished stainless steel surface and 0.9 for a glass and metal wall for the subsonic wind tunnel. The most critical values in the heat balance equation are in the third term. The local mass-flow rate $(\rho v)_w$ must be known accurately and the accuracy of measurement over a small finite area is primarily dependent on the uniformity of porosity of the wall and on the local pressure difference across it. The relative mass-flow measurements of figure 2 show quite good uniformity from thermocouple 1 to 7 for 1/2-inch-diameter circular areas measured. The gas internal coolant temperatures, T_g, are normally correctly indicated by the internal thermocouples, but for the low injection rates of Freon, air, and occasionally helium, corrections to the thermocouple readings must be taken into account. Considerations applicable to the measurement of the true internal coolant temperature are presented in appendix C. For low Freon injection rates corrections were necessary so the temperature of the gas emanating from the internal glass fiber cone (average temperature of internal thermocouples 5 and 6) was used as the corrected T_g for internal thermocouples 1, 2, 3, and 4 located in the forward area of the cone. (See fig. 5.)

The heat-transfer coefficient, h, in equation (1) was evaluated graphically from a plot of q versus T_w/T_t for each surface thermocouple location.

Normally, the heat transfer was measured at four wall temperature levels for each gas injection rate; and this usually provided sufficient definition of a straight line through the data. The stagnation temperature, T_t, was held to within a 6.0°, 2.7°, and 2.6° F range for any given injection rate from run to run for Mach numbers 0.7, 3.67, and 4.35, respectively. For some low injection runs where the wall temperature level could not be changed appreciably, a small change in T_t could cause a considerable error in determining heat-transfer coefficient if q were plotted as a function of only T_w.

The heat-transfer coefficients presented in this report are uncorrected for external radiation heat transfer and porous wall heat conduction. The sum of the radiation and wall conduction corrections is negligible (less than 2 percent) for the Mach number 0.7 tests. For the Mach number 3.67 tests, the total corrections are less than 5 percent at the lower injection rates, and for the highest injection rates are generally less than 10 percent with a maximum correction of 15 percent. For the Mach number 4.35 tests, the total corrections are generally less than 8 percent with a maximum of 10.5 percent (except for the highest Freon injection rate where a maximum correction of 28 percent was noted). In all cases, the corrections would reduce the value of the heat-transfer coefficient. Also, the largest percent corrections apply to the smallest heat-transfer coefficients which were measured at the higher injection rates.

The heat-transfer data obtained at thermocouple locations 1 and 8 generally are not included in this report. For thermocouple 1, large surface conduction corrections, boundary-layer-trip effects, a variable porosity distribution preceding the location, the effect of the impermeable surface preceding the test station, and nonuniform surface temperature effects caused too many uncertainties to account for the behavior of the heat-transfer data. Thermocouple 8 was located in a region of rapidly decreasing porosity along cone rays B and C and was near to the nonporous area at the back of the cone; these conditions caused some of the heat-transfer results to behave in an unexplainable manner.

Because of the many test runs, the porous wall temperature distributions along the cone are not presented in this report. When a coolant gas is injected through the surface the temperature generally decreases along the cone ray as is shown for a low Freon injection rate in figure 5. For higher injection rates, and especially for air and helium injection, the temperature is essentially uniform along the cone.

PRESENTATION OF BASIC RESULTS

The fundamental usable results of this experiment are the Stanton numbers and the associated recovery factors. For each external thermocouple location (nos. 2 through 7) the local Stanton number was plotted as a function of the local air injection rate, and the smooth curve drawn through the data was extrapolated to the zero injection value to define the St_0 value. The ordinate and abscissa for all injection gases were normalized by dividing by the St_0 value obtained by air injection and these results are presented in a series of graphs (see figs. 6(a) to 8(f)), corresponding to each Mach number and local Reynolds

number (or thermocouple location). The curves drawn through the experimental points are primarily for identification of the data; certain exceptions are for the low Freon injection rates where the faired curves are forced through the zero injection St_o values. The St_o at each thermocouple is tabulated on each graph.

Before discussing these Stanton number results one might ask why the air injection heat-transfer data were used exclusively to define the St_o value. First, for low Freon injection rates, the internal heat-transfer coefficient to the internal thermocouples is smallest; therefore $\epsilon_i \sigma / h_i$ (eq. (C1)) is highest and internal radiation has the maximum effect. For helium injection, one of the theories for turbulent boundary-layer flow (ref. 10) predicts St/St_o values over 1.0 at low injection rates, and, if correct, this would prohibit extrapolation to the one correct zero injection value. These considerations compelled the authors to select the St_o value from the air injection heat-transfer results. These St_o results will be considered again in this report when comparison will be made with turbulent theory and other results.

$M_\infty = 0.7$ Heat Transfer and Recovery Factor

The series of graphs of St/St_o vs. F/St_o (figs. 6(a) through 6(f)) show an odd behavior of Freon-12 injection Stanton numbers. For the high injection rates, the Freon-12 Stanton numbers are in the expected relative position to the air injection values, but with decreasing injection, the values increase to a value greater than the zero injection value, St_o, and then decrease to a value just above the air injection values. (See thermocouples 4 to 7, figs. 6(c) to 6(f), inclusive.) For thermocouples 2 and 3 (figs. 6(a) and 6(b)) the increase is noted but not a subsequent decrease with decreasing injection rate. The associated recovery factors (figs. 9(a) through 9(f)) show a small decrease generally with increased injection for Freon with no apparent unexpected behavior. The possibility exists that the flow is transitional for the low Freon injection rates and the high Stanton values are a direct result of this type of flow; however, the fact that the Stanton number peak occurs at a higher injection rate for thermocouple locations at higher Reynolds numbers essentially nullifies this conjecture. The anomalous behavior of the Stanton number at low Freon injection rates was finally determined to be primarily a result of not knowing with sufficient accuracy the local injection rate of the heavy gas Freon-12 through the porous cone when the external pressure varies along the cone surface. The method used to determine the local flow injection rates is described in appendix A. Also, at low injection rates of Freon, it is difficult to change the porous wall temperature by varying the coolant temperature to adequately define the q vs. T_w curve by which to determine a heat-transfer coefficient.

The theoretical predictions of reference 10 for $M \approx 0$ are shown on the thermocouple 6 (fig. 6(e)) St/St_o graph for comparison purposes. Generally, the relative effectiveness on a mass injection basis of the three injection gases is in accordance with the theoretical predictions, but the absolute values do not agree. The theory is for distributed injection where F is proportional to the skin-friction coefficient. The possibility of the slight increase in Stanton

number over the zero injection value for helium injection, as predicted by the theory, exists in the data but the experimental definition is not sufficient at the low injection rates.

The effect of Reynolds number (or thermocouple location) on the St/St_o variation with injection rate, F/St_o, is hardly noticeable at the subsonic Mach numbers for these tests. The theories (refs. 2 and 10) predict little effect of Reynolds number on the St/St_o value for air and Freon injection, and for helium injection the theory predicts a lower St/St_o value for higher Reynolds numbers at a given F/St_o value.

In conjunction with the discussion of the Stanton number variation, the effect of injection on the recovery temperature, T_r, or the recovery factor, $(T_r - T_c)/(T_t - T_c)$, must be considered since $q = h(T_r - T_w)$. For helium injection the recovery factor rises from the zero injection value near 0.84 and peaks out for $F \approx 0.001$ at a maximum value of about 1.35 or 62.7° R above the free-stream temperature or 16.3° R above the total temperature of the stream. By definition, this is the wall temperature condition for zero heat transfer to the wall. At higher injection rates $F > 0.001$ the recovery temperature decreases. Tewfik, Eckert, and Shirtliffe (ref. 3) have noted an increase in recovery temperature for F values up to their maximum test value of 0.001. They attribute the increase in recovery temperature to thermal diffusion within the laminar sublayer. Another possible cause of the high recovery temperature may be the vortical action of the injection gas causing a separation of energy within the boundary layer. Large swirls and eddies are evident in the boundary layer photographs at the higher Mach numbers.

The recovery temperature with air injection shows a slight peak at about the same mass injection rate as with helium injection and then decreases gradually to a value near 0.79 at the highest air injection mass flow. Since both helium and air recovery temperatures peak at the same injection mass flow, the effect is probably not due to transitional flow effects because helium is more apt to trip the boundary layer for the same mass injection rate. (See ref. 1.)

$M_c = 3.67$ Heat Transfer and Recovery Factor

Here again, some unexpected behavior of the heat-transfer coefficients (figs. 7(a) through 7(f)) and the recovery factors (figs. 10(a) through 10(f)) is immediately evident. First, the Stanton numbers for helium injection at low injection rates are greater than the zero injection Stanton number obtained from extrapolation of the air data. Second, the Stanton numbers for Freon injection do not tend to the zero injection value except for thermocouple 6 (ray A and C) and thermocouple 7. Third, the air injection Stanton numbers for some lowest injection cases tend to deviate away from the trend to the zero injection Stanton value. (Equal weight was given to all air injection Stanton values when the St_o values were defined for this Mach number, $M_c = 3.67$.) The first observation is bolstered by the fact that straight line extrapolation of the low helium injection Stanton values would yield St_o values 130 to 140 percent of the value obtained for air. For the Stanton value trends as $F \to 0$, this 30- to 40-percent

discrepancy is too large and consistent to be explained on any other basis than that the low injection Stanton values for helium are, in fact, greater than the zero injection value. To explain the second observation, two possible conditions may exist: (1) the heavy gas Freon may tend to stabilize and thicken the laminar sublayer at low injection rates and reduce the heat transfer, (2) internal radiation effects may not be completely accounted for in the measurement of the coolant gas temperature, T_g. The internal radiation correction applied to the coolant gas temperature did not raise the lowest injection St values completely into line with the expected trend. The correction was usually about a 10-percent increase with a maximum correction of a 20-percent increase in Stanton number. The third observation is most likely due to the fact that internal radiation corrections do not quite yield the true internal gas coolant temperature. A final observation of the normalized St/St_o representation as a function of F/St_o indicates an essential independence of Reynolds number for all injection gases.

Again when heat transfer is considered, the behavior of the recovery factor is equally important. For air and Freon injection the recovery factor decreases from its initial zero injection value to a minimum value and then increases to near its initial value at the higher injection rates. With helium injection the recovery factor decreases initially and then rises rapidly for injection rates near $F = 0.001$ to values near 1.30; thermocouple 7 is the only exception. These high values for recovery factor with accompanying low Stanton numbers suggest an evaluation of the heat transfer on a basis other than $St(T_{r_o} - T_w)$ or $St(T_t - T_w)$. Further discussion of this point is required and will follow later in the report.

$M_c = 4.35$ Heat Transfer and Recovery Factor

The heat-transfer data (figs. 8(a) through 8(f)) for $M_c = 4.35$ are not so well defined as the previously presented $M_c = 3.67$ data, again, especially at the low injection rates of air and Freon. The zero injection Stanton numbers for this series of tests ($M_c = 4.35$) were extrapolated from the air injection data but ignoring the lowest injection rate Stanton values at each thermocouple location. These extrapolated St_o values are somewhat lower than the correct values that would have been obtained if reliable low injection rate Stanton numbers were available; therefore, the St/St_o ratios when plotted against F/St_o are moved in the positive ordinate and abscissa direction giving a conservative value relative to the correct result. Except for the low injection rates of air and Freon the relative effectiveness of the three gases in reducing Stanton number follows the theory and is consistent with the results at other Mach numbers. The effect of Reynolds number (or thermocouple location) on the reduction in the normalized St/St_o ratio as a function of F/St_o is small, as in the $M_c = 3.67$ results. The theoretical $M \approx 0$ results of reference 10 are presented (fig. 8(e)) for thermocouple 6 for reference purposes.

The recovery factors (figs. 11(a) through 11(f)) for helium, air, and Freon rise very rapidly at the highest injection rates of each gas. For higher helium injection rates, $F \approx 0.002$, the heat transfer cannot be defined on the basis of $q = h(T_r - T_w)$ because T_r becomes undefinable and q is essentially constant

with T_w. The change in recovery temperature must be taken into account when the present Stanton numbers are used to calculate heat transfer. The heat-transfer data obtained at the high injection rates will be presented later on as a direct heat-transfer measurement q rather than a heat-transfer coefficient. One last statement on the recovery factor representation. A dimensionless plot of r/r_o vs. $c_{p_g}F/c_{p_c}St_o$ does not particularly correlate the representation of the recovery factor for the three injection gases at $M_c = 4.35$.

Stanton Number Variation With Reynolds Number

The effect of Reynolds number on the local heat-transfer coefficient at fixed rates of injection is shown in the series of figures 12 through 15(c). The data points were obtained from the smooth curves drawn through the Stanton number data plotted as a function of local injection rate for each thermocouple location. The zero injection Stanton numbers shown separately in figure 12 are the extrapolated values obtained from the air injection data. Given as a reference for the zero injection heat transfer are the curves based on the Blasius incompressible turbulent skin-friction formula modified to cone flow and converted to heat transfer through the Rubesin analogy and finally adapted to the compressible turbulent boundary layer by the intermediate temperature method (T' method, ref. 13). Using the Sutherland viscosity variation with temperature gives the final relation for the reference curves as

$$St_{\substack{\text{cone}\\\text{local}}} = \frac{0.0415}{R_c^{0.2}} \left(\frac{T'}{T_c}\right)^{-0.5} \left(\frac{1 + \frac{200}{T_c}}{\frac{T'}{T_c} + \frac{200}{T_c}} \right)^{0.2} \tag{2}$$

where

$$\frac{T'}{T_c} = 1 + 0.035M_c^2 + 0.45\left(\frac{T_w}{T_c} - 1\right) \tag{3}$$

$$\frac{T'}{T_c} = 1 + 0.115M_c^2 \qquad \text{for} \quad r = 0.89$$

The zero injection St_o values for all Mach numbers appear to decrease more rapidly with increasing Reynolds number than the commonly accepted variation $St_o = K/R_c^n$, where $n \approx 0.2$ and $K = K(M_c)$ for $T_w = T_r$. The Reynolds number for each full line symbol is based on a length from the cone tip to the thermocouple location. The dotted symbols, shown only for stations 2 and 8, denote the effective boundary-layer Reynolds number based on a length from the effective start of the porous material as obtained from shadowgraph pictures of the boundary layer without a boundary-layer trip.

The effective run of the boundary layer is $s_j - s_o$, where $s_j = (j + 1.187)$ inch, $s_o = 1.417$ inch, and $j = 1, 2, \ldots, 8$. The effective Reynolds number is $R_c(s_j - s_o)/s_j$. With injection, then, the effective boundary-layer Reynolds number would be near the dotted symbols. Since the St_o (zero injection) values are extrapolated from St values with air injection, then the effective Reynolds number corresponding to St_o values should be near the effective boundary-layer Reynolds numbers with injection. The variation of St_o with this effective Reynolds number agrees more closely to the analytical trend of equation (2). One further statement with regard to the effective turbulent boundary-layer Reynolds number for small test models is that the boundary-layer trip can also alter the effective starting position of the boundary layer. For these cone tests, the forward location of the trip would most likely cause the effective Reynolds number to increase from the dotted symbol, that is, from the effective start of the porous region of the cone.

The effect of Mach number on the extrapolated St_o values for Reynolds numbers near 2.5 million is quite close to that predicted by the intermediate enthalpy method applied to the present Stanton formulation (eq. (2)).

Generally, the St_o values are slightly higher than the predicted values for the limited Reynolds number range of this test. Previous measurements of total skin friction (ref. 1) were higher than similarly predicted skin-friction values. It is noted that the Kármán-Schoenherr incompressible skin-friction relation modified to the compressible heat-transfer relation gives Stanton numbers from 5 to 9 percent below the Blasius relation for a Reynolds number of near 2 million.

A general observation is that the Stanton numbers for air, helium, and Freon-12 injection (figs. 13(a) through 15(c)) decrease with increasing Reynolds number more rapidly than the usual -0.2 power of Reynolds number, and for higher injection rates the Stanton numbers decrease more rapidly with Reynolds number than the St_o values. The effective Reynolds numbers based on a boundary-layer run starting at the effective beginning of the porous material are shown for the zero injection values, St_o, on each figure for the lowest and highest Reynolds numbers. A possible shift in effective Reynolds number is also applicable to all test cases with injection. As is quite evident at each Mach number $M_c = 0.7$, 3.67, and 4.35, substantial reductions in Stanton number were obtained at the highest injection rates of these tests. As previously noted, the behavior of the Stanton number at the lower Freon injection rates for $M_c = 0.7$ and 4.35 is not accurately defined; therefore, the St vs. R_c variation is shown only for the higher Freon injection rates for the two Mach numbers.

Mach Number Effects on Heat Transfer

In a previous paper (ref. 1) measurements on a porous cone of the total skin-friction coefficients showed a dependence on Mach number, with greater effectiveness of the foreign gas injection in reducing the skin friction at the subsonic Mach numbers. These present tests were initially proposed to determine the effect of Mach number on the reduction in heat-transfer coefficient. The

Mach number effect is shown in figures 16(a) through 16(c). For air, helium, and Freon injection there is generally a decreased effectiveness in reducing the Stanton number from its zero injection value for a given injection rate, F/St_o, with increasing Mach number. The variation of St/St_o with Mach number is similar but not as great as that of C_F/C_{F_o} with Mach number. Also for the highest air, helium, and Freon injection rates at $M = 0.7$ the drop-off in St/St_o values levels off with increased injection; the skin-friction C_F/C_{F_o} variation with $2F/C_{F_o}$ continued to decrease with increased injection at the low Mach numbers. The St/St_o variation with Mach number is quite incomplete for Freon injection because of the limitations of the present test methods in obtaining low injection data. The St/St_o values (closed points) are measured values. The St/St_o values (dotted points) for F/St_o up to 1.5 were obtained from the faired curves through the higher injection Freon data and terminate at the extrapolated air value of St_o. There is a small variation in St/St_o with Mach number for the limited Freon tests; this result is not quite in agreement with skin-friction results of reference 1, where greater effectiveness in reducing the skin friction is shown at the subsonic Mach numbers.

A final comparison of the St/St_o variation should be made with some of the existing theories because for turbulent flow the experimental results are usually the standard on which the theories are tested. The faired curves through the St/St_o vs. F/St_o data for the two thermocouple locations 4 and 6 at each Mach number are used here in figure 17 for comparison. Thermocouple locations 4 and 6 were selected because (1) the St/St_o curves are defined at each location by four thermocouples, one on each instrumented cone ray, (2) the flow at these locations is more likely to be fully developed turbulent flow, and (3) for all the test Mach numbers the results are representative of most cone locations. The comparison will be made using the Rubesin theory for air injection into the compressible turbulent boundary layer and the theory of Rubesin and Pappas for the incompressible turbulent boundary layer with foreign gas injection. As contrasted to the previous skin-friction measurements (ref. 1) the Stanton number ratio St/St_o vs. F/St_o curves agree fairly well with the predictions of Rubesin for distributed air injection over the Mach number range 0 to 4. The primary disagreement is at $M = 0.7$ where the data show a slightly greater reduction in Stanton number than predicted. The comparisons are made for a flat-plate Reynolds number of 1 million, which is approximately one-half the average of the local cone Reynolds numbers of 2.6 million for this series of data. It is noted that for turbulent boundary-layer flows, Van Driest has shown that the cone boundary-layer characteristics are equivalent to the flat-plate values at one-half the flat-plate Reynolds number.

In order to compare the relative effectiveness of the foreign gases with theory, the predictions of reference 10 for incompressible flow are shown on the thermocouple 6 results in figures 6(e), 7(e), and 8(e) for each Mach number, for reference purposes. The effect of Reynolds number on the theoretical prediction of St/St_o vs. F/St_o curves is very small for both Freon and air injection; therefore, the prediction for only a flat-plate Reynolds number of 10^6 is shown. For helium injection the theoretical effect of Reynolds number is quite pronounced; therefore, the theoretical predictions for $R_x = 10^6$ and 10^7 are shown for comparison on the $M = 0.7$ data plot. For all Mach numbers the spread in effectiveness is greater than the theory predicts but the relative values are in

the right order. The important conclusion is that the effect of Mach number on the heat-transfer coefficient with air injection is very small and in quite good agreement with the theoretical predictions of Rubesin. Previous skin-friction results showed a marked effect of Mach number on the effectiveness of air injection to reduce the skin-friction coefficient; this was not in accordance with the theory.

Cooling Effectiveness

Of direct interest to many applications of transpiration cooling is the effectiveness in reducing the temperature of the porous wall. The effectiveness, $(T_w - T_g)/(T_{ro} - T_g)$, is a useful measure of the ability of the heat-transfer systems (or methods) in cooling an aerodynamically heated wall. A simple heat balance on a porous wall area neglecting heat conduction along the wall and radiation to the wall yields the relation

$$\frac{q}{(\rho u c_p)_c} = St(T_r - T_w) = F \frac{c_{p_g}}{c_{p_c}} (T_w - T_g) \tag{4}$$

and after some algebra this may be written as

$$E \equiv \frac{T_w - T_g}{T_{ro} - T_g} = \frac{T_r - T_g}{T_{ro} - T_g} \frac{1}{\frac{Fc_{p_g}}{St_o c_{p_c}} \left(\frac{St_o}{St}\right) + 1} = \frac{1}{1 + \frac{F}{St_o} \frac{c_{p_g}}{c_{p_c}} \left(\frac{q_o}{q}\right)} \tag{5}$$

Since, for air injection, Rubesin (ref. 14) found from theory for a wide range of Reynolds numbers, Mach numbers, and wall to free-stream temperature ratios and for both distributed and uniform injection that $St/St_o \approx f(F/St_o)$, one can expect that $E \approx E(F/St_o)$ for air; and if the other gases behave similarly, then one might expect $E \approx E[(F/St_o)(c_{p_g}/c_{p_c}),(St/St_o)]$ or perhaps, as some have proposed (see ref. 11), that $E \approx E[(F/St_o)(c_{p_g}/c_{p_c})]$. When the temperature data in the form of the effectiveness, E, are plotted as a function of $(F/St_o)(c_{p_g}/c_{p_c})$ in figure 18, a broadband correlation is obtained. Only the effectiveness data for the largest $(T_w - T_g)$ values are presented. The empirical curve of Bartle and Leadon (ref. 11) $E = 1/[1 + (1/3)(F/St_o)(c_{p_g}/c_{p_c})]^3$ is shown on the figure only for reference purposes when comparing the present data. Similar effectiveness curves may be obtained from the various turbulent theories available. It should be noted that the variation in effectiveness ratio is considerable at any given abscissa value of $(F/St_o)(c_{p_g}/c_{p_c})$ over the range of Mach numbers and Reynolds numbers for the various injection gases. Also, for small temperature differences between wall and coolant and for the high helium injection rates at $M = 4.35$, no apparent correlation was observed. The effectiveness data that are presented may be used as a rough guide to predict the coolant ability of a transpiration system on an aerodynamically heated porous wall.

The temperature effectiveness ratio relation

$$E \equiv \frac{T_w - T_g}{T_{ro} - T_g} = \frac{1}{1 + \frac{F}{St_o}\frac{c_{p_g}}{c_{p_c}}\left(\frac{q_o}{q}\right)}$$

is not recommended as a method for calculating q/q_o for turbulent flows with foreign gas injection, because $E \neq E[(F/St_o)(c_{p_g}/c_{p_c})]$ for many of the test conditions for all test Mach numbers. This statement is not in agreement with reference 15, where the effectiveness ratio is recommended as a universal means for calculating heat transfer with gas injection for wall temperatures outside the range $0.9 < T_w/T_{ro} < 1.1$.

High-Injection-Rate Heat Transfer

For the highest injection rates of the foreign gases at Mach numbers 3.67 and especially 4.35 the recovery temperature has increased above its lowest value and for some cases (see figs. 10 and 11) was well above the total temperature of tunnel air stream. At Mach number 4.35, two additional runs were made at higher rates of helium injection. The concept of a recovery temperature is not applicable for these runs since the heat transfer was essentially constant for a wall temperature change of over 100° F. The heat transfer to the wall actually increased with increased injection rate for the same wall temperature level. For conditions where the recovery temperature is initially well above the zero injection recovery temperature a comparison must be made based on the actual heat entering the wall rather than on a heat-transfer coefficient with its attendant recovery temperature; but even heat-transfer ratio must be used with care for wall temperatures near recovery temperature. A comparison is made in figure 19 for helium injection at $M_c = 4.35$ of the heat entering the porous wall for a wall temperature 100° F below the zero injection recovery temperature. The maximum reduction in Stanton number for the last three test stations for $F = 0.00101$ yields St/St_o values of 0.120, 0.127, and 0.173 with corresponding q/q_o ratios of 0.585, 0.535, and 0.447; however, the maximum reduction in q (which occurs at other injection rates) gives q/q_o values of 0.551, 0.444, and 0.398. For the highest injection rate at test stations 4, 5, and 6, the heat entering the wall is about equal to the zero injection value; that is, $q/q_o \approx 1.0$. This discussion again emphasizes the caution that St/St_o ratios should not be used as heat-transfer ratios at the higher gas injection rates for the turbulent boundary layer. At high injection rates, high-speed gas jets may emanate from the porous surface and affect the heat transfer differently than uniform gas injection.

SUMMARY OF RESULTS

Local heat transfer and recovery temperatures of the turbulent boundary layer with foreign gas injection of helium, air, and Freon-12 were measured on a porous cone for cone Mach numbers up to 4.35 and in a local Reynolds number range from 1 to 5 million. The heat-transfer data generally were presented as the ratio of local Stanton number to the Stanton number with zero injection, St/St_o, as a function of the dimensionless local injection value, F/St_o. The recovery factor $(T_r - T_c)/(Tt - T_c)$ was presented as a function of the local injection rate F because no other type parameter considered would generally improve the correlation of the data at one particular test Reynolds number. The important results of the tests were as follows.

$$M_c = 0.7$$

The relative effectiveness of the gases helium, air, and Freon-12 in reducing the Stanton number is as expected on a mass injection basis, but the absolute magnitude of the reduction is not in agreement with the low-speed theory of Rubesin and Pappas. The experimental results indicate little effect on Stanton number ratio with increased Reynolds number for all the injection gases; whereas the theory predicts a reduction in Stanton number with increased Reynolds number for helium and essentially no Reynolds number effect for air and Freon injection.

The recovery factor for helium injection increases from the zero injection value near 0.84 to a maximum value near 1.35 ($T_r = T_t + 16.3^\circ$ R) and then decreases with increasing injection. Tewfik, Eckert, and Shirtliffe also measured a recovery temperature higher than the free stream (or total temperature) with increasing helium injection but did not note a subsequent decrease at the higher injection values. They attribute the rise in recovery temperature to effects of thermal diffusion. The recovery temperatures for the present tests for air and Freon-12 injection decrease generally with increased injection.

$$M_c = 3.67 \text{ and } M_c = 4.35$$

The relative effectiveness of the gases helium, air, and Freon-12 in reducing the Stanton number is as expected on a mass injection basis.

The effects of Mach number on the reduction in Stanton number ratio are not as great as the effect on the reduction in skin friction but the general trends are the same, that is, the effectiveness generally decreases with increasing Mach number at given injection rates F/St_o.

For air injection, the experimental values of St/St_o vs. F/St_o curves agree quite well with the theoretical predictions of Rubesin for distributed air

injection over the Mach number range from 0 to 4. This result is in contrast with the skin-friction results of Pappas and Okuno, where the reduction in C_F/C_{F_o} ratio was dependent on Mach number for air injection.

The recovery factor for all injection gases initially decreases as expected from the zero injection value and then increases at the higher injection rates to values above the total temperature. The concept of a Stanton number and temperature potential based on a recovery temperature do not apply at high injection rates for the turbulent boundary layer.

The actual heat transfer to a porous wall can increase with increased injection at the high test injection rates, and in fact may be about the same value as that at zero injection.

Ames Research Center
National Aeronautics and Space Administration
Moffett Field, Calif., Nov. 15, 1963

APPENDIX A

RELATIVE MASS FLOW RATE DISTRIBUTION OF THE HEAT-TRANSFER MODEL

An accurate determination of the local mass flow rate is essential for reliable local heat-transfer measurements. Although various methods have been used (refs. 1 and 9) to measure the relative mass flow rate, the procedure described below is considered to be the most appropriate and accurate method for the present test. The setup shown schematically in figure 3 was used to measure the porosity distribution of the cone. The cone was sealed inside of a polyester film bag 4 mils thick. The one opening in the bag was a 1/2-inch-diameter hole which was sealed and positioned over the area to be tested. The bag was evacuated with a vacuum pump until the rotameter indicated no flow. The seal over the hole was then removed and the valve was throttled until the desired pressure difference across the porous surface material was obtained. The rotameter reading, pressure, and temperature were then recorded. Figure 2 shows the relative flow rate results of the test along four equally spaced rays of the cone. Ray A is the ray with the eight thermocouples. For an indication of the accuracy of the results, the integrated average of the flow rates measured along the four rays was compared with the flow rate through the total porous cone at the same pressure differential. The integrated value was 16 percent greater than the total as shown by figure 4. This difference of 16 percent is probably a result of insufficient number of measurements over the total cone surface.

These tests were conducted while the gas flow was in the direction opposite to that of the actual test. To verify that the direction of gas flow had no effect on the mass flow rate, the measured flow rate through the total porous cone in one direction was compared with that in the opposite direction for a given pressure. Figure 4 shows that the flow rates in both directions were essentially the same.

The local mass injection rate at each thermocouple was determined from the relative mass flow measurements and the total metered mass flow rate through the cone for the test cases $M_c = 3.67$ and 4.35, where the external cone pressure is essentially constant along any cone ray. Measurements of the external pressure distribution made in conjunction with the test results of reference 1 for a 15° cone at supersonic Mach numbers $M_c = 3.21$ and 4.30 show that the pressure level may change slightly with injection gas and rate of injection but is essentially uniform over the cone.

For the subsonic $M = 0.7$ tests, the external pressure on the 15° cone decreases along the cone ray; and for the present tests, the variation from thermocouple 1 ($s = 2.187$ in.) to 8 ($s = 9.187$ in.) is only 3 percent from about 10.8 to 10.5 psia, but certainly of sufficient change to decrease the calculated local injection rate at thermocouple 1 a maximum of 55 percent at the lowest Freon injection rate. The method of determining the local flow at each thermocouple location was as follows. The pressure inside the internal glass fiber

cone was measured at each injection rate during the heat-transfer tests. The pressure drop across the glass fiber cone was measured for the three injection gases for various flow rates and correlated on the basis of Δp^2 vs. G based on the relation for flow through porous materials

$$\frac{\Delta p^2}{t} = \alpha(2bT\mu)G + \beta\left(2b\frac{T}{g}\right)G^2 \qquad (A1)$$

From this correlation, the pressure on the inside of the stainless steel test cone was determined. A calibration of total unit flow rate was obtained for the stainless steel cone as a function of Δp^2 across the cone, where the outside pressure was the outside area-weighted-average pressure; this calibration along with the relative local porosity measurements of figure 2 was sufficient to calculate the local unit flow rate $(\rho v)_w$ for each test injection rate for all the injection gases. Corrections for gas temperature level were included in these calculations by equation (A1). These determinations of local flow rate at each thermocouple location were still not adequate to account for the odd behavior of the local Stanton numbers with Freon injection at the lower injection rates. A better method is required to determine the local flow rate of a heavy gas through a porous cone with an external pressure variation.

APPENDIX B

CONDUCTIVITY MEASUREMENT

The conductivity of the porous stainless steel was found to be 4.7 Btu/hr ^{o}F ft at 80^{o} F. This was determined by measuring the temperature distributions along a porous stainless steel circular ring and an identical solid stainless steel specimen of a known conductivity, each heated from one side of the ring. The heat loss to the ambient air was assumed to be the same for both specimens (since the temperature levels were approximately the same) and the thermal conductivity was calculated from the temperature distributions.

APPENDIX C

INTERNAL TEMPERATURE MEASUREMENT OF COOLANT

The temperature of the coolant gas indicated by the internal thermocouples and the external surface temperature are plotted in figure 5 for a test with a low Freon injection rate. The indicated internal temperature tends to follow the external wall temperature. This variation in the temperature of the internal thermocouple can only result from the net heat exchange to the internal thermocouple from (1) the convective heat transfer of the internal coolant gas, (2) the radiation from the surrounding surfaces, (3) conduction to the thermocouple from the lead wires, and (4) conduction through the gas from the higher temperature porous wall. Heat-transfer mode (3) contributes very little, and an analysis of the temperature distribution in a gas flowing normally to a porous wall shows that the gas temperature distribution cannot possibly extend into the gas as far as the internal thermocouple locations; therefore mode (4) does not contribute to the temperature of the thermocouple. Consideration of heat-transfer modes (1) and (2) results in a heat balance on an internal thermocouple which yields the following expression for the coolant gas temperature

$$T_g = T_i + \frac{\epsilon_i \sigma}{h_i}\left[\left(\frac{T_i}{100}\right)^4 - \left(\frac{T_w}{100}\right)^4\right] \tag{C1}$$

The term $\epsilon_i\sigma/h_i$ can be evaluated from one particular test run with air injection for the internal thermocouples $i = 1, 2, 3,$ and 4 since all the temperatures in the equation are known; then knowing the variation of h_i as a function of the internal flow conditions at an internal film temperature T_f will allow a check of the measured temperature difference, $T_g - T_i$. The convective heat transfer to a spherical-shaped blob is for laminar flow

$$\frac{h_i D}{k_f} = 0.37\ \mathrm{Pr}_f^{1/3}\left[\frac{B_i(\rho v)_w D}{\mu_f}\right]^{0.6} \tag{C2}$$

Then for any other gas and injection rate

$$\frac{h_{air}}{h_g} = \left(\frac{k_{air}}{k_g}\right)_f \left(\frac{\mathrm{Pr}_{air}}{\mathrm{Pr}_g}\right)_f^{1/3}\left[\frac{\mu_g}{\mu_{air}}\,\frac{(\rho v)_{w_{air}}}{(\rho v)_{w_g}}\right]^{0.6} \tag{C3}$$

where

$$B_i = \frac{(\rho u)_i}{(\rho v)_w} = \frac{1}{\sin \theta}\left(1 - \frac{s_o^2}{s_i^2}\right), \quad i = 1,2,3,4 \tag{C4}$$

By this means the indicated internal thermocouple temperature rise, $T_i - T_g$, see figure 5, for thermocouples 1, 2, 3, and 4 was predicted quite accurately from one test to the others, where the internal flow rate and coolant gas and the fourth power temperature difference were changed. The ability to predict the temperature of the thermocouples generally confirmed the postulated heat exchange. The true temperature, T_g, of the coolant gas in the forward part of the cone was taken to be the average of the temperature of the gas emanating from the internal glass fiber cone at thermocouples 5 and 6.

Now, the internal junctions for thermocouples 5, 6, 7, and 8 are also subject to a radiant and convective heat balance as are the others in the forward part of the cone. For the high injection flow rates all the internal coolant indicated temperatures are essentially the same value, and the temperature difference between the porous cone wall and the internal thermocouples is small and the internal radiation correction is negligible. With decreasing coolant flow (for the case where $T_g \ll T_{ro}$), the internal temperatures, starting with thermocouple 1, begin to increase and follow the external wall temperature; that is, the $\epsilon_i \sigma / h_i$ term and the $(T_i^4 - T_w^4)$ term both increase. Internal thermocouples 5, 6, 7, and 8 are located on the surface of the inner glass fiber cone and therefore the junction and leads see (in a radiation sense) the outer porous cone from one side and the inner porous cone surface from the other, and the effective emissivity to the outer cone is reduced by about one-half. Lead wire conduction would tend to change the junction temperature to the correct coolant temperature because the lead wires pass through the glass fiber cone wall. Also at all injection rates the true temperature rise of the coolant is much less at thermocouple locations near the back of the cone. An analysis of the gas flow over the internal thermocouples 1 through 8 reveals that the maximum mass flow occurs over thermocouple 5 and near maximum over 6 with corresponding minimal values of $\epsilon_i \sigma / h_i$ for these thermocouples. This discussion is deliberately somewhat qualitative with regard to the effect of internal radiation on the thermocouples 5, 6, 7, and 8 because exact calibration of the effect of $\epsilon_i \sigma / h_i$ term is not easily made. Examination of the response of the internal indicated temperature distribution to the external cone wall distribution was the best possible way to determine whether radiation influenced the indicated internal coolant temperature at thermocouple locations 5, 6, 7, and 8.

REFERENCES

1. Pappas, Constantine C., and Okuno, Arthur F.: Measurements of Skin-Friction of the Compressible Turbulent Boundary Layer on a Cone With Foreign Gas Injection. Jour. Aero. Sci., vol. 27, no. 5, May 1960, pp. 321-333.

2. Rubesin, Morris W.: An Analytical Estimation of the Effect of Transpiration Cooling on the Heat-Transfer and Skin-Friction Characteristics of a Compressible, Turbulent Boundary Layer. NACA TN 3341, 1954.

3. Tewfik, O. E., Eckert, E. R. G., and Shirtliffe, C. J.: Thermal Diffusion Effects on Energy Transfer in a Turbulent Boundary Layer With Helium Injection. Proceedings of the 1962 Heat Transfer and Fluid Mech. Inst., June 1962, pp. 42-61.

4. Craven, A. H.: Boundary Layers With Suction and Injection. Rep. 136, The College of Aeronautics (Gt. Brit.), Sept. 1960.

5. Hartnett, J. P., Masson, D. J., Gross, J. F., and Gazley, C., Jr.: Mass-Transfer Cooling in a Turbulent Boundary Layer. Inst. Aero. Sci. Paper 60-66.

6. Tewfik, O. E., Eckert, E. R. G., and Jurewicz, L. S.: Measurement of Heat Transfer from a Circular Cylinder to an Axial Stream With Air Injection Into a Turbulent Boundary Layer. Univ. of Minnesota, Inst. of Tech., HTL TR no. 38, AFOSR 1397, Aug. 1961.

7. Bartle, E. R., and Leadon, B. M.: The Effectiveness as a Universal Measure of Mass Transfer Cooling for a Turbulent Boundary Layer. Proc. 1962 Heat Transfer and Fluid Mech. Inst., June 1962, pp. 27-41.

8. Rubesin, Morris W.: A Modified Reynolds Analogy for the Compressible Turbulent Boundary Layer on a Flat Plate. NACA TN 2917, 1953.

9. Rubesin, Morris W., Pappas, Constantine C., and Okuno, Arthur F.: The Effect of Fluid Injection on the Compressible Turbulent Boundary Layer - Preliminary Tests on Transpiration Cooling of a Flat Plate at $M = 2.7$ With Air as the Injected Gas. NACA RM A55I19, 1955.

10. Rubesin, Morris W., and Pappas, Constantine C.: An Analysis of the Turbulent Boundary-Layer Characteristics on a Flat Plate With Distributed Light-Gas Injection. NACA TN 4149, 1958.

11. Leadon, B. M., and Scott, C. J.: Measurement of Recovery Factors and Heat-Transfer Coefficients With Transpiration Cooling in a Turbulent Boundary Layer at $M = 3.0$ Using Air and Helium as Coolants. Univ. of Minnesota, Rosemount Aeronautical Lab. Res. Rep. 126, 1956.

12. Staff of the Computing Section, M. I. T. (under the direction of Zdênek Kopal): Tables of Supersonic Flow Around Cones. Tech Rep. 1, Center of Analysis, M. I. T., Cambridge, 1947.

13. Sommer, Simon C., and Short, Barbara J.: Free-Flight Measurements of Turbulent-Boundary-Layer Skin-Friction in the Presence of Severe Aerodynamic Heating at Mach Numbers From 2.8 to 7.0 NACA TN 3391, 1955.

14. Rubesin, Morris W.: The Influence of Surface Injection on Heat Transfer and Skin-Friction Associated With the High-Speed Turbulent Boundary Layer. NACA RM A55L13, 1956.

15. Leadon, B. M., and Bartle, E. R.: On Mass Transfer Effectiveness. AIAA Jour., vol. 1, no. 5, May 1963, pp. 1185-86.

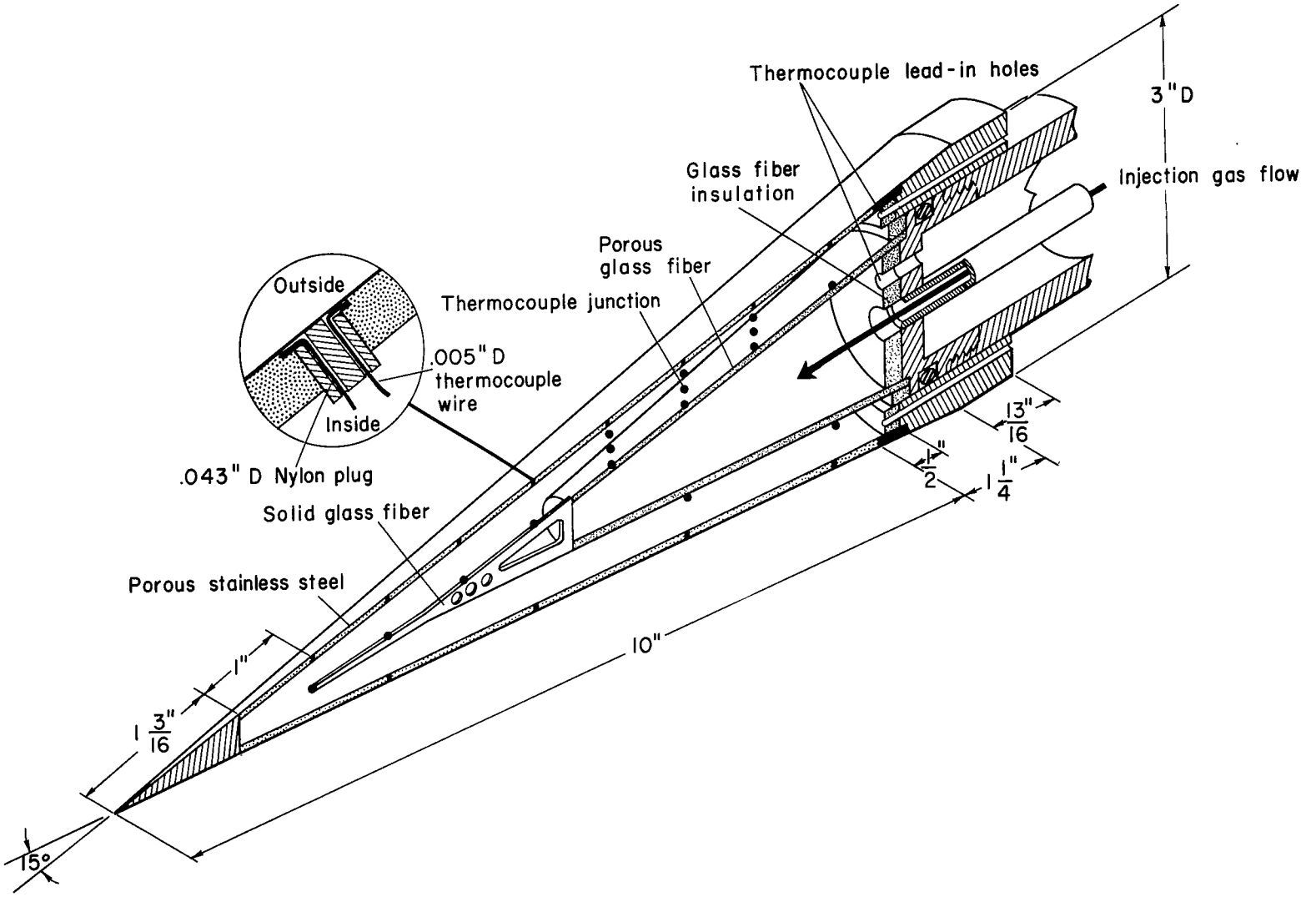

Figure 1.- Cone heat-transfer model.

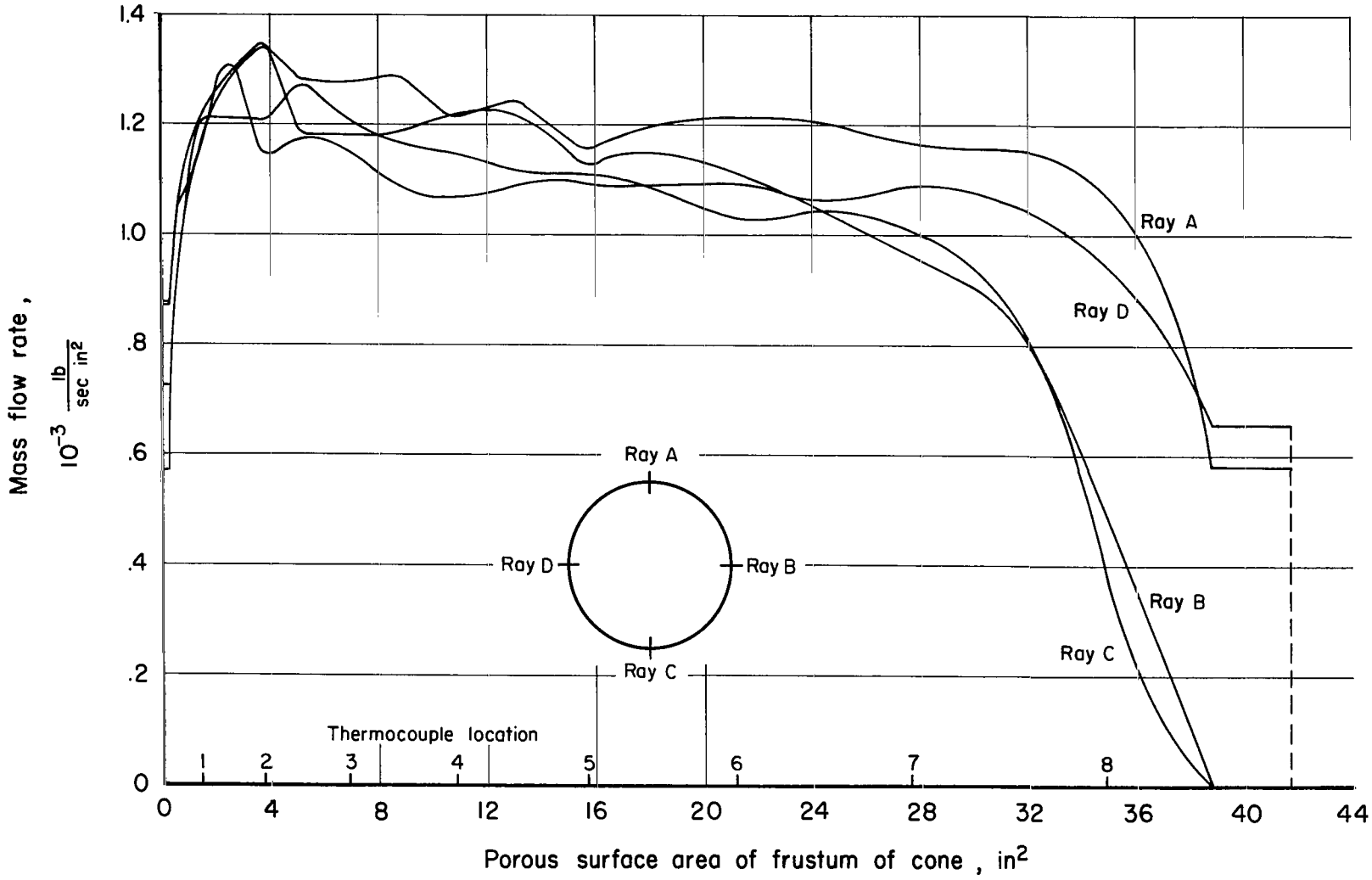

Figure 2.- Mass flow rate distribution through porous cone.

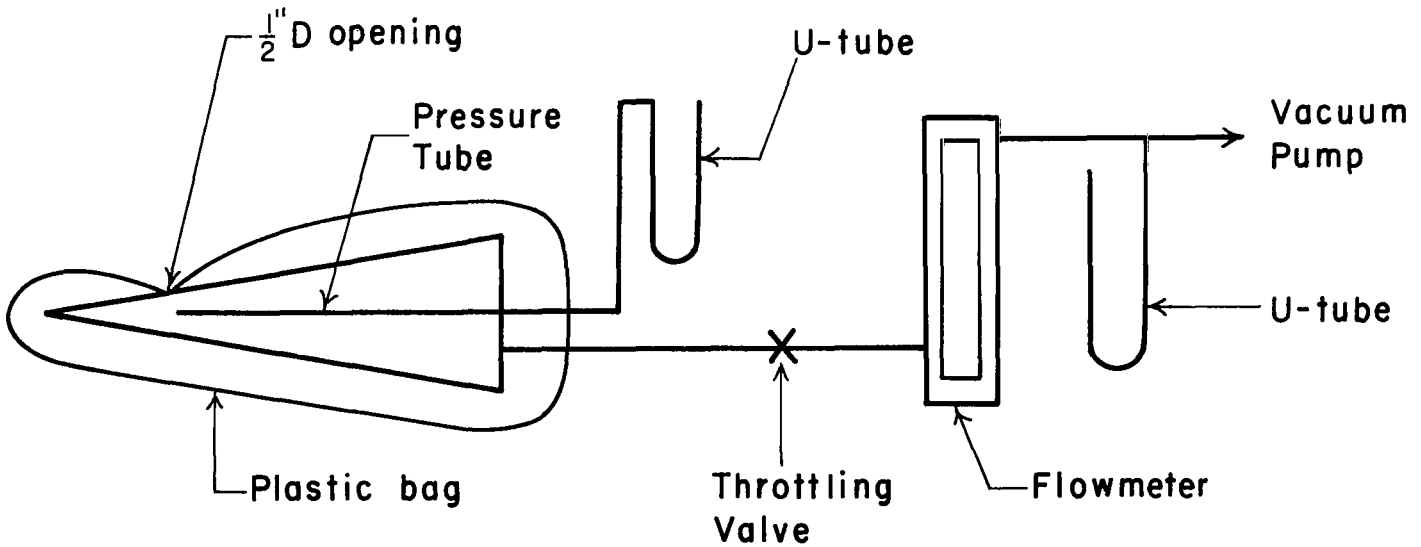

Figure 3.- Test technique for porosity measurements.

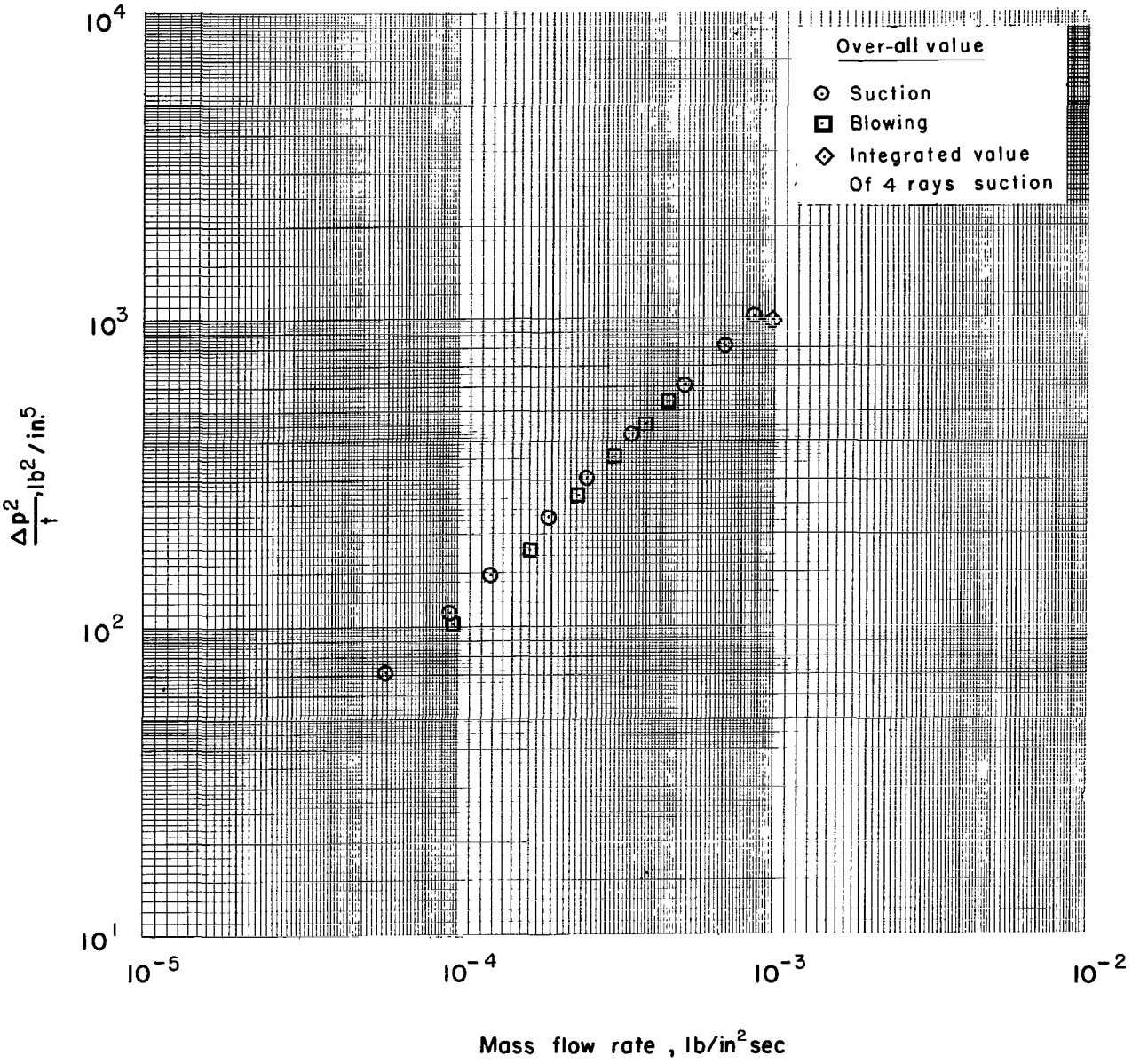

Figure 4.- Mass flow rate characteristics of porous cone model.

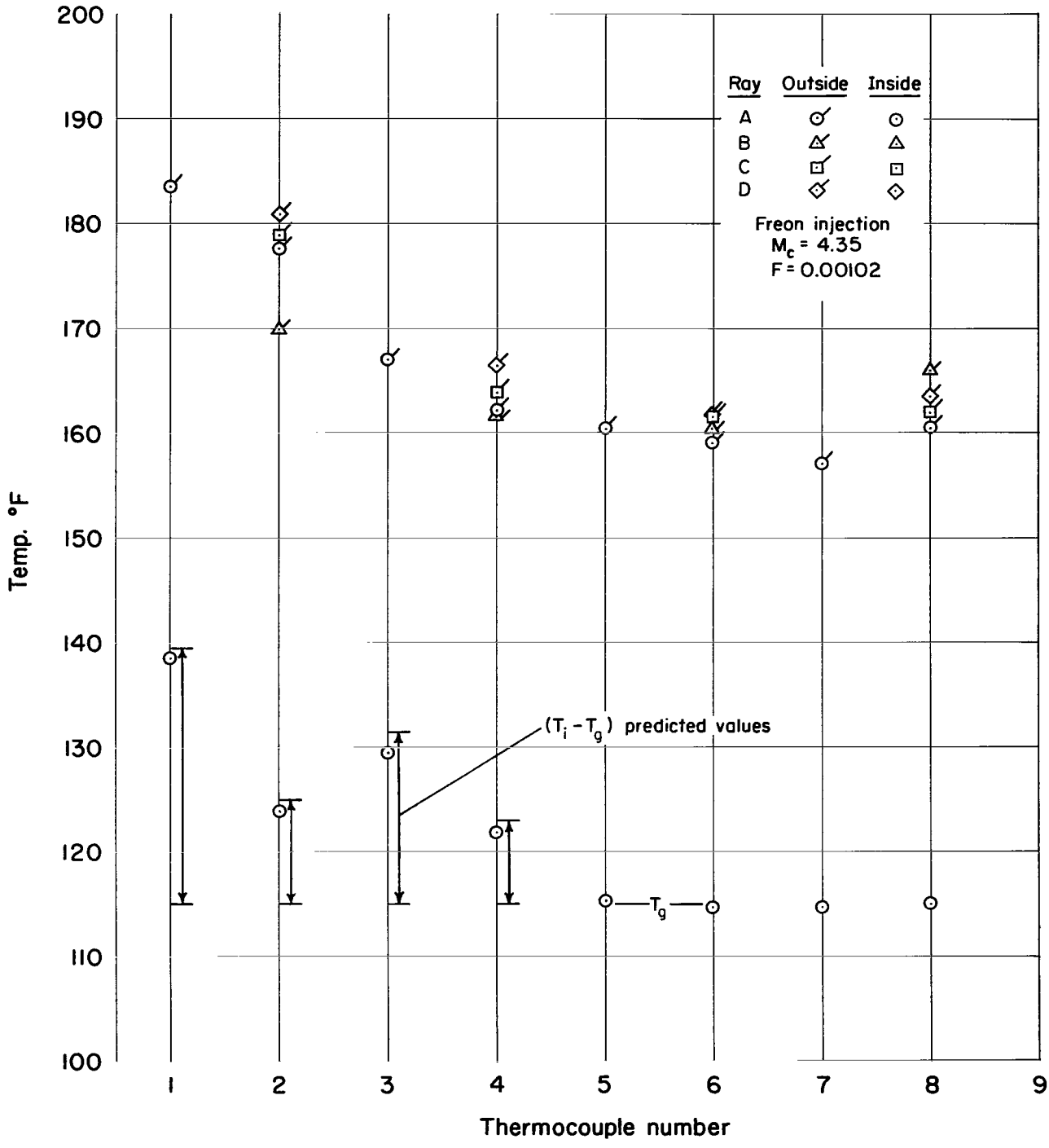

Figure 5.- Cone and internal gas temperatures.

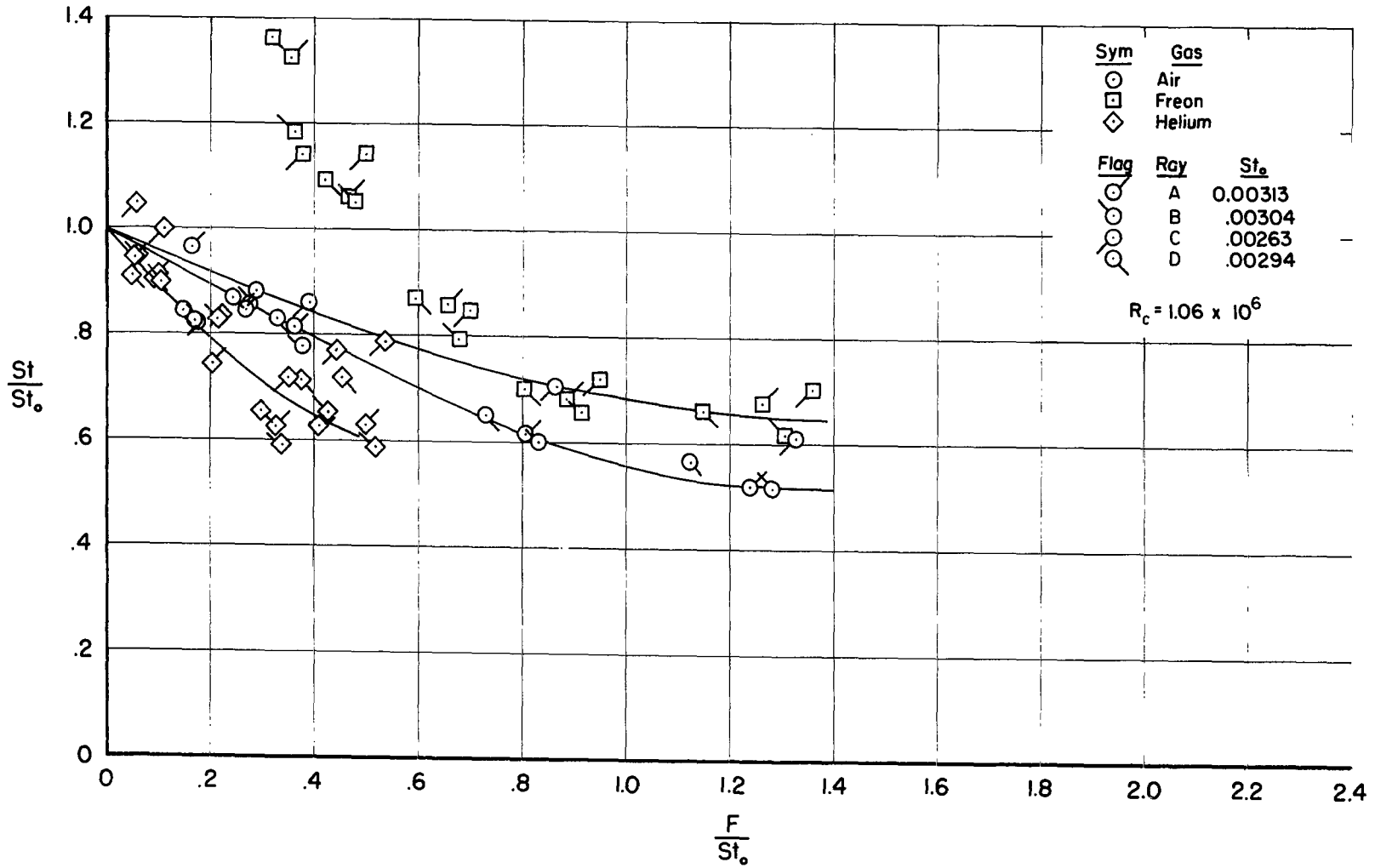

(a) Thermocouple no. 2.

Figure 6.- Effect of gas injection on the Stanton number, $M_c = 0.7$.

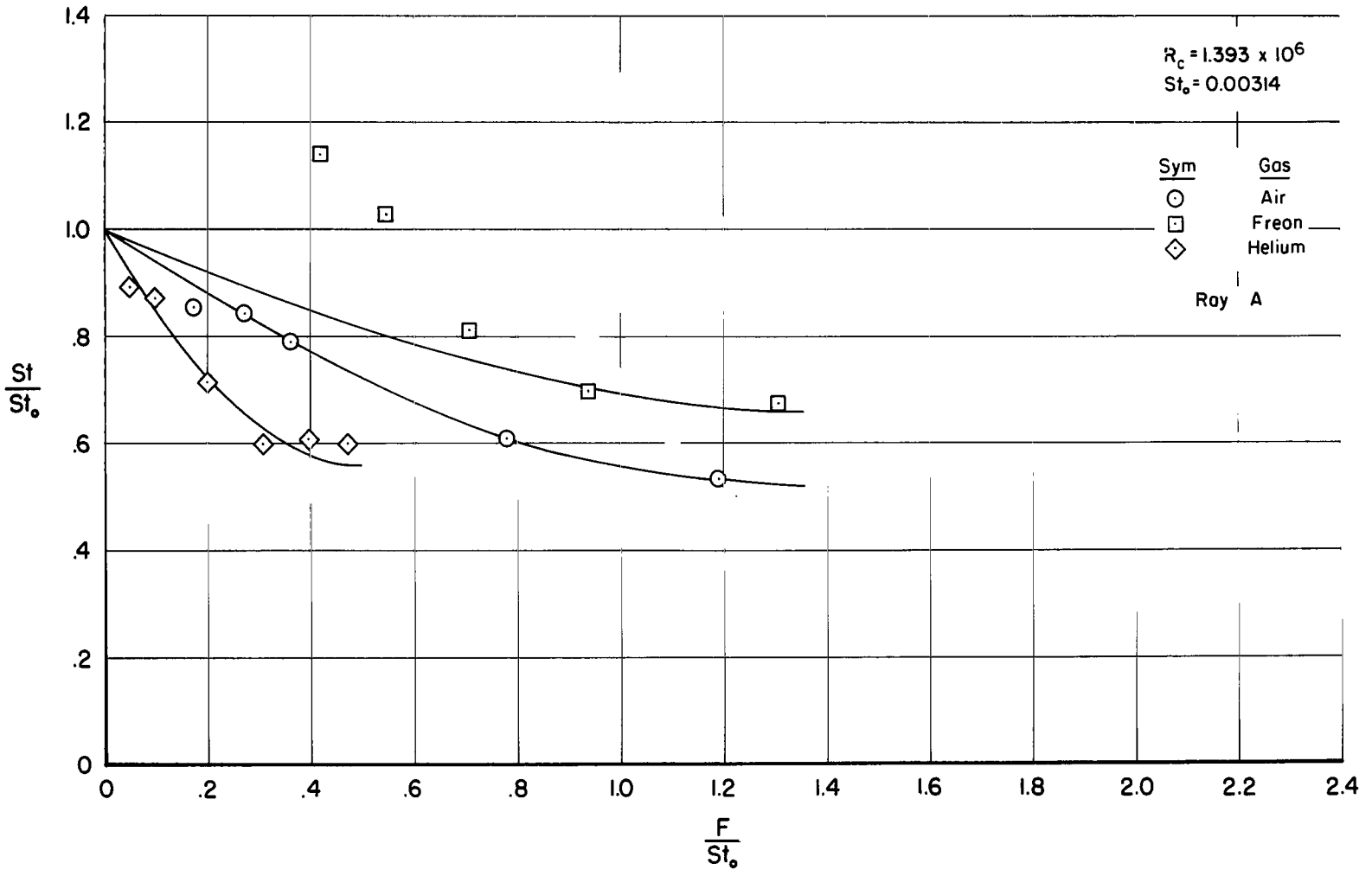

(b) Thermocouple no. 3.

Figure 6.- Continued.

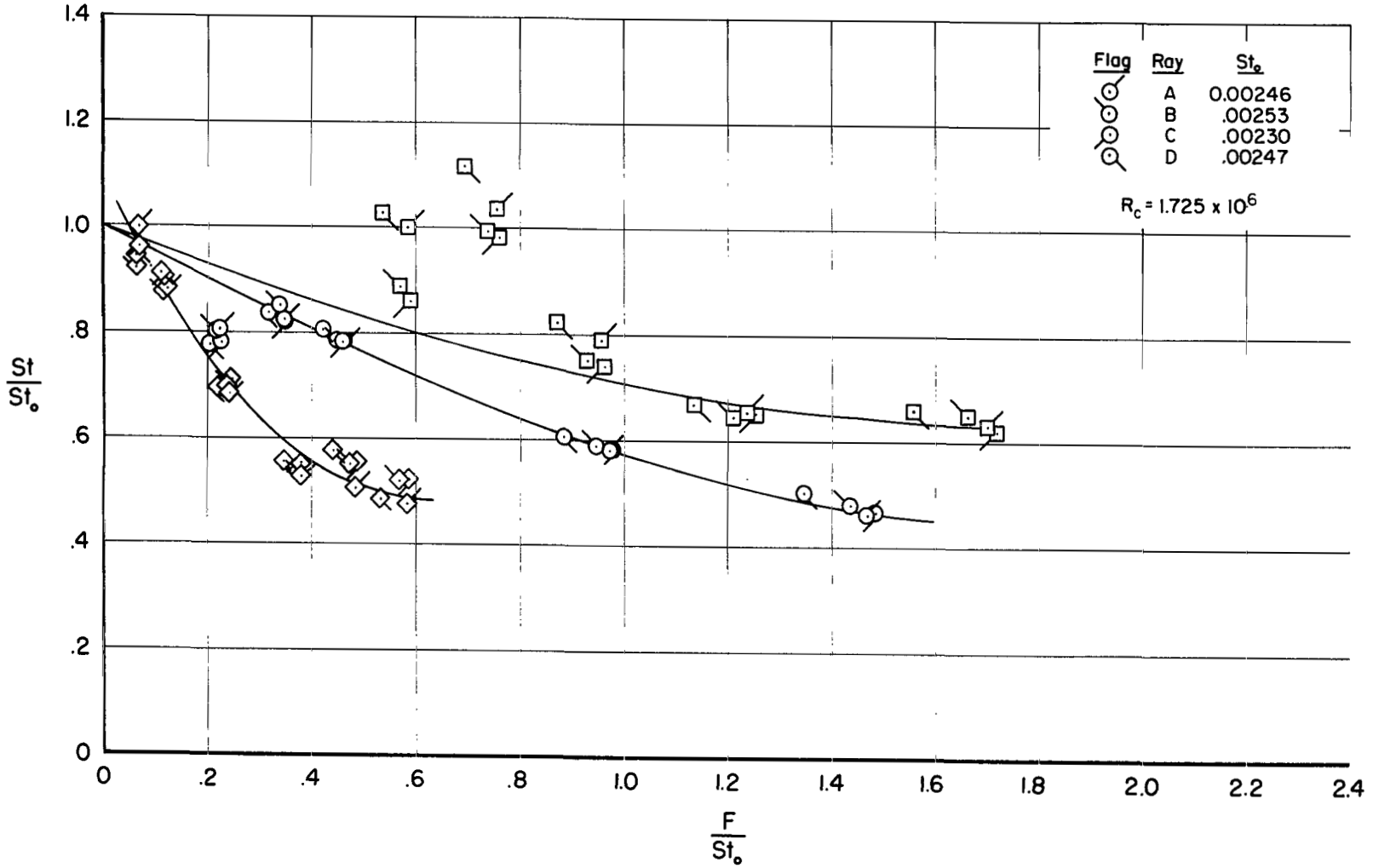

(c) Thermocouple no. 4.

Figure 6.- Continued.

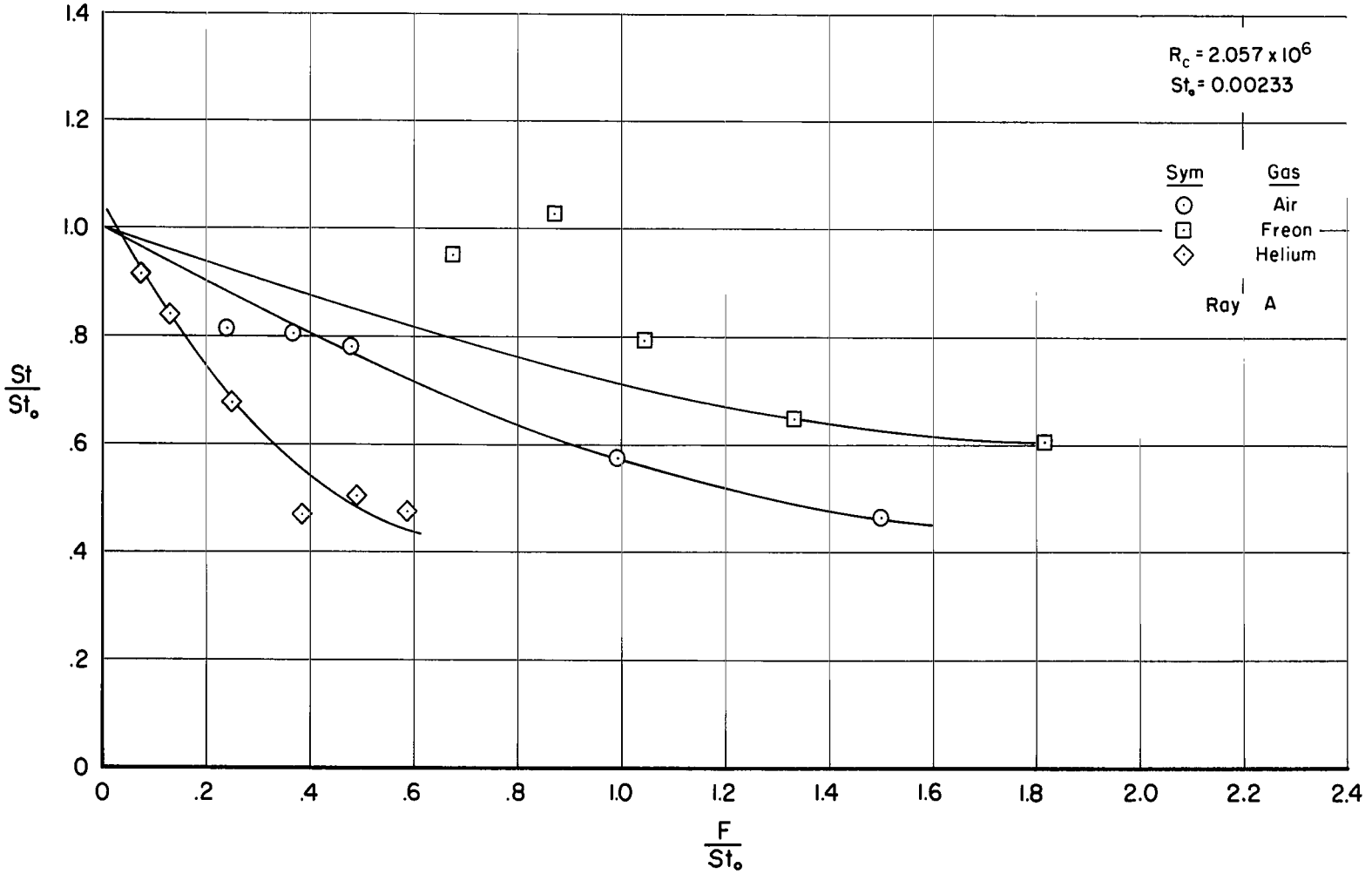

(d) Thermocouple no. 5.

Figure 6.- Continued.

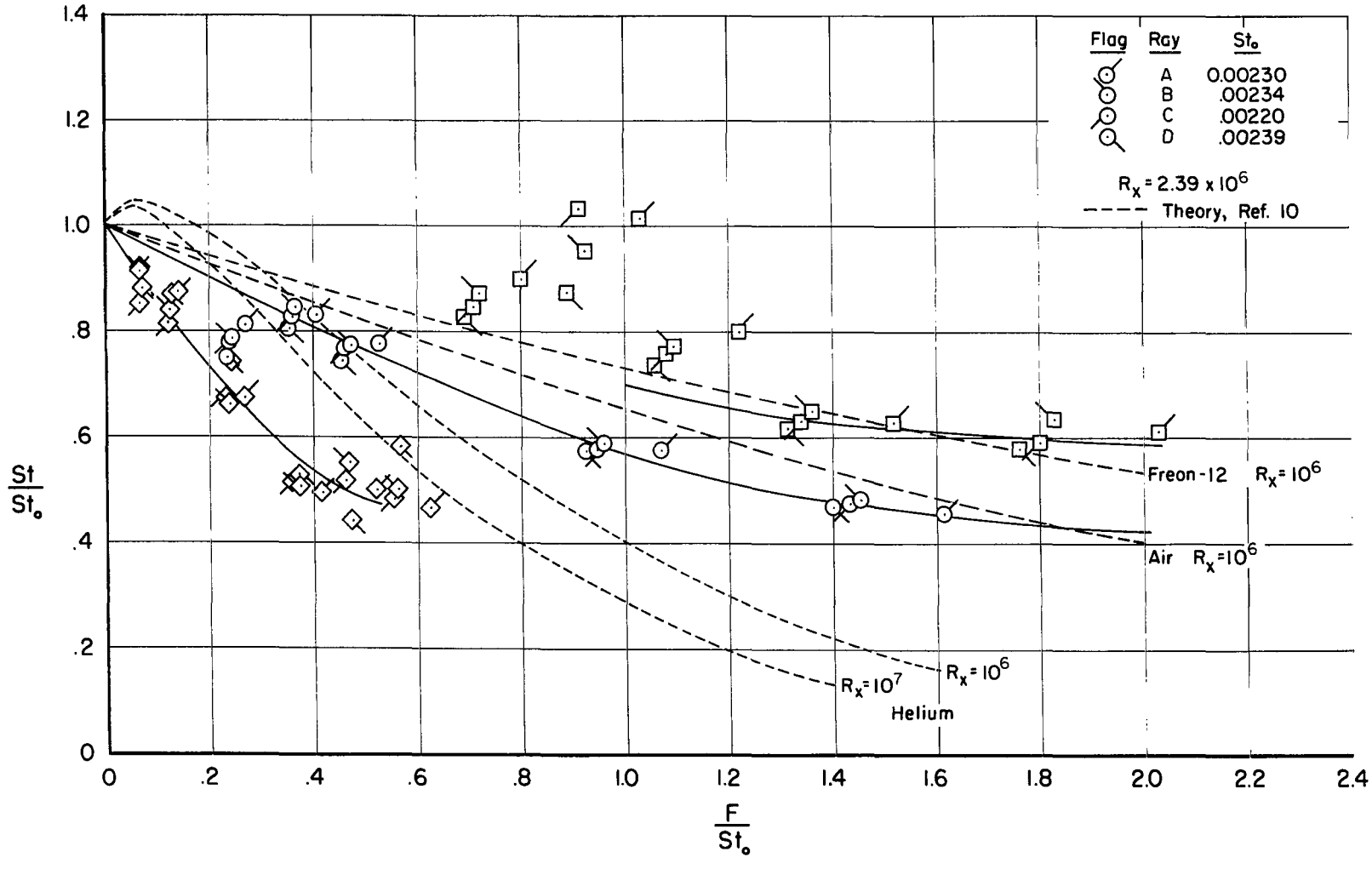

(e) Thermocouple no. 6.

Figure 6.- Continued.

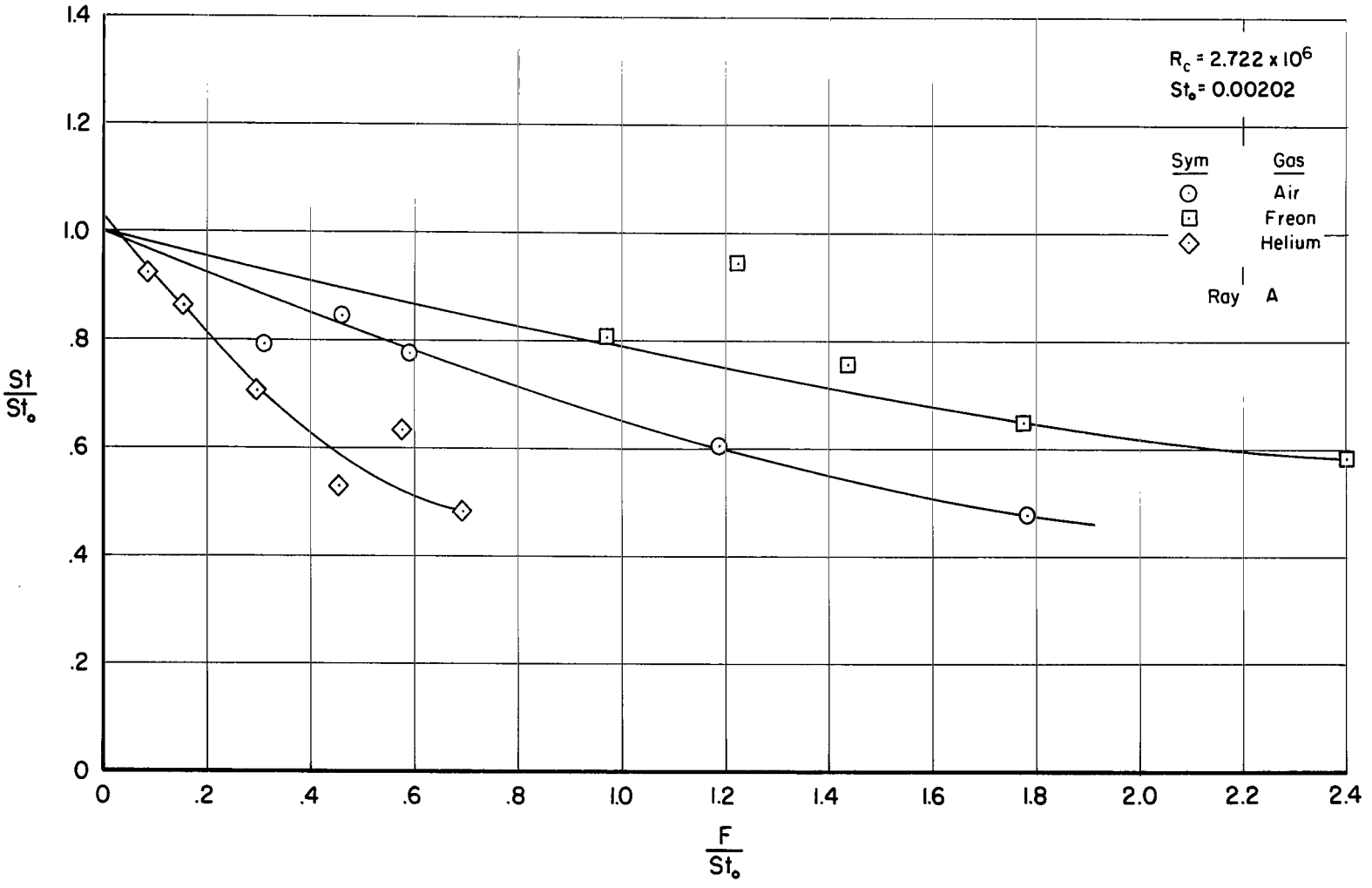

(f) Thermocouple no. 7.

Figure 6.- Concluded.

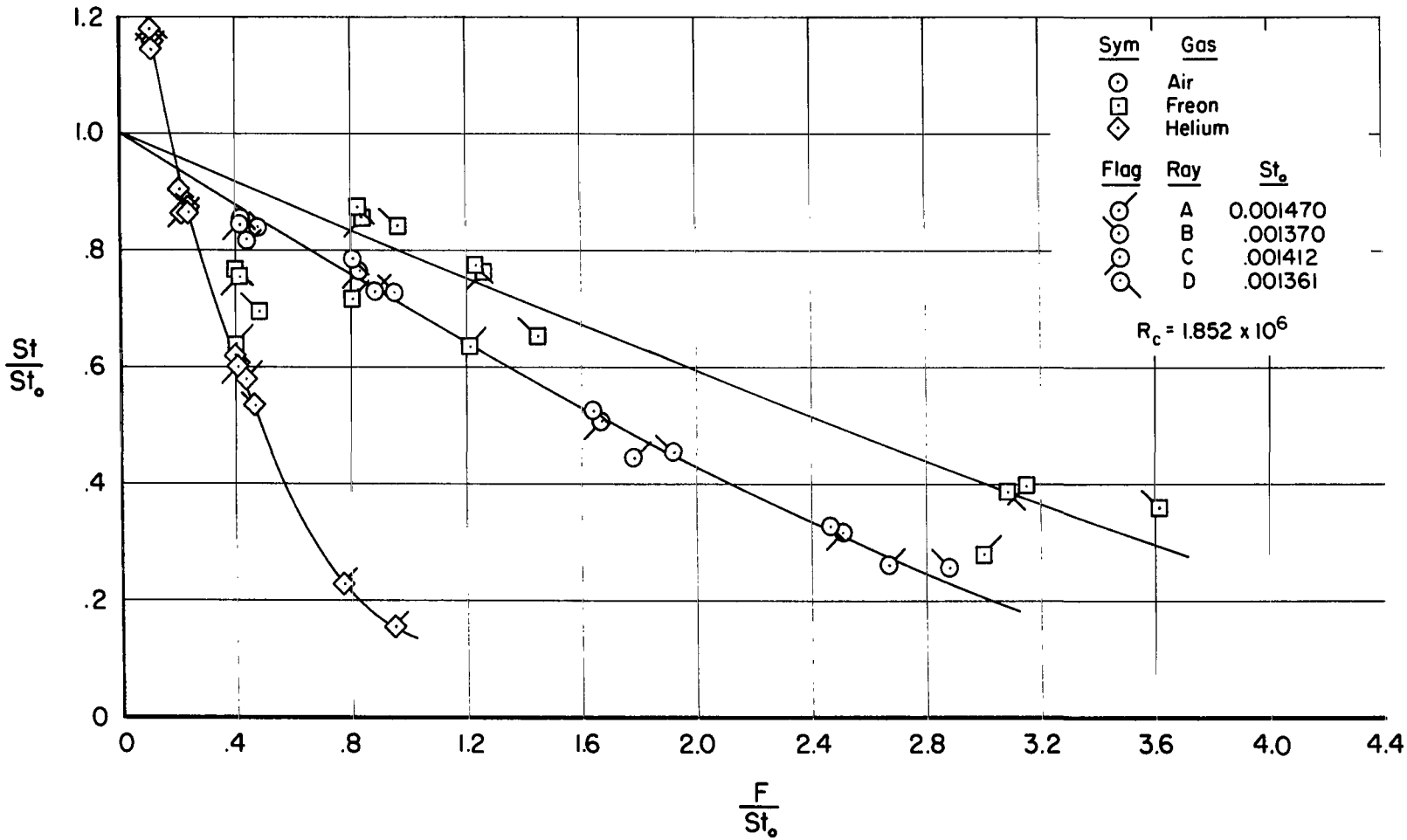

(a) Thermocouple no. 2.

Figure 7.- Effect of gas injection on the Stanton number, M_c = 3.67.

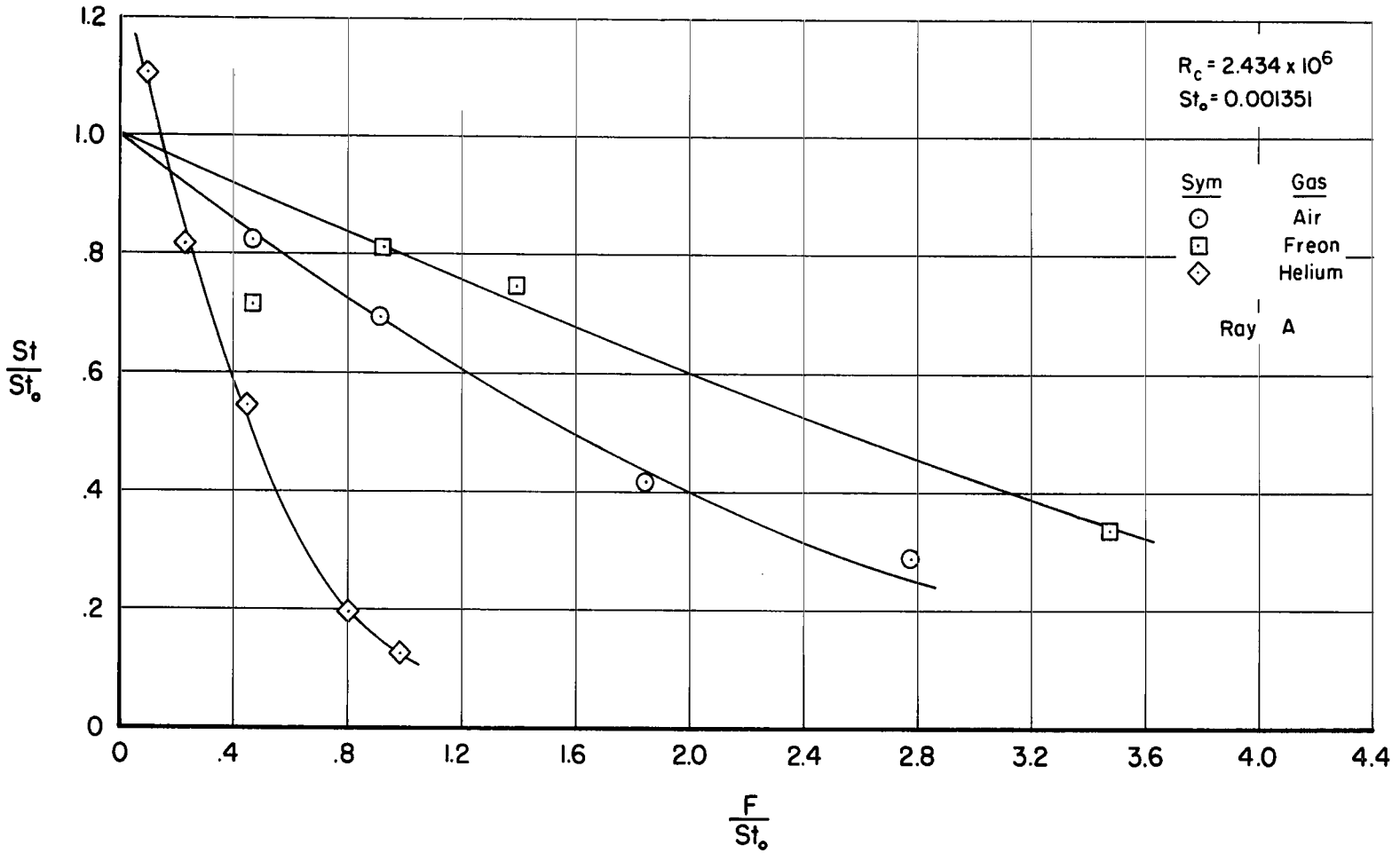

(b) Thermocouple no. 3.

Figure 7.- Continued.

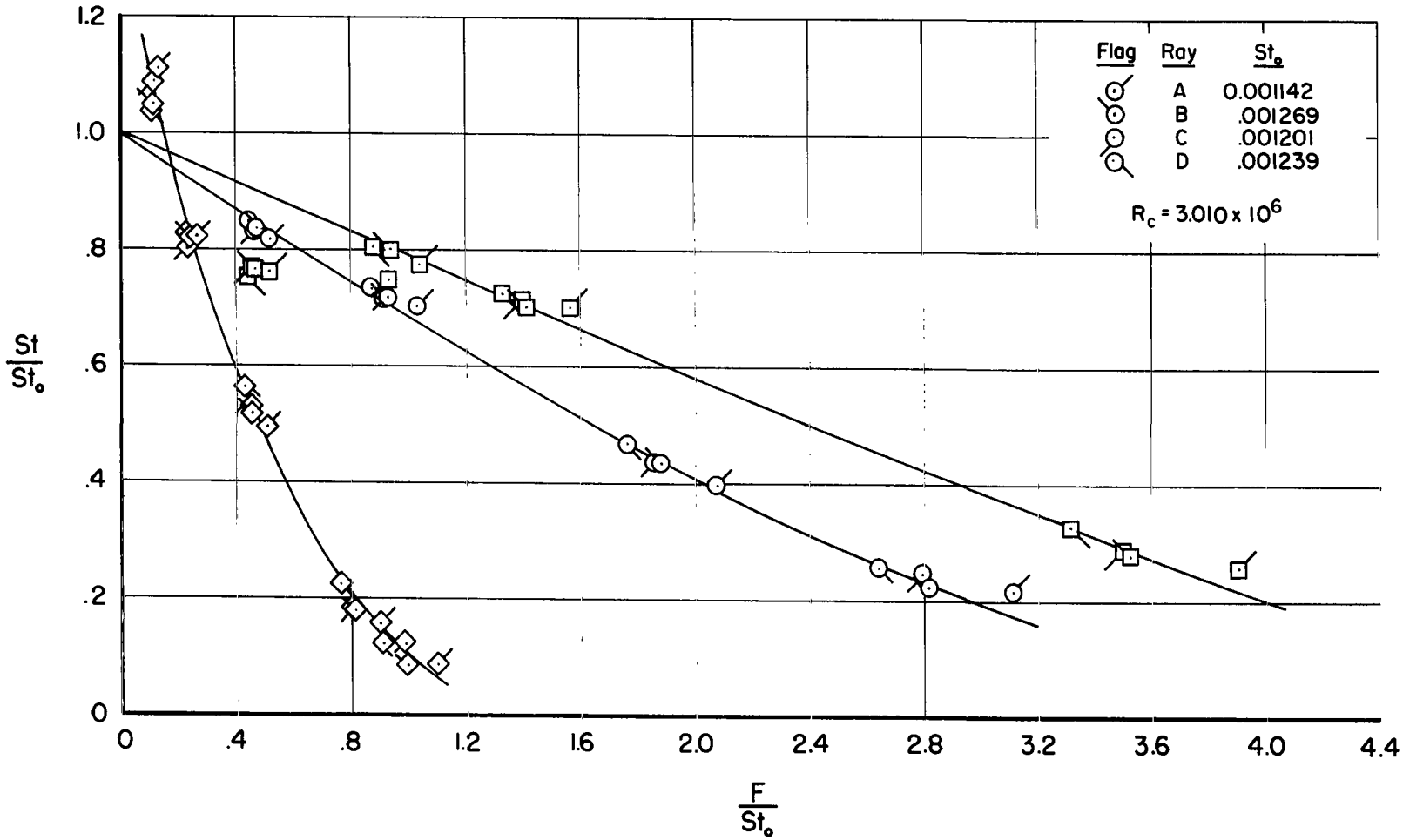

(c) Thermocouple no. 4.

Figure 7.- Continued.

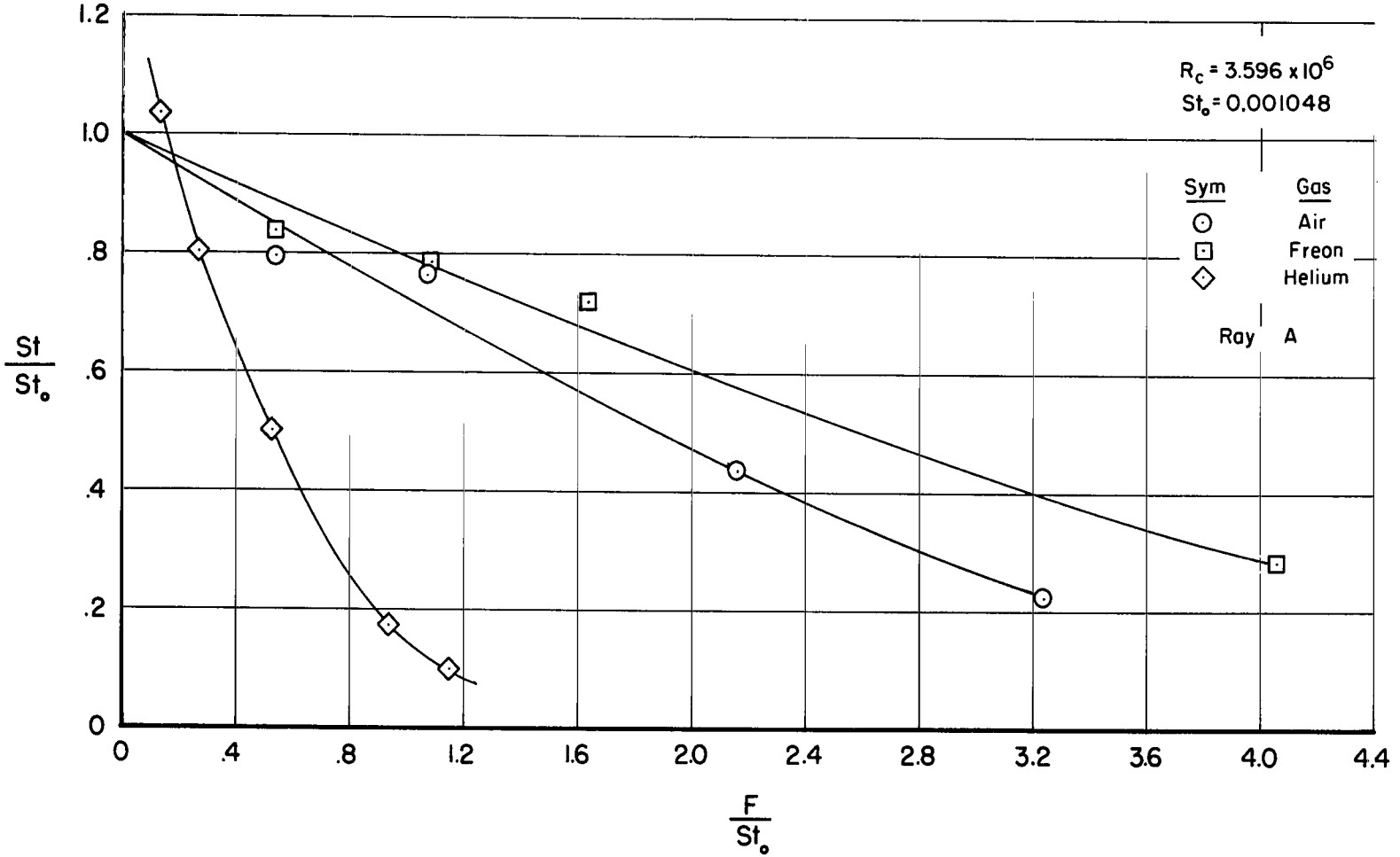

(d) Thermocouple no. 5.

Figure 7.- Continued.

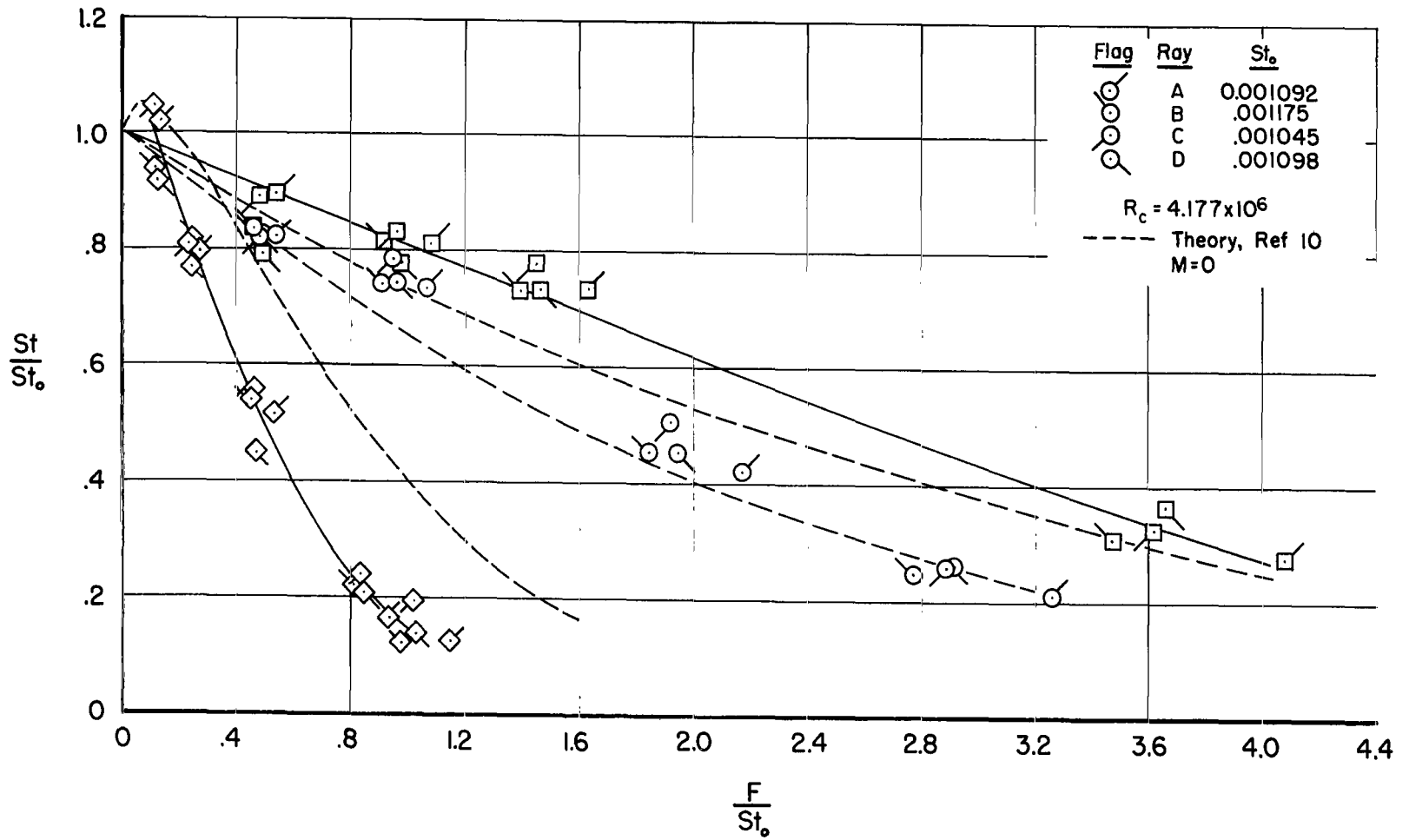

(e) Thermocouple no. 6.

Figure 7.- Continued.

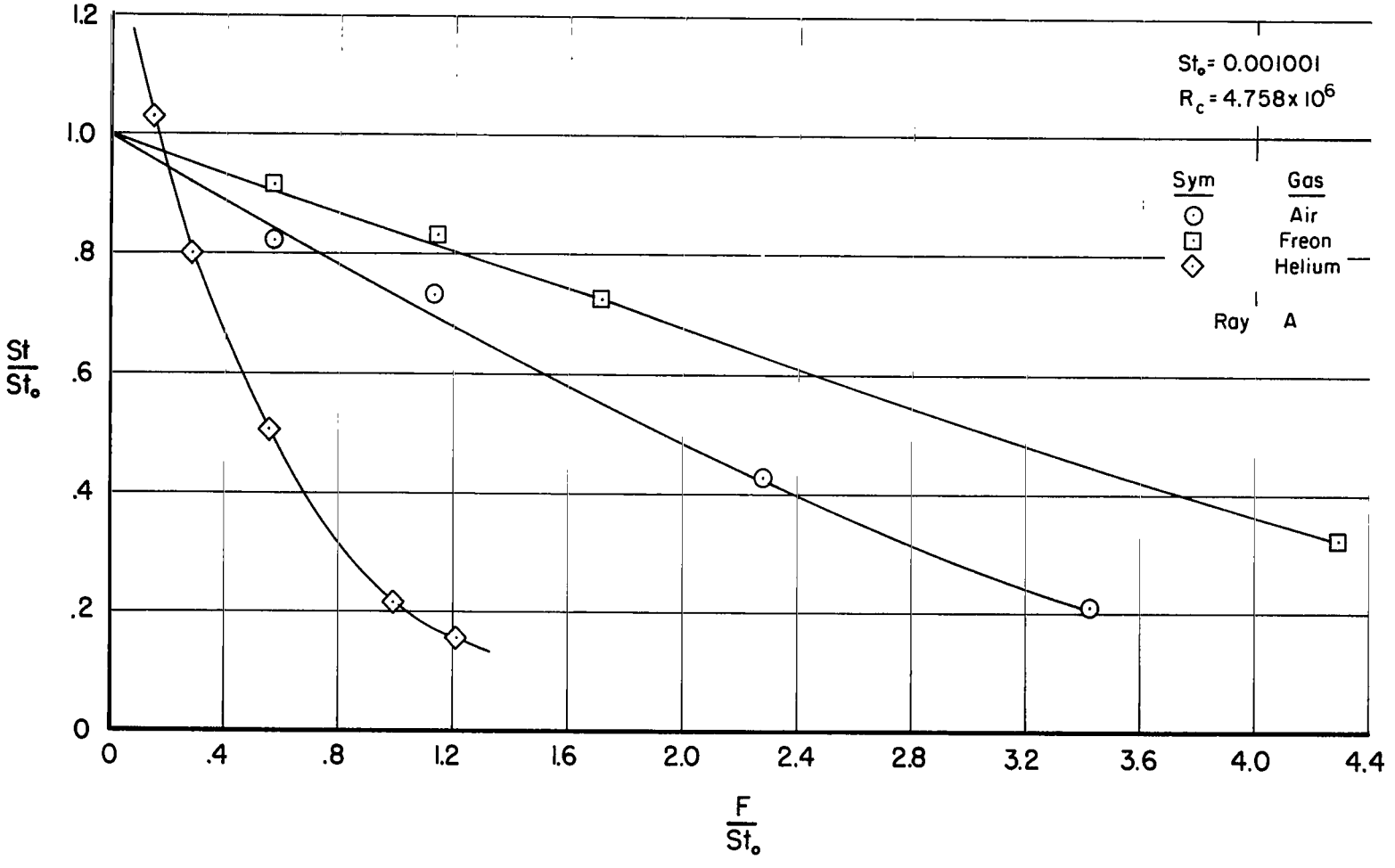

(f) Thermocouple no. 7.

Figure 7.- Concluded.

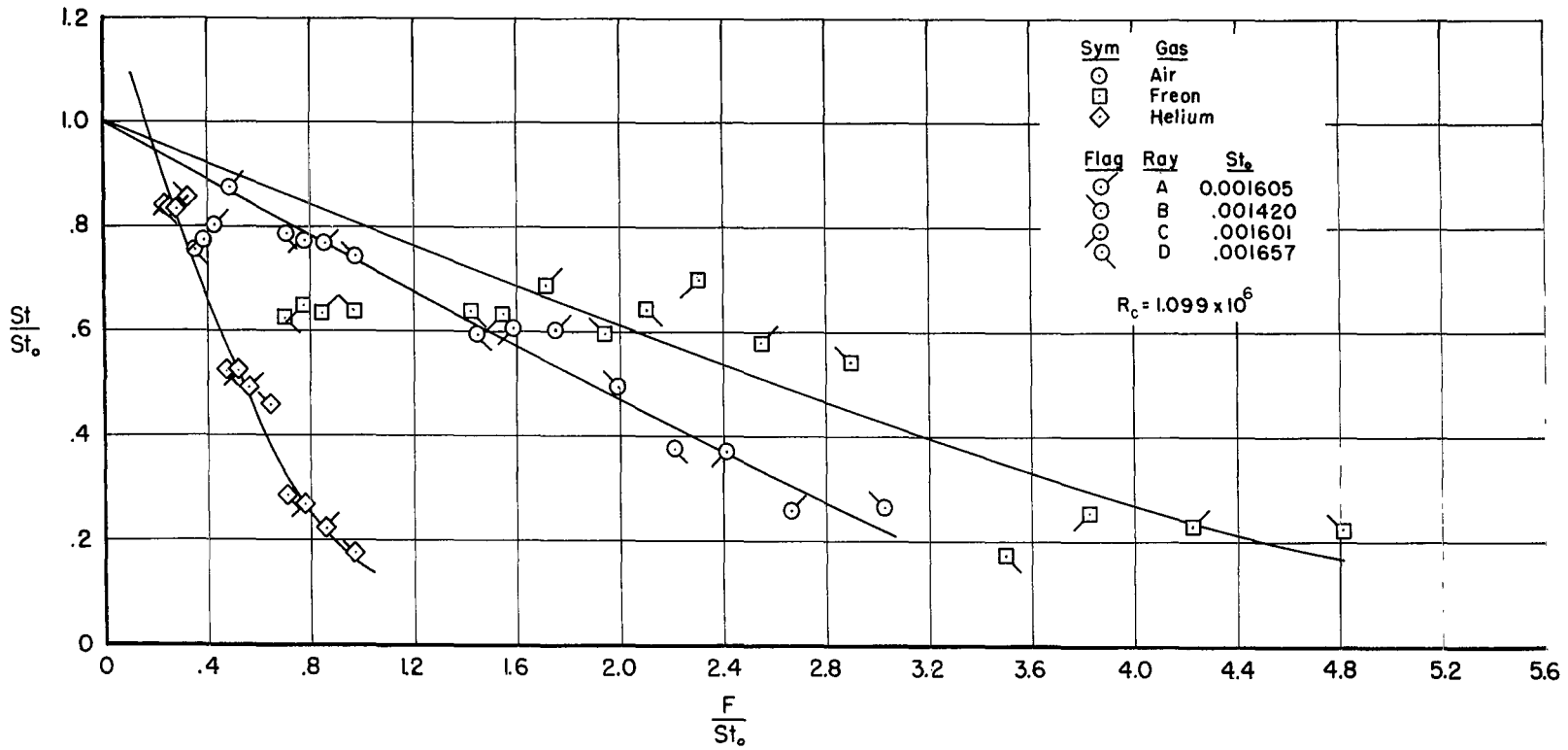

(a) Thermocouple no. 2.

Figure 8.- Effect of gas injection on the Stanton number, $M_c = 4.35$.

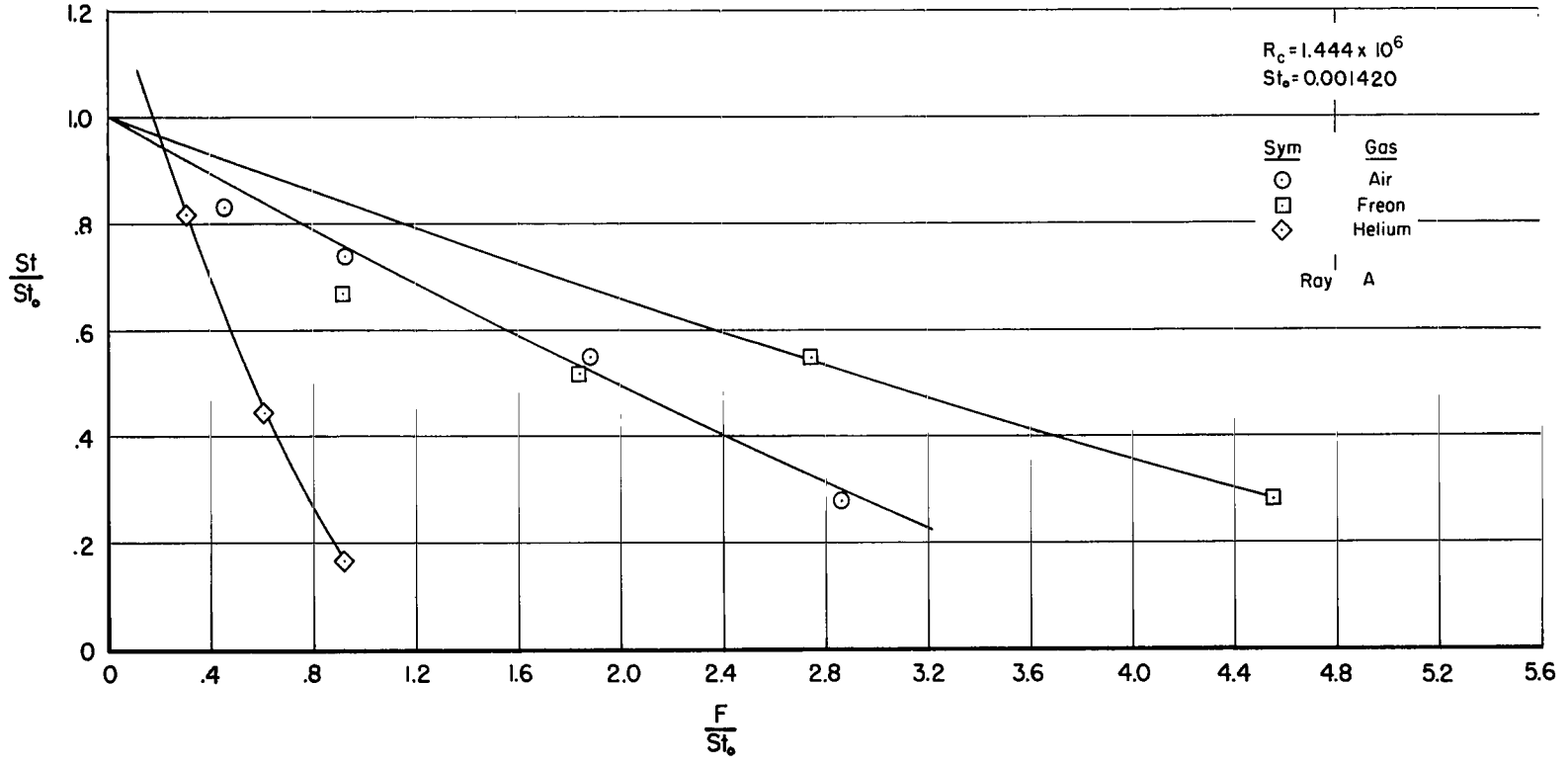

(b) Thermocouple no. 3.

Figure 8.- Continued.

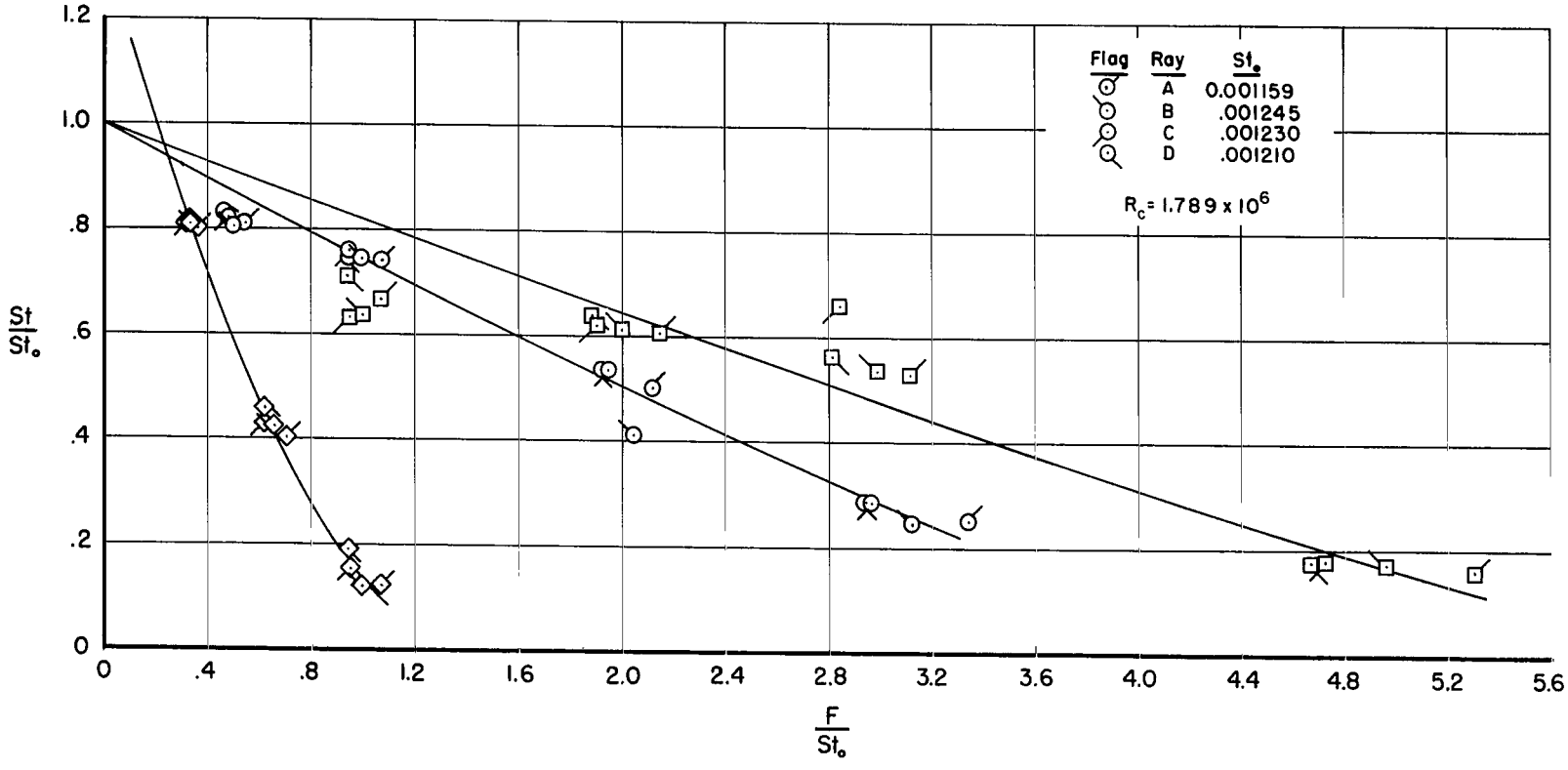

(c) Thermocouple no. 4.

Figure 8.- Continued.

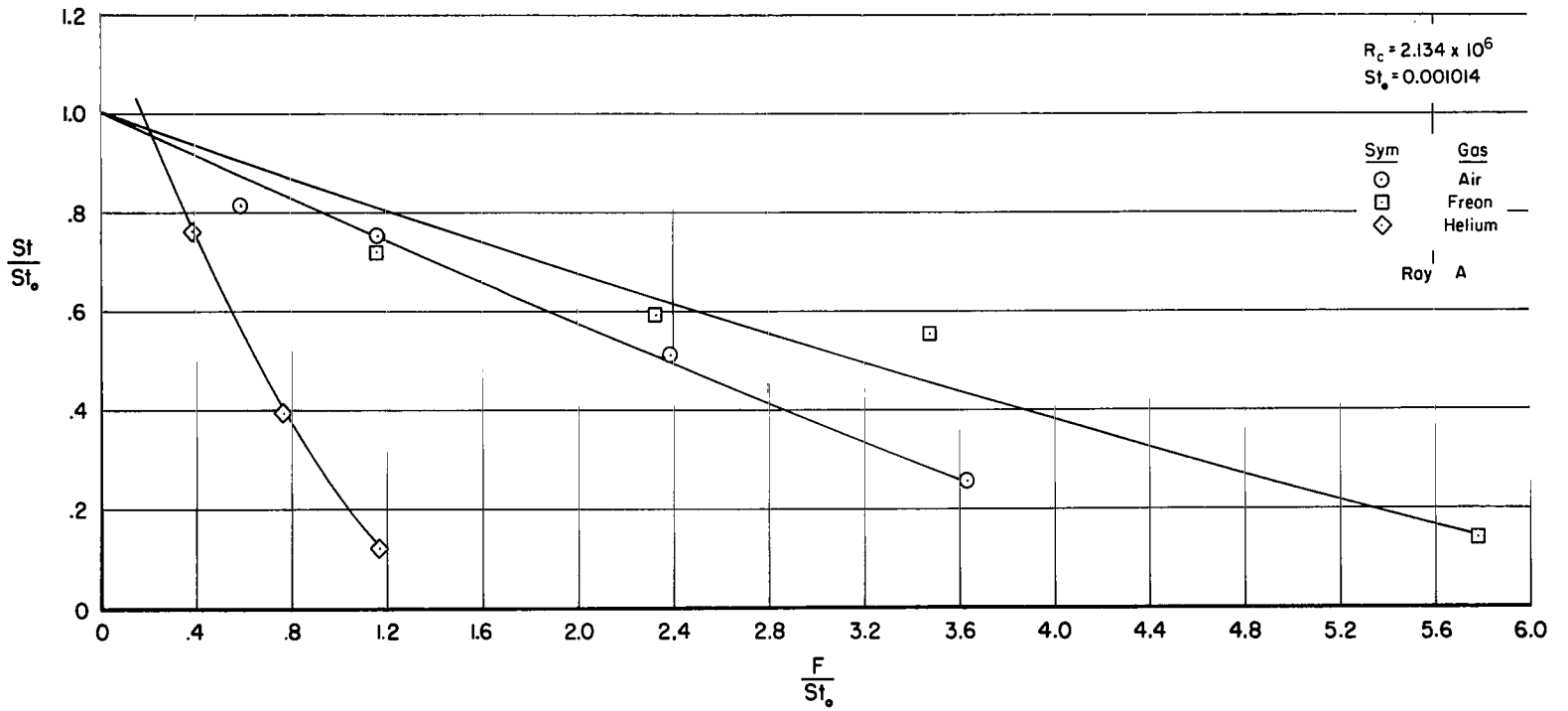

(d) Thermocouple no. 5.

Figure 8.- Continued.

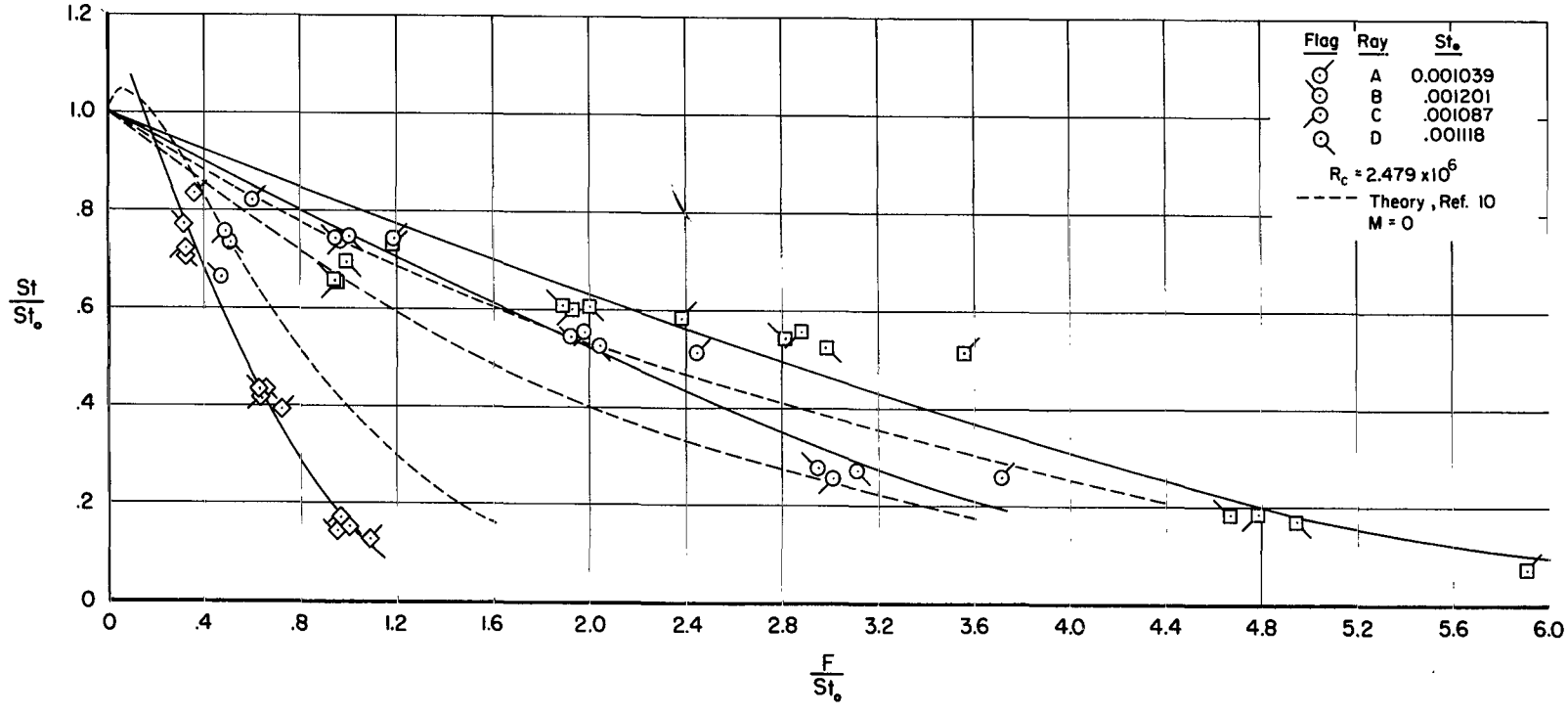

(e) Thermocouple no. 6.

Figure 8.- Continued.

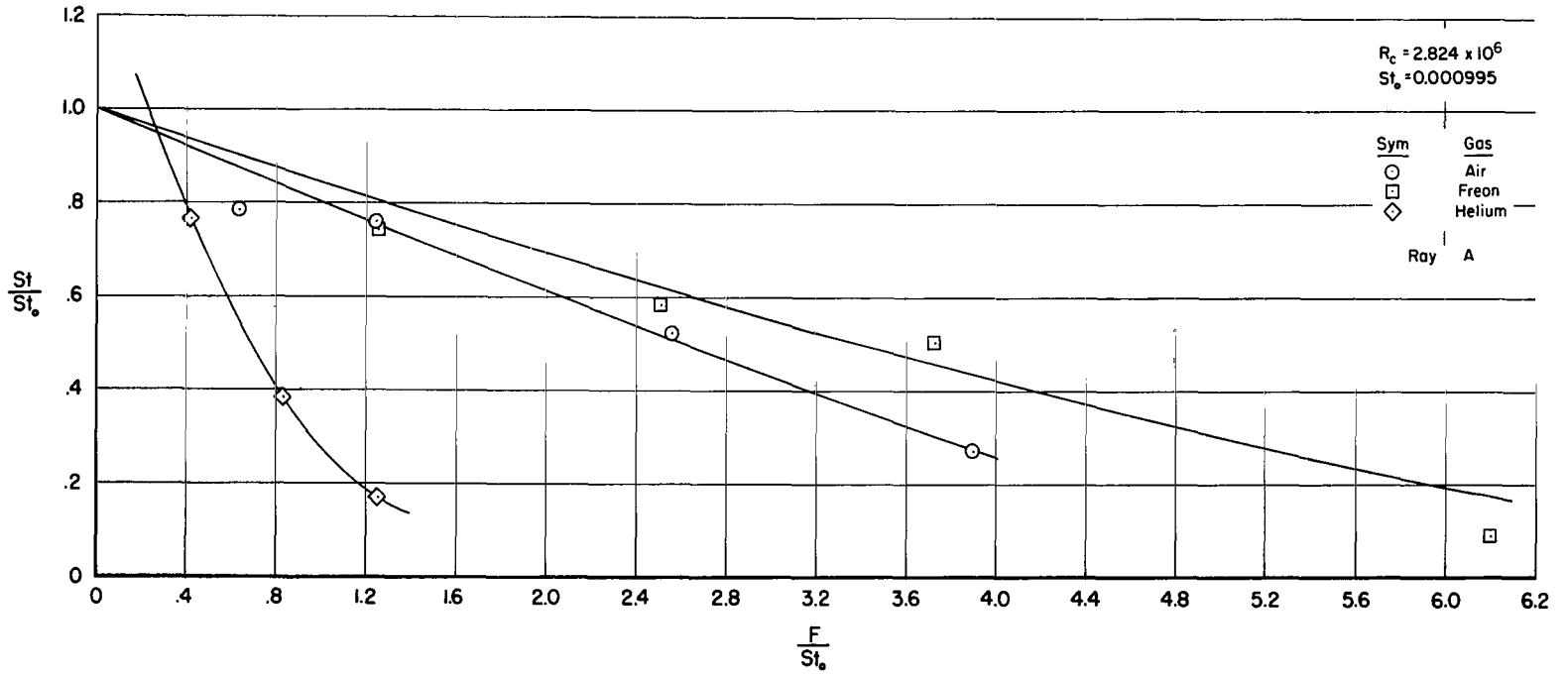

(f) Thermocouple no. 7.

Figure 8.- Concluded.

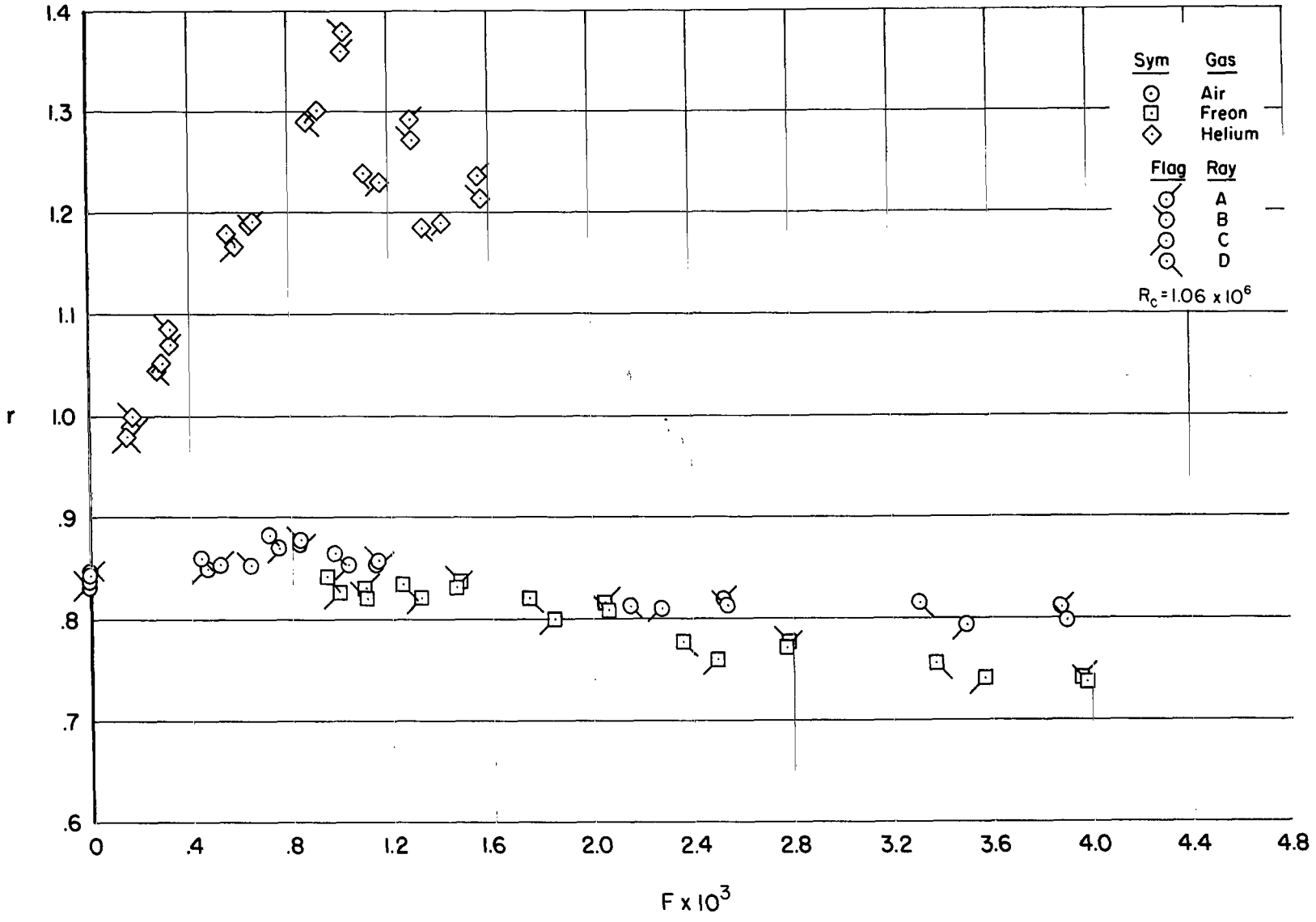

(a) Thermocouple no. 2.

Figure 9.- Recovery factor with gas injection, $M_c = 0.7$.

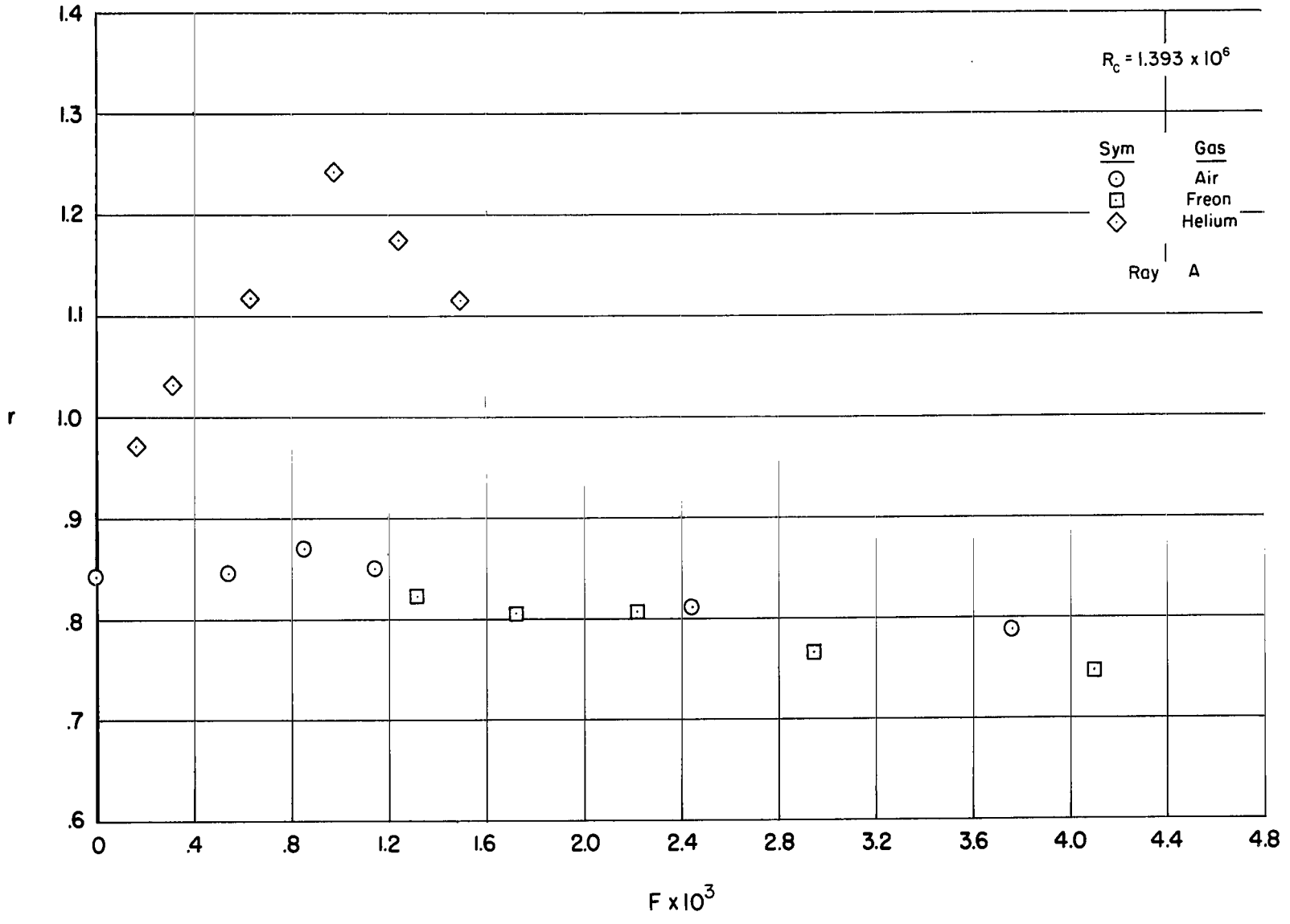

(b) Thermocouple no. 3.

Figure 9.- Continued.

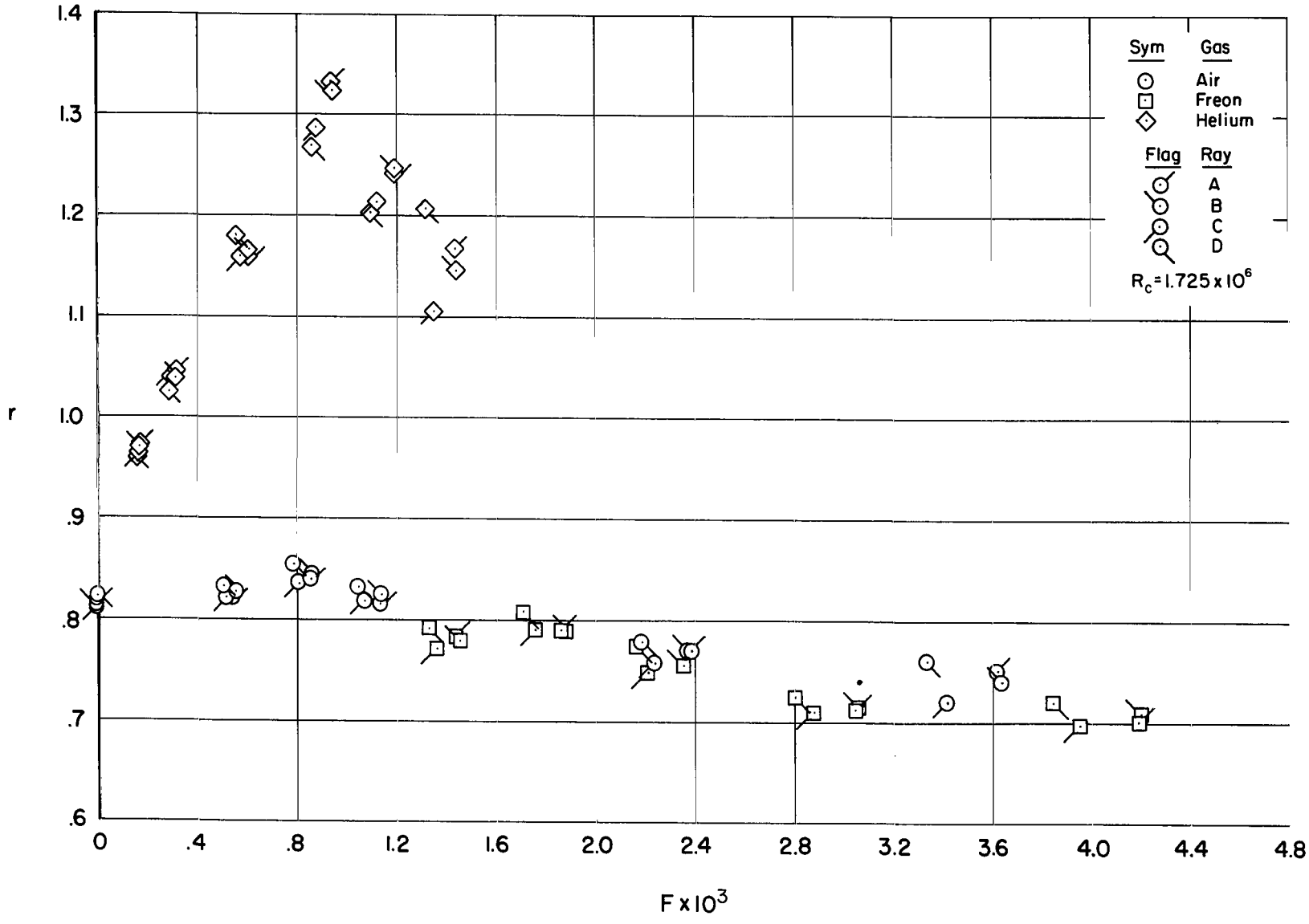

(c) Thermocouple no. 4.

Figure 9.- Continued.

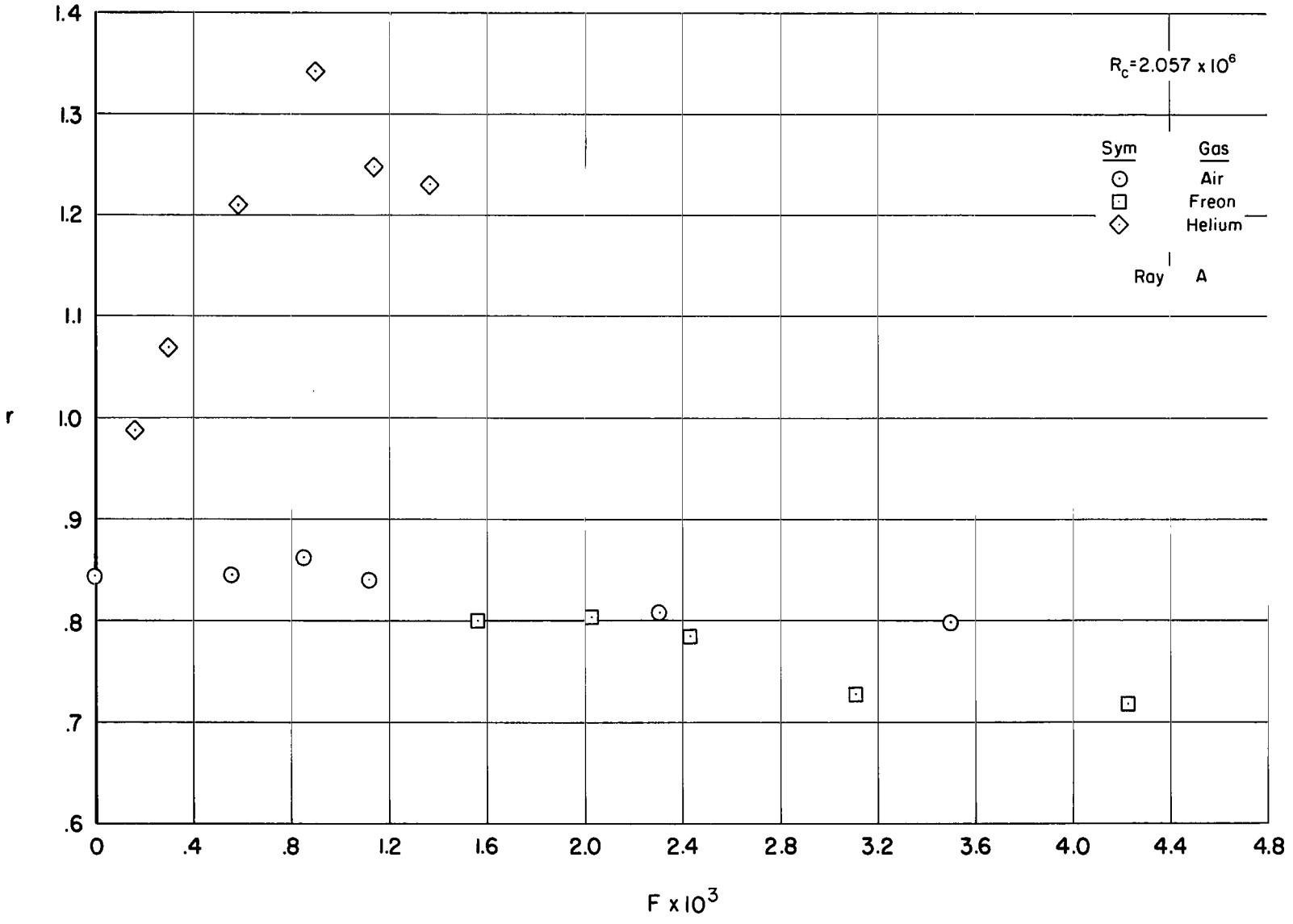

(d) Thermocouple no. 5.

Figure 9.- Continued.

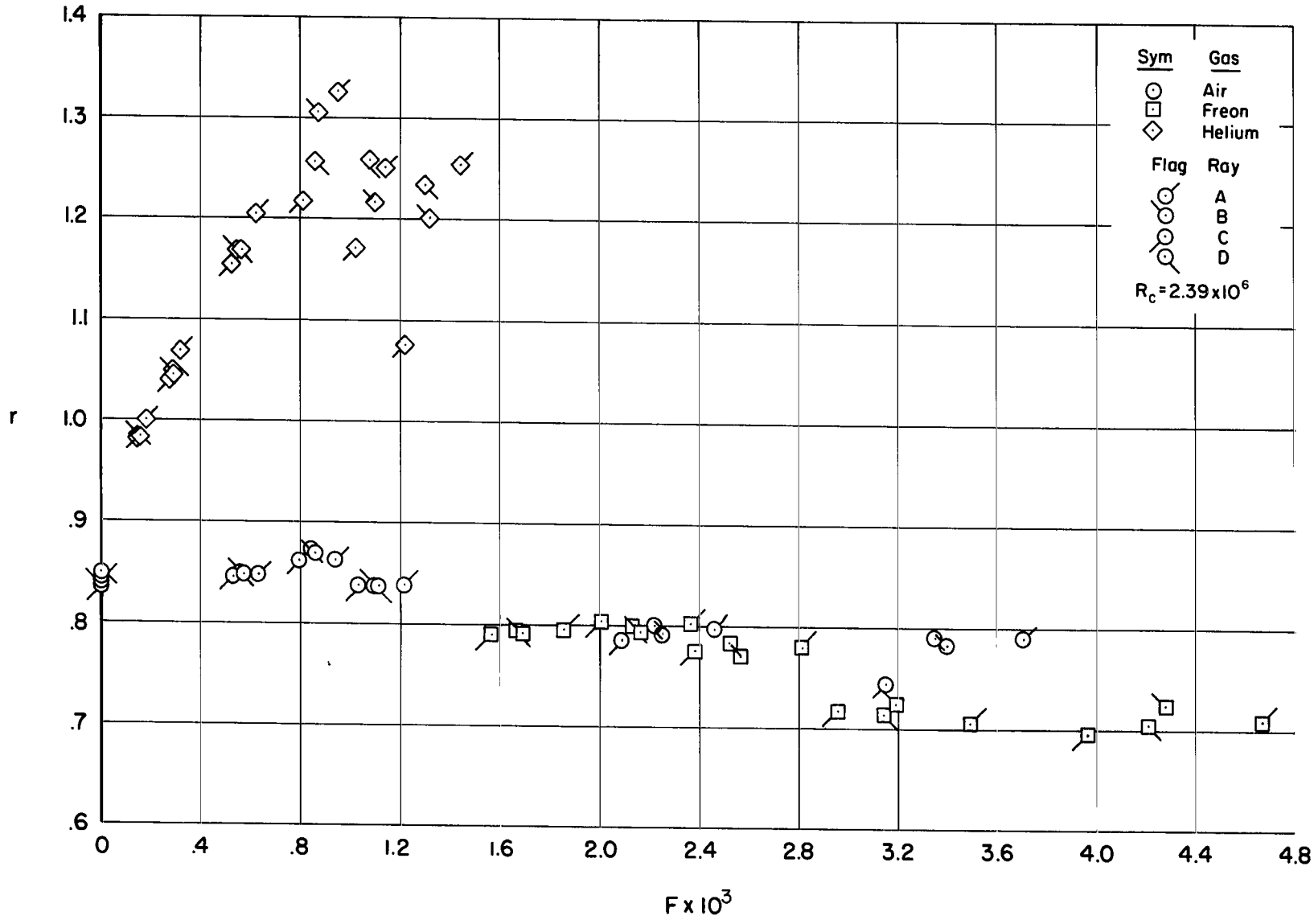

(e) Thermocouple no. 6.

Figure 9.- Continued.

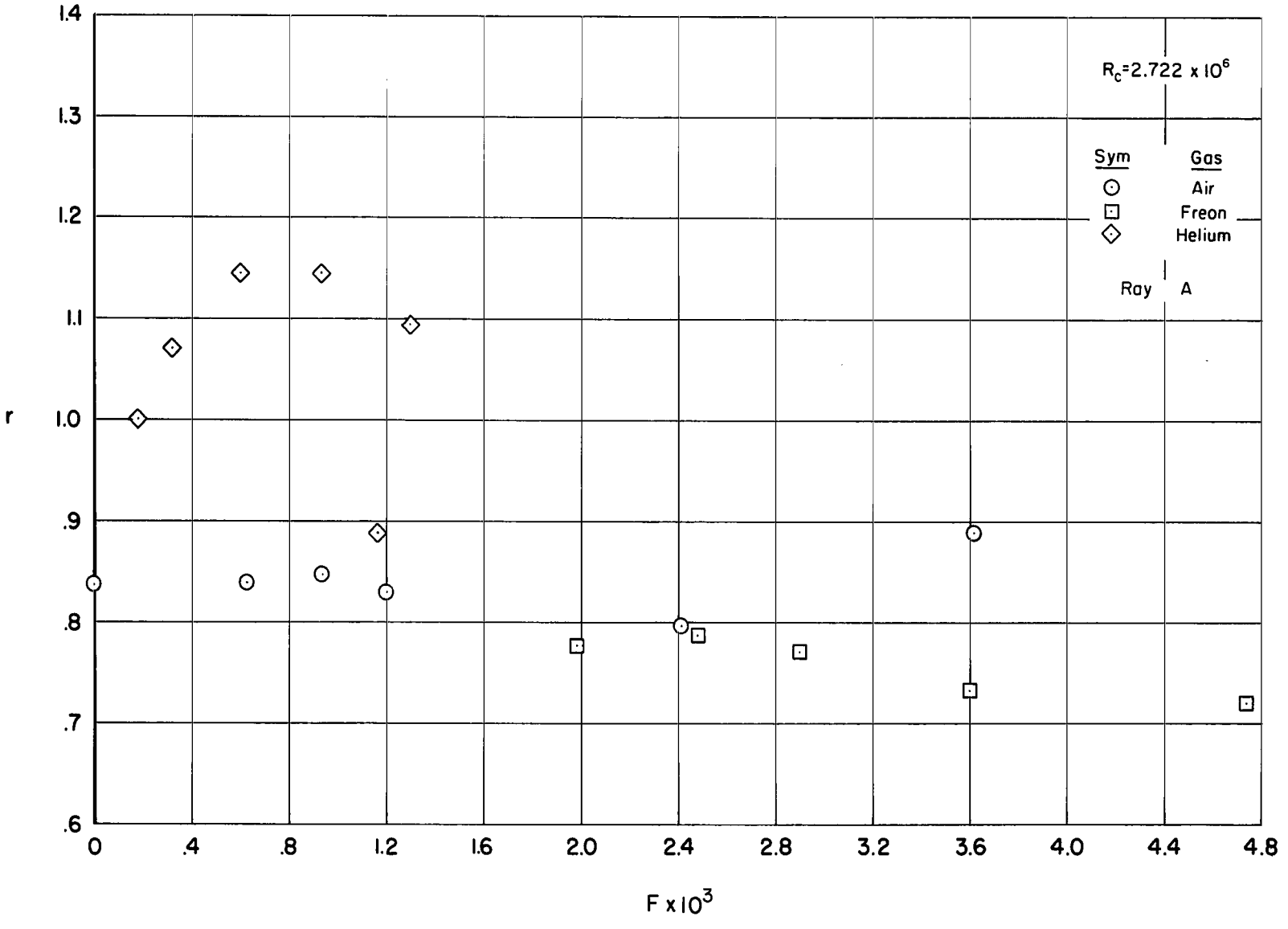

(f) Thermocouple no. 7.

Figure 9.- Concluded.

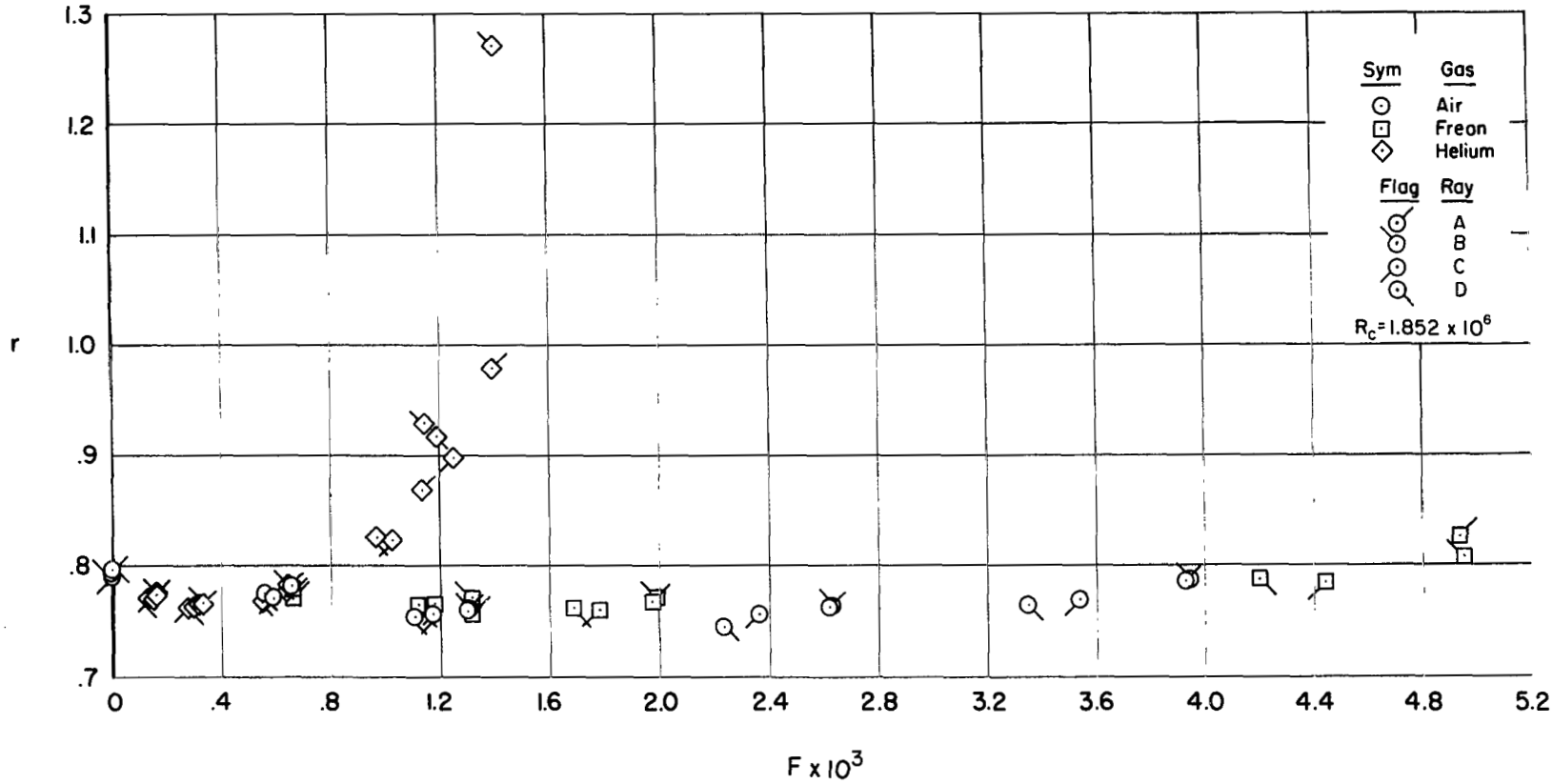

(a) Thermocouple no. 2.

Figure 10.- Recovery factor with gas injection, M_c = 3.67.

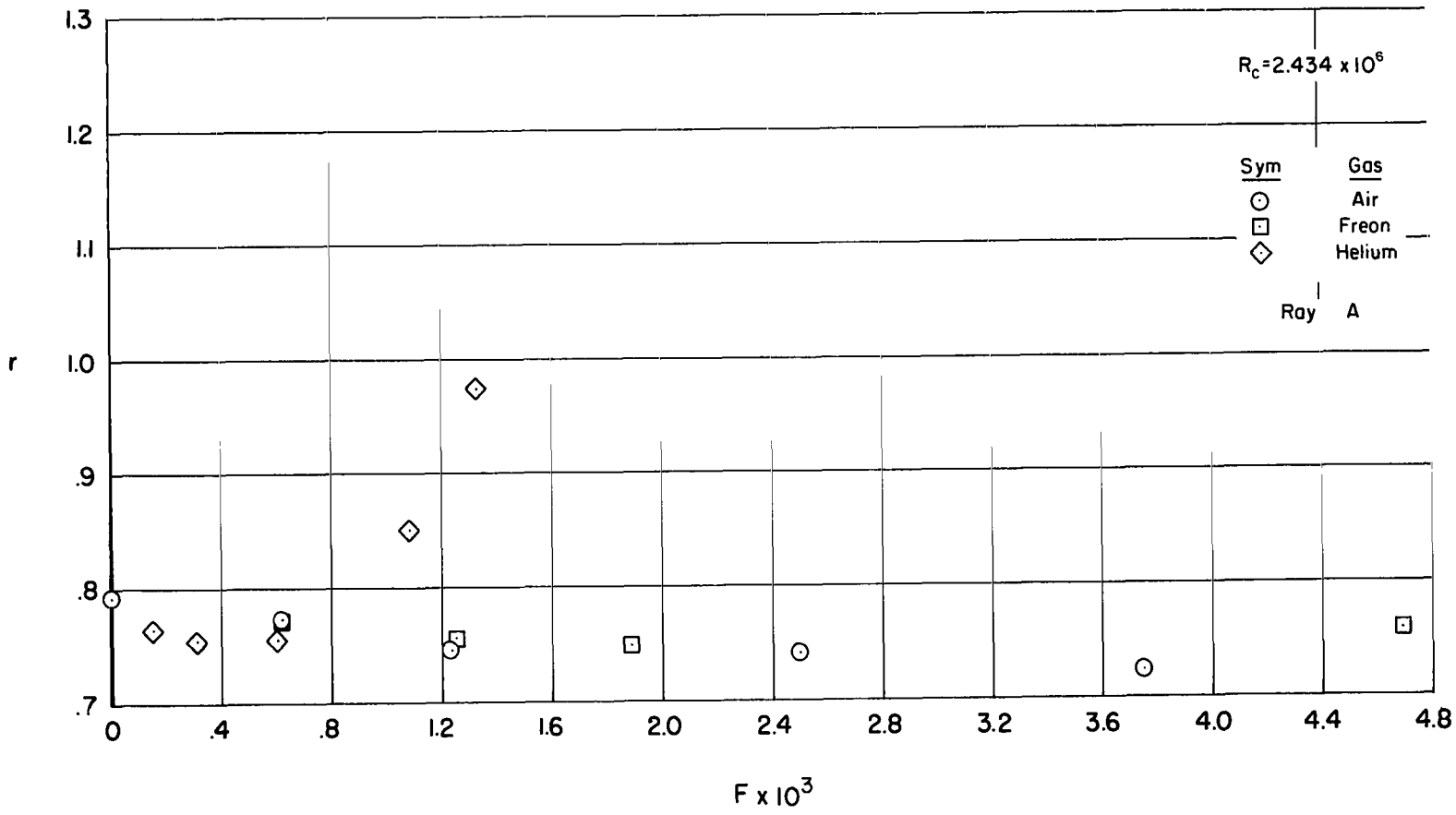

(b) Thermocouple no. 3.

Figure 10.- Continued.

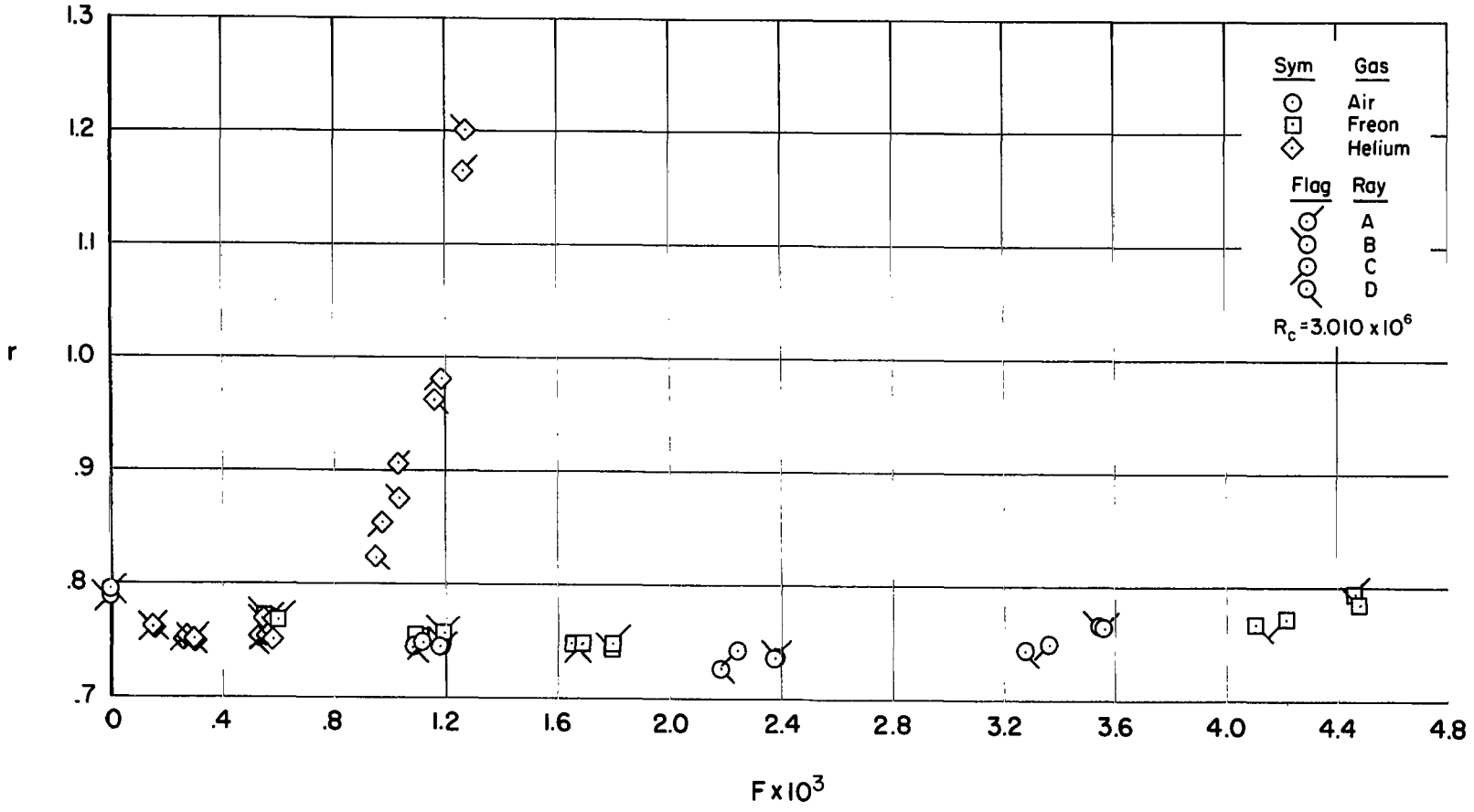

(c) Thermocouple no. 4.

Figure 10.- Continued.

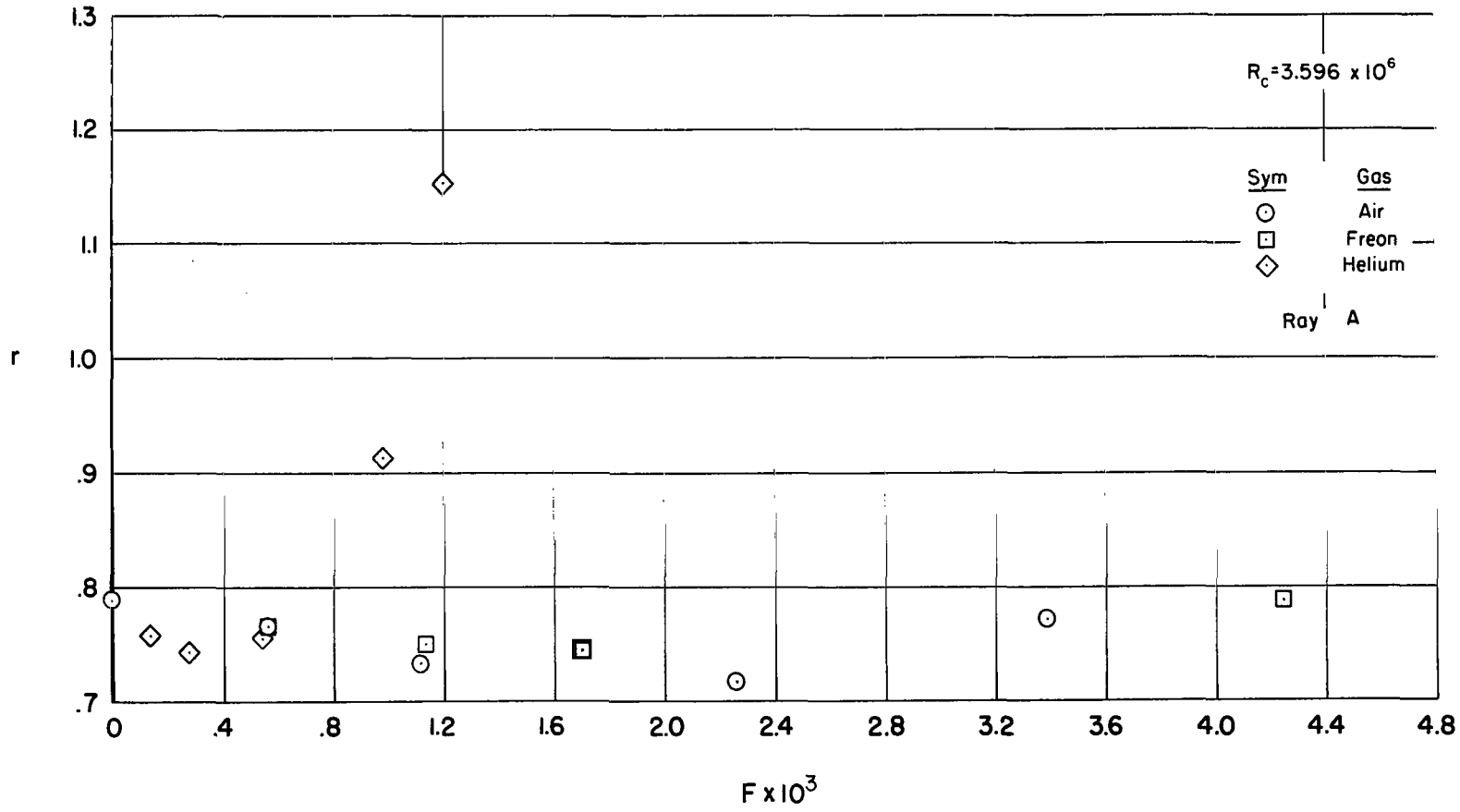

(d) Thermocouple no. 5.

Figure 10.- Continued.

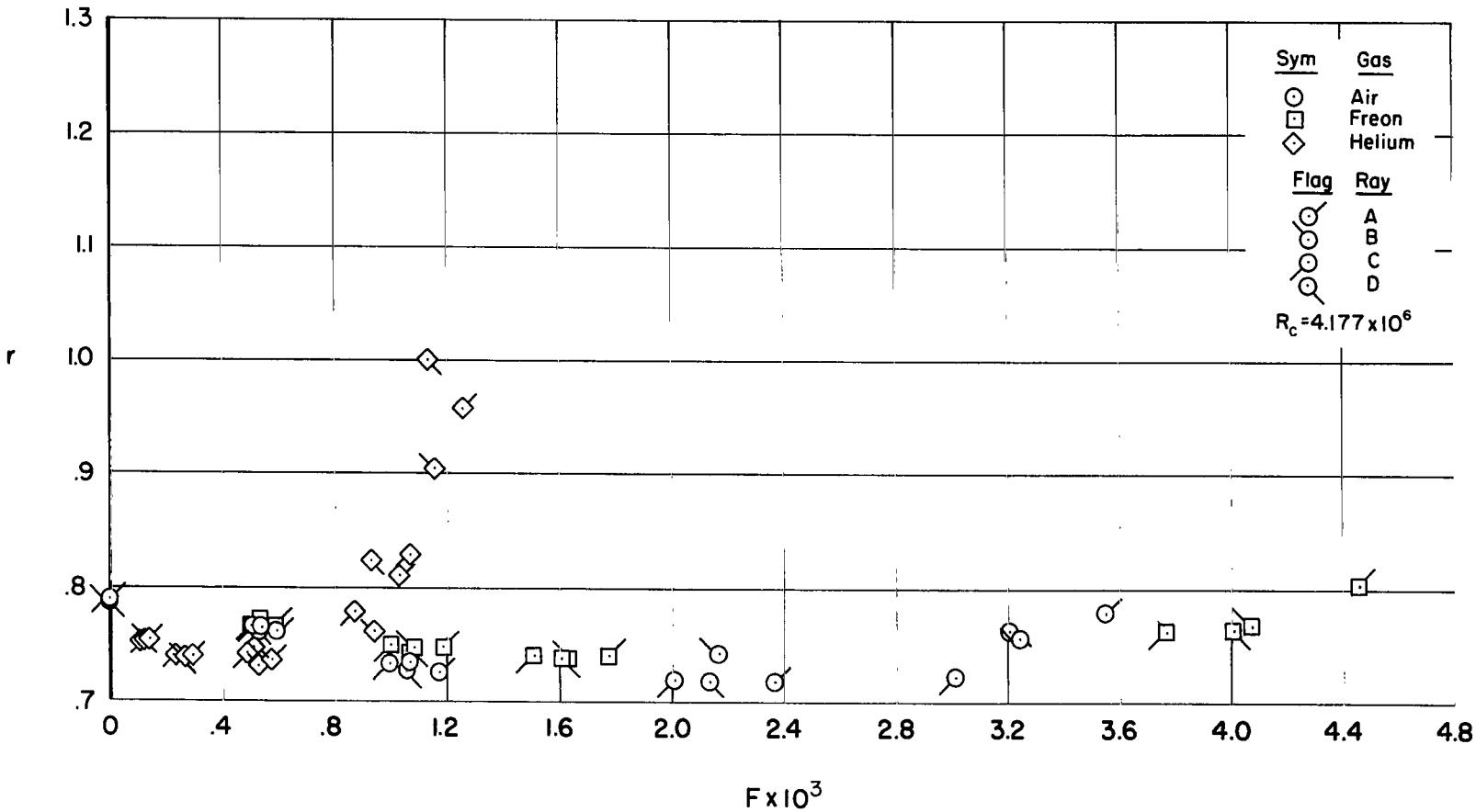

(e) Thermocouple no. 6.

Figure 10.- Continued.

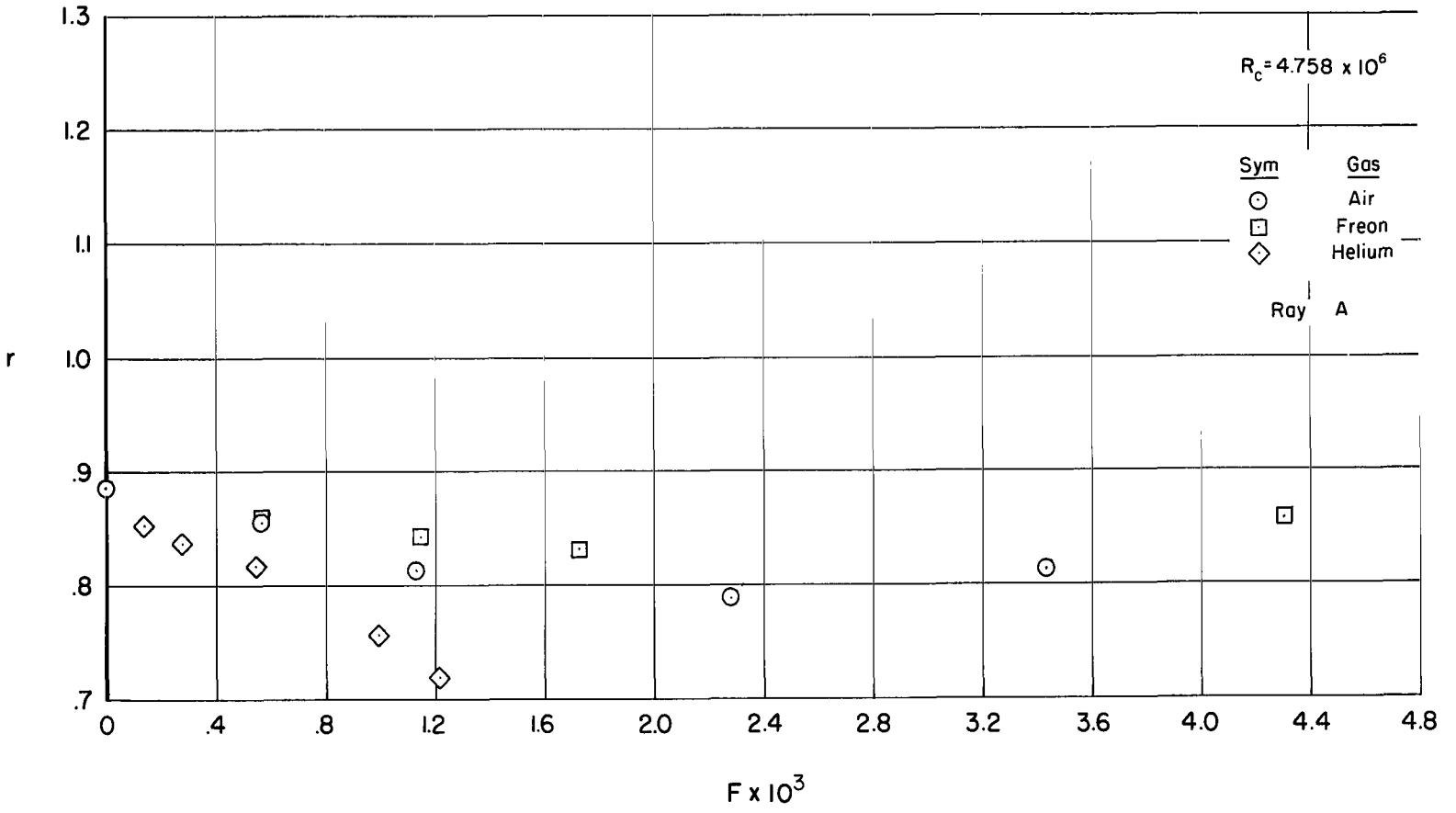

(f) Thermocouple no. 7.

Figure 10.- Concluded.

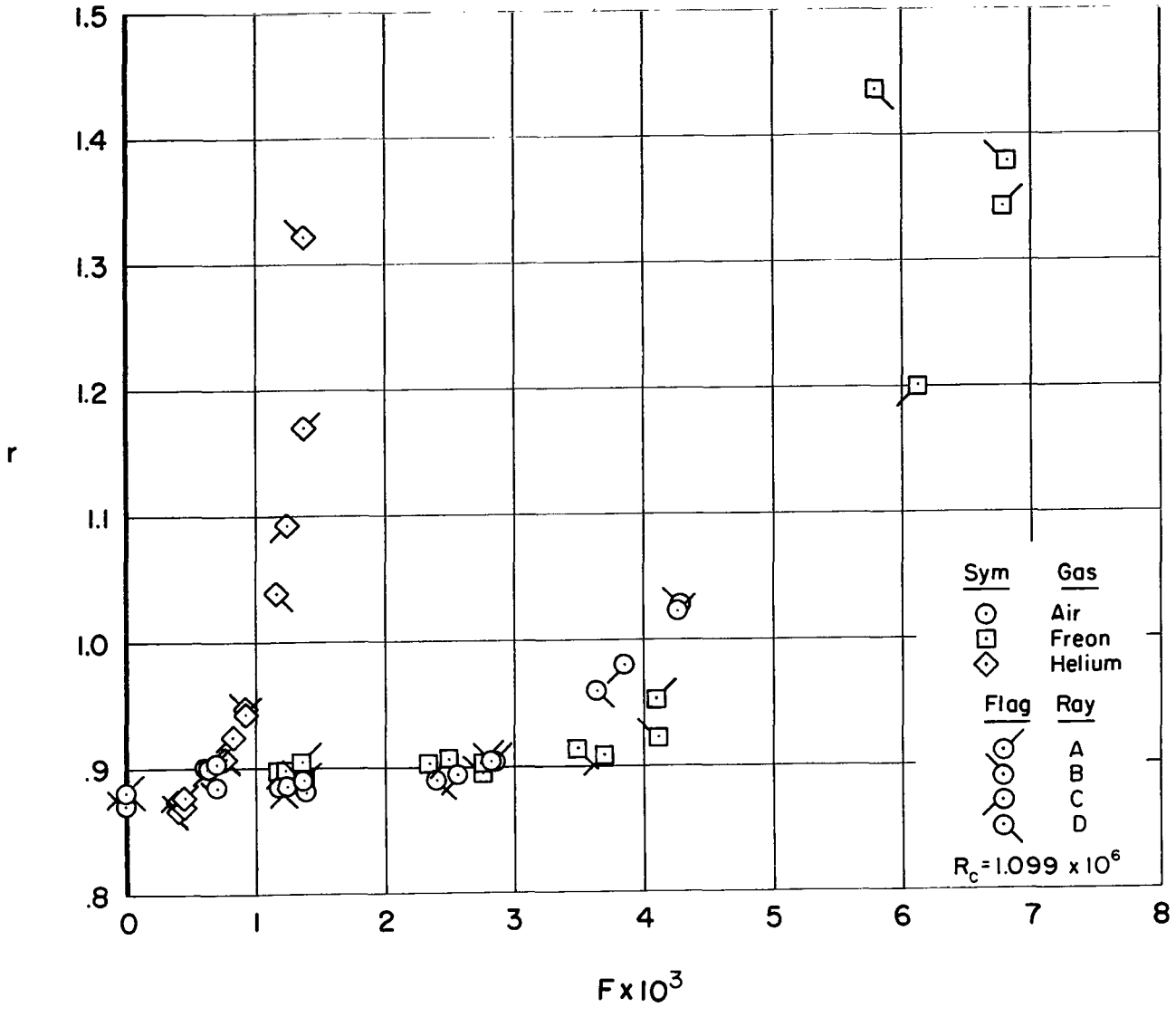

(a) Thermocouple no. 2.

Figure 11.- Recovery factor with gas injection, M_c = 4.35.

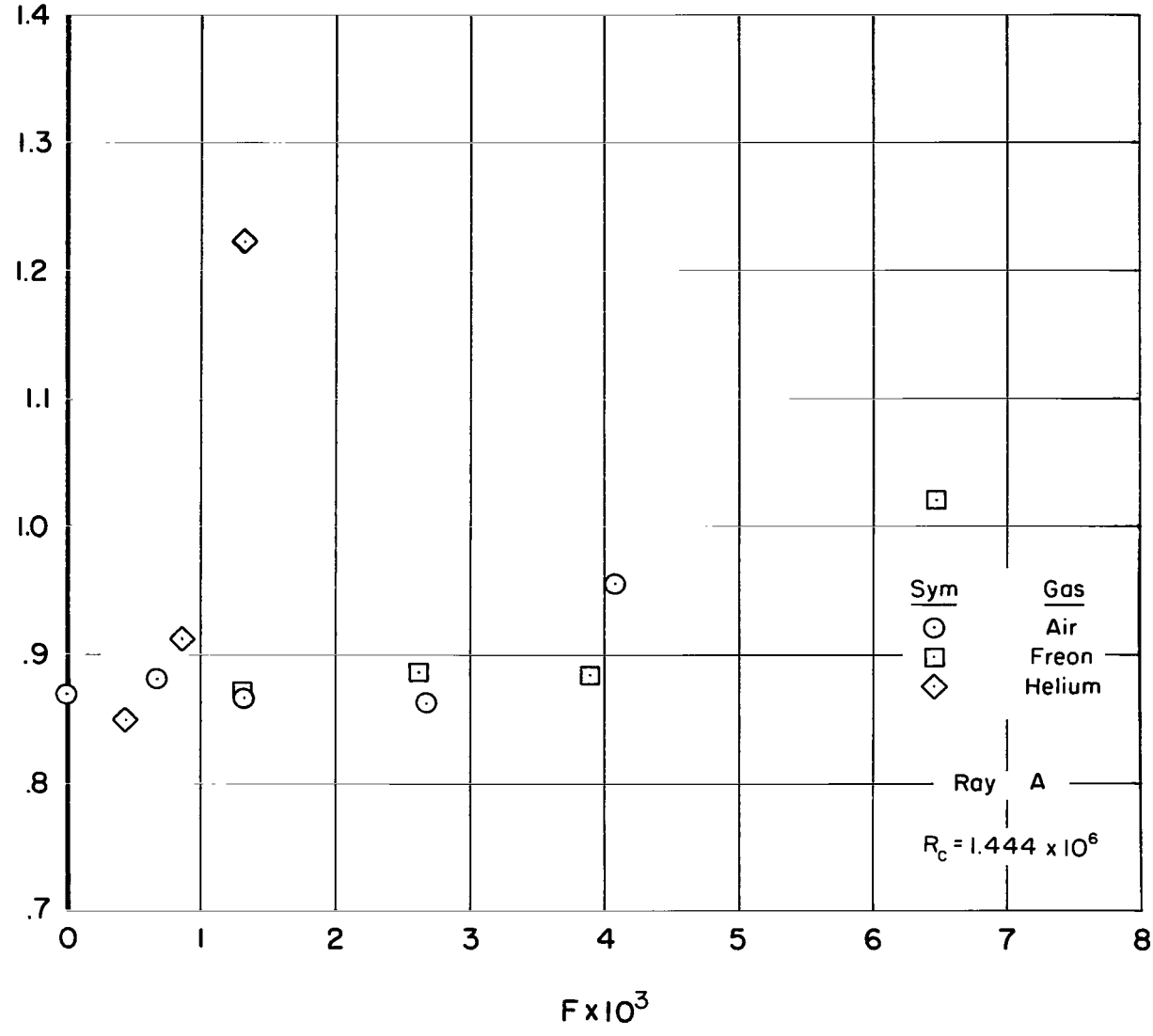

(b) Thermocouple no. 3.

Figure 11.- Continued.

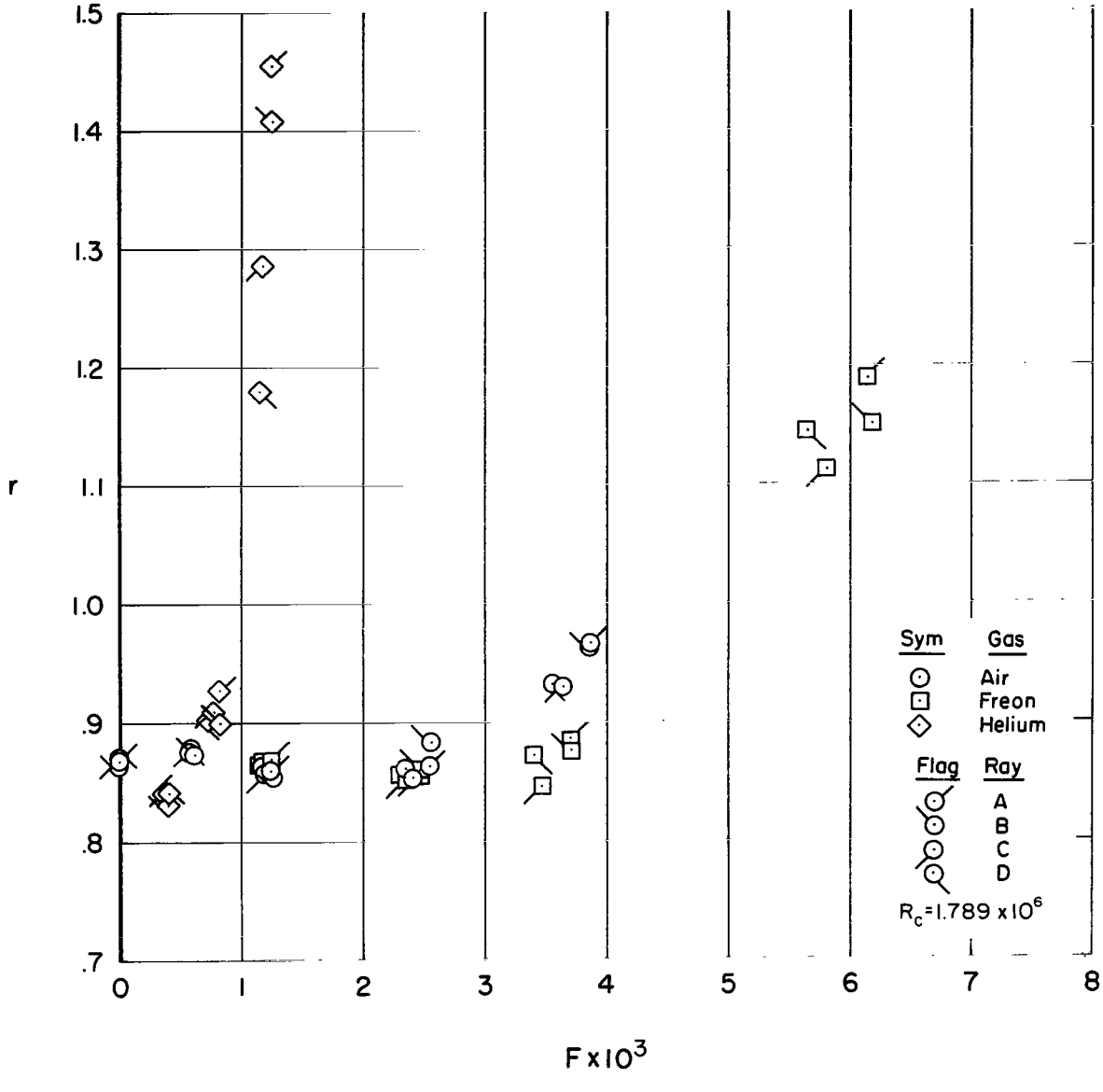

(c) Thermocouple no. 4.

Figure 11.- Continued.

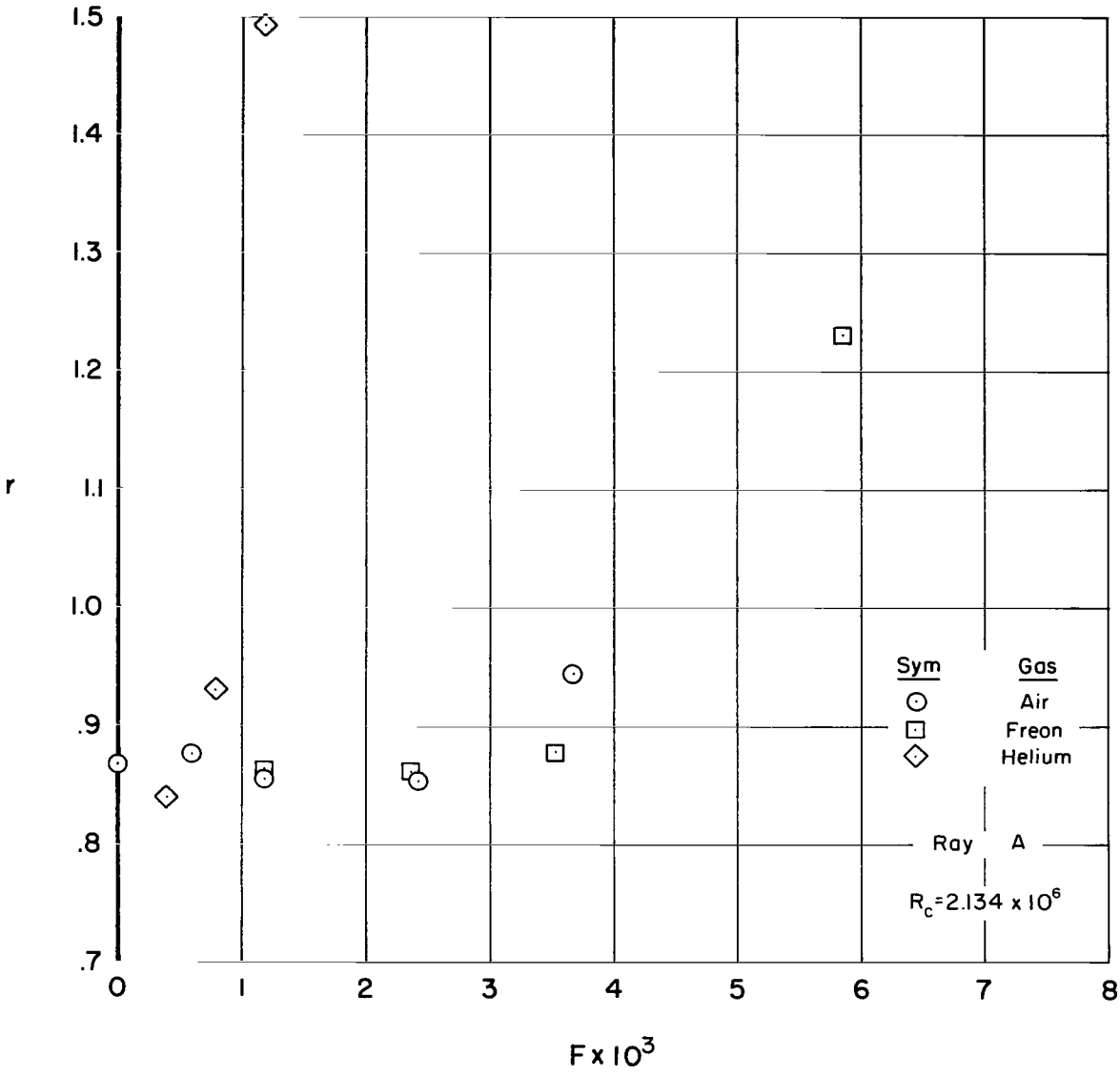

(d) Thermocouple no. 5.

Figure 11.- Continued.

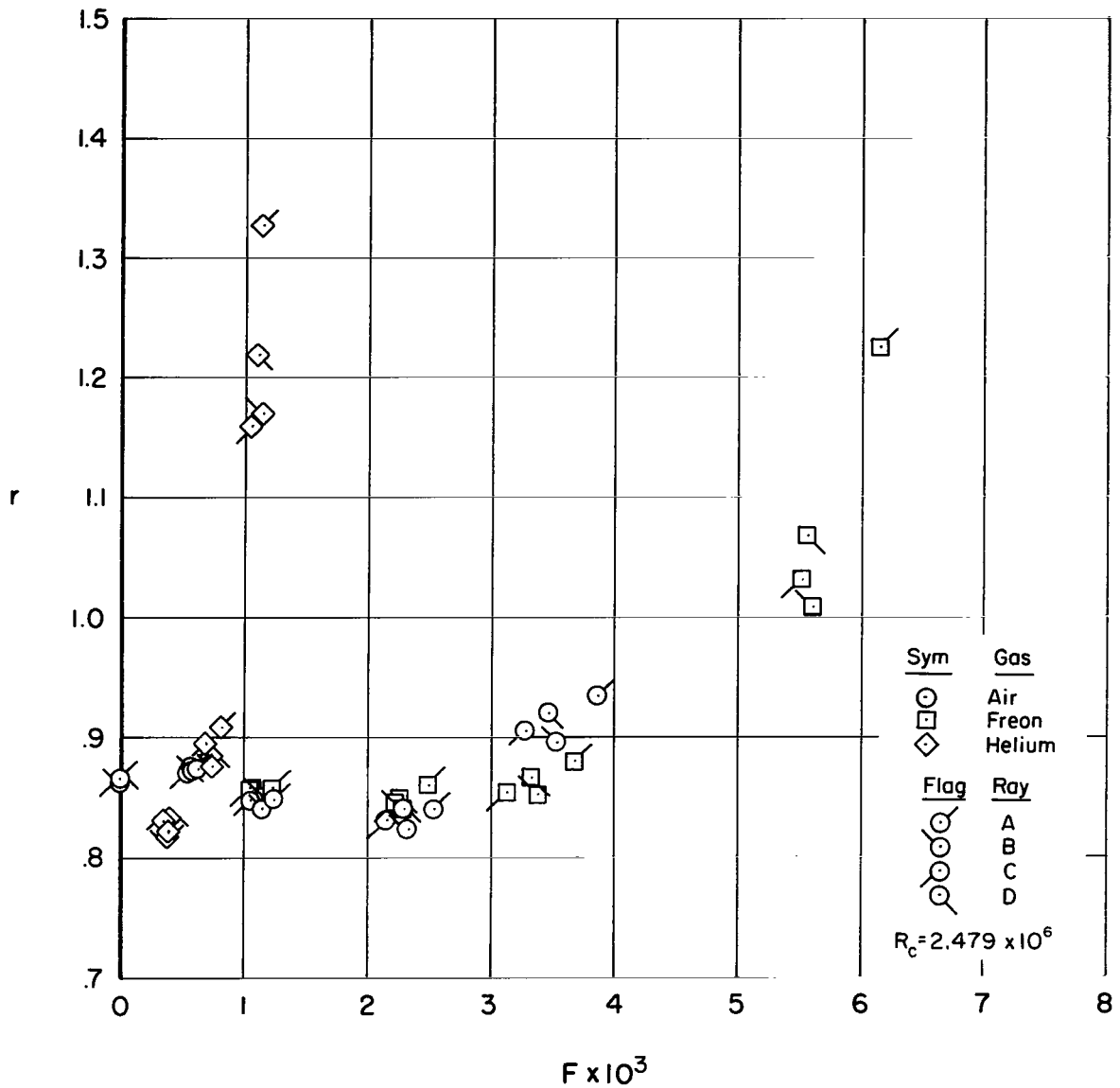

(e) Thermocouple no. 6.

Figure 11.- Continued.

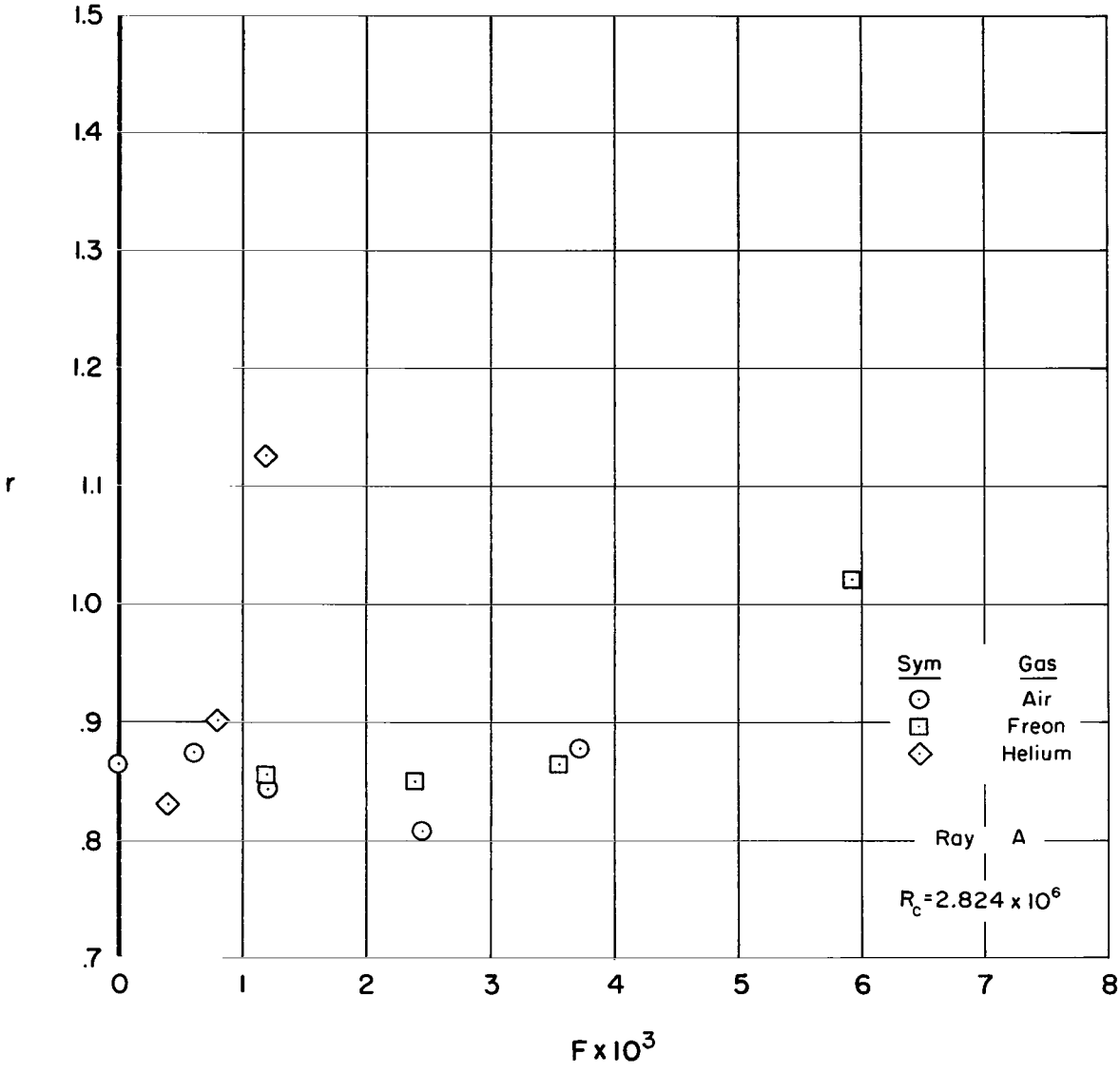

(f) Thermocouple no. 7.

Figure 11.- Concluded.

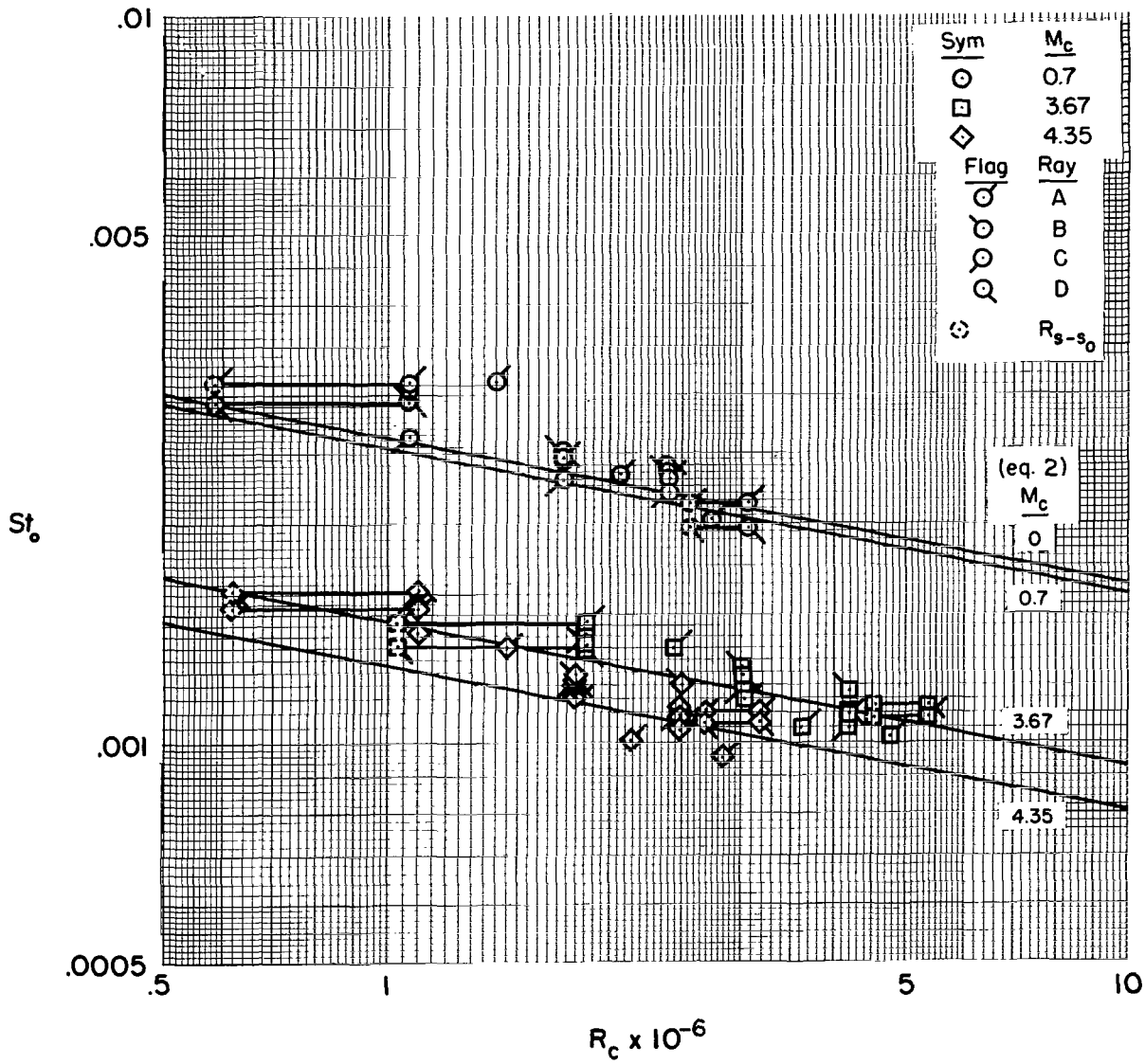

Figure 12.- Effect of Reynolds number on Stanton number without injection.

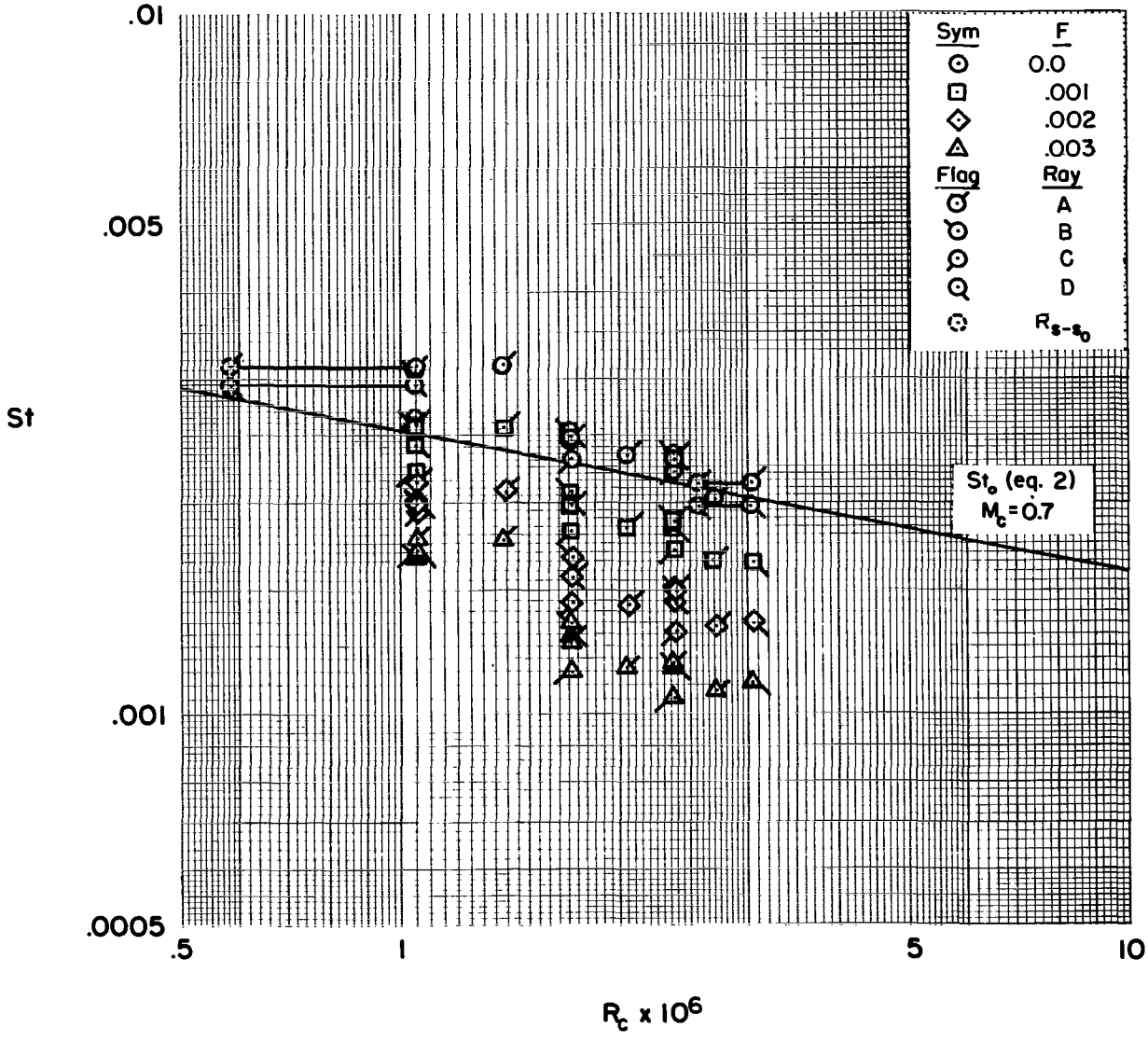

(a) Air injection, M_c = 0.7.

Figure 13.- Effect of Reynolds number on Stanton number.

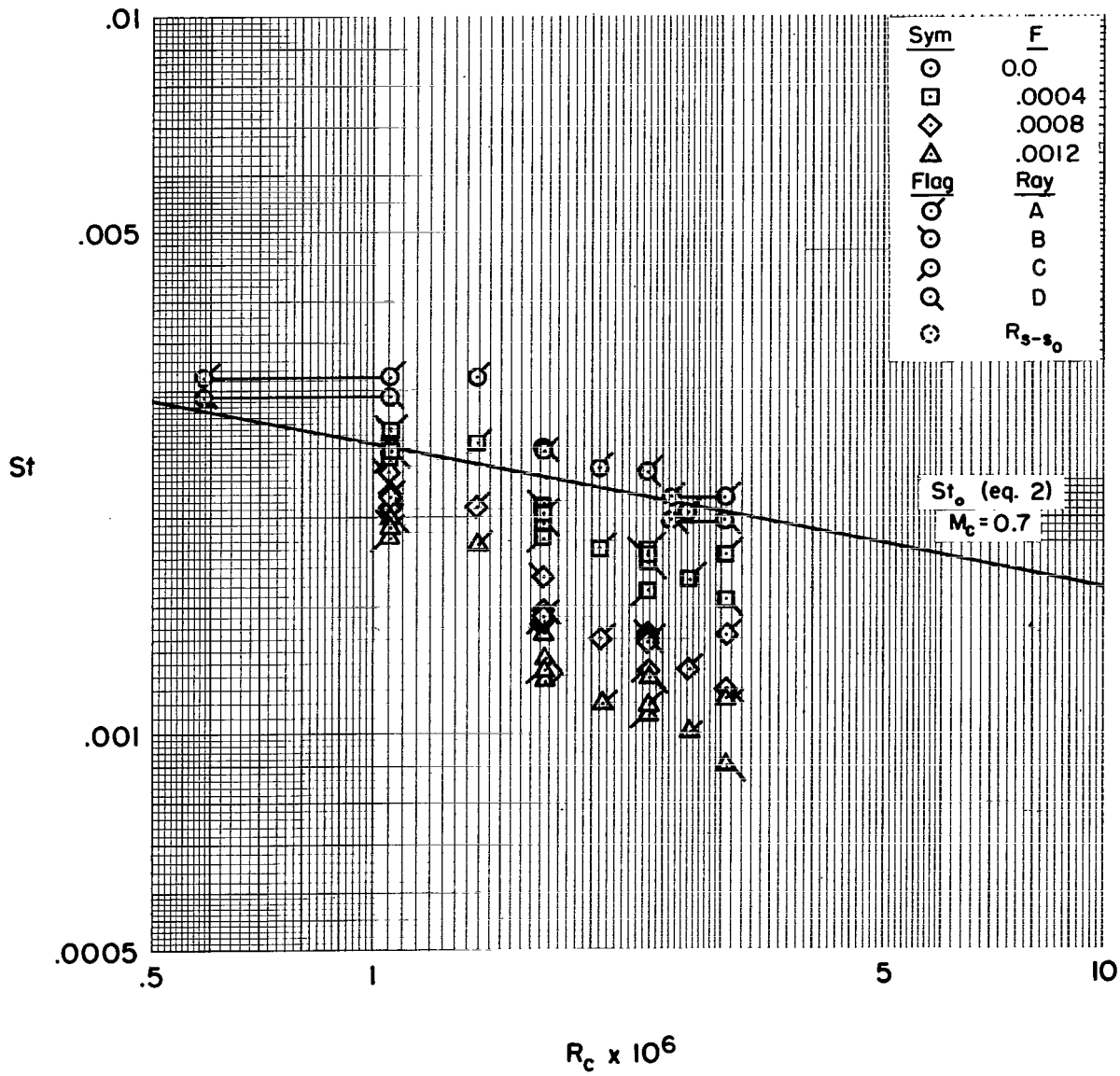

(b) Helium injection, $M_c = 0.7$.

Figure 13.- Continued.

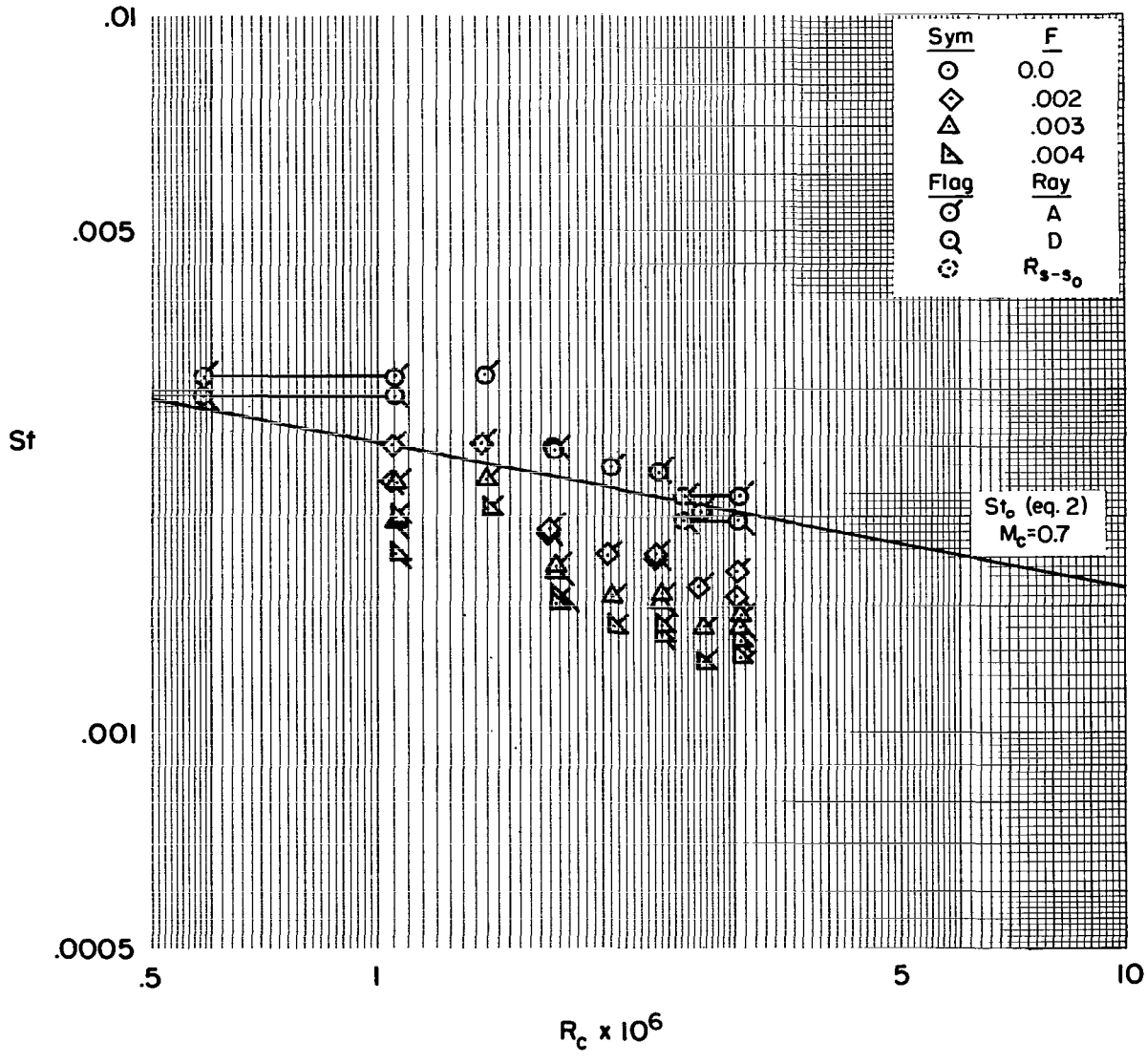

(c) Freon-12 injection, M_c = 0.7.

Figure 13.- Concluded.

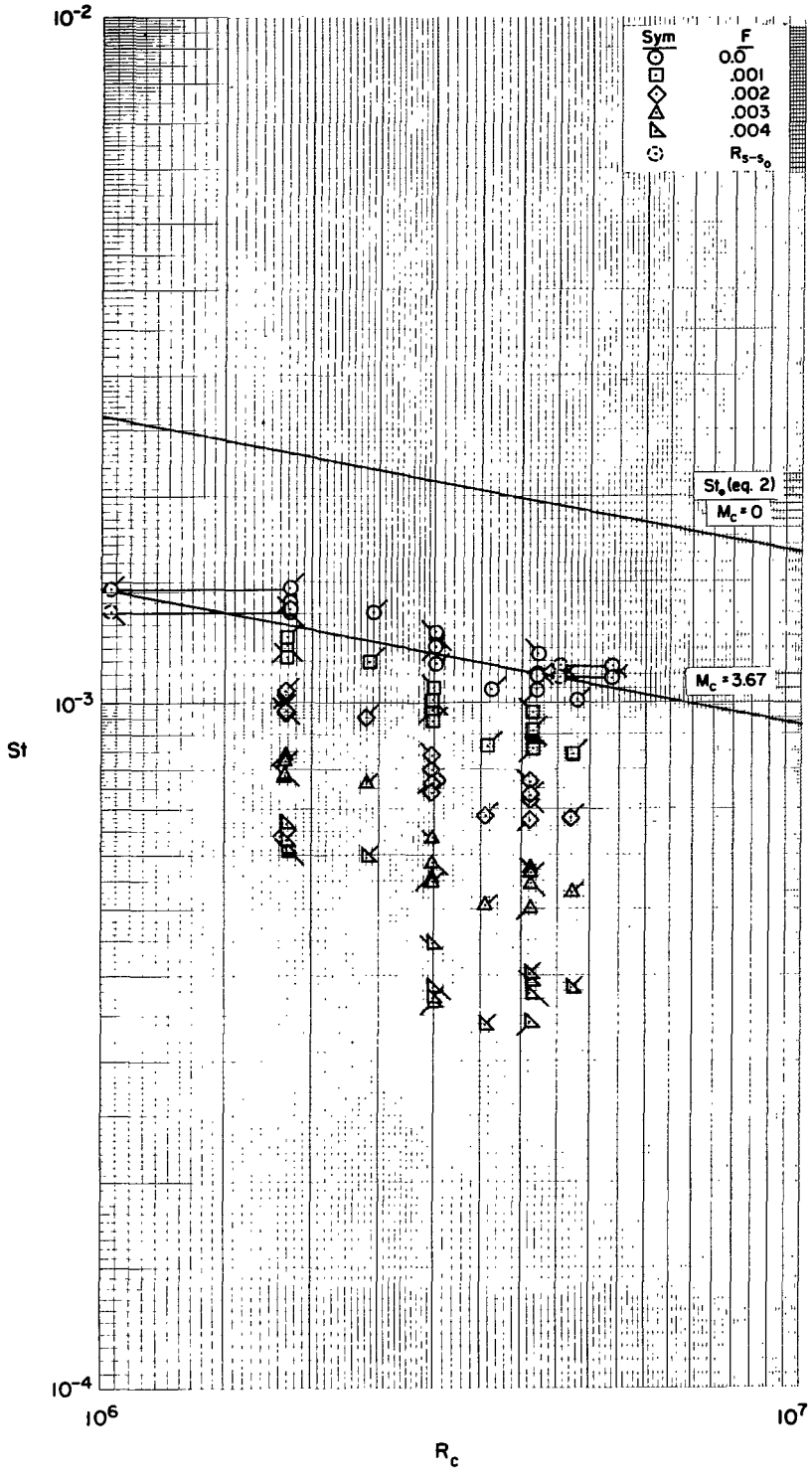

(a) Air injection, $M_c = 3.67$.

Figure 14.- Effect of Reynolds number on Stanton number.

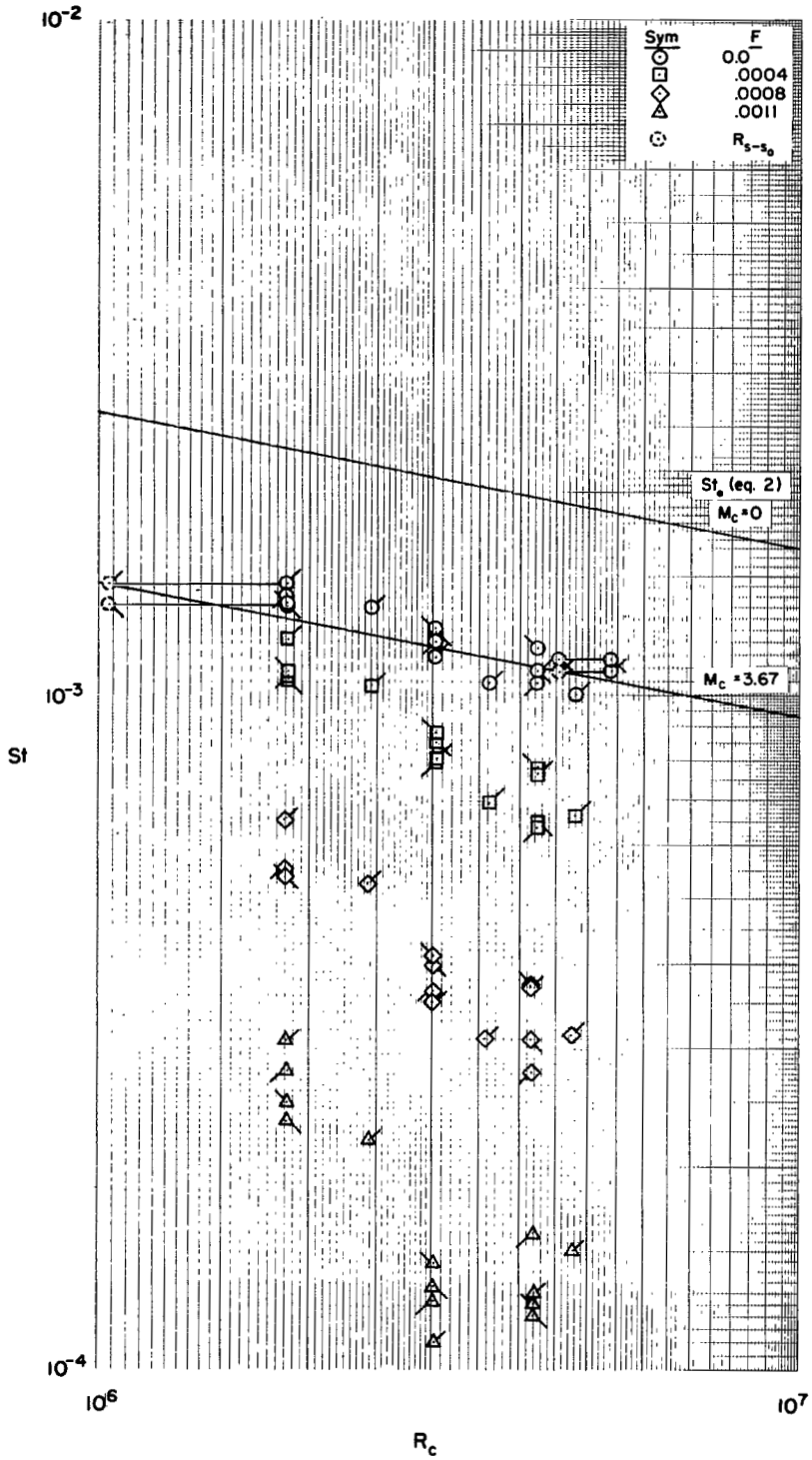

(b) Helium injection, M_c = 3.67.

Figure 14.- Continued.

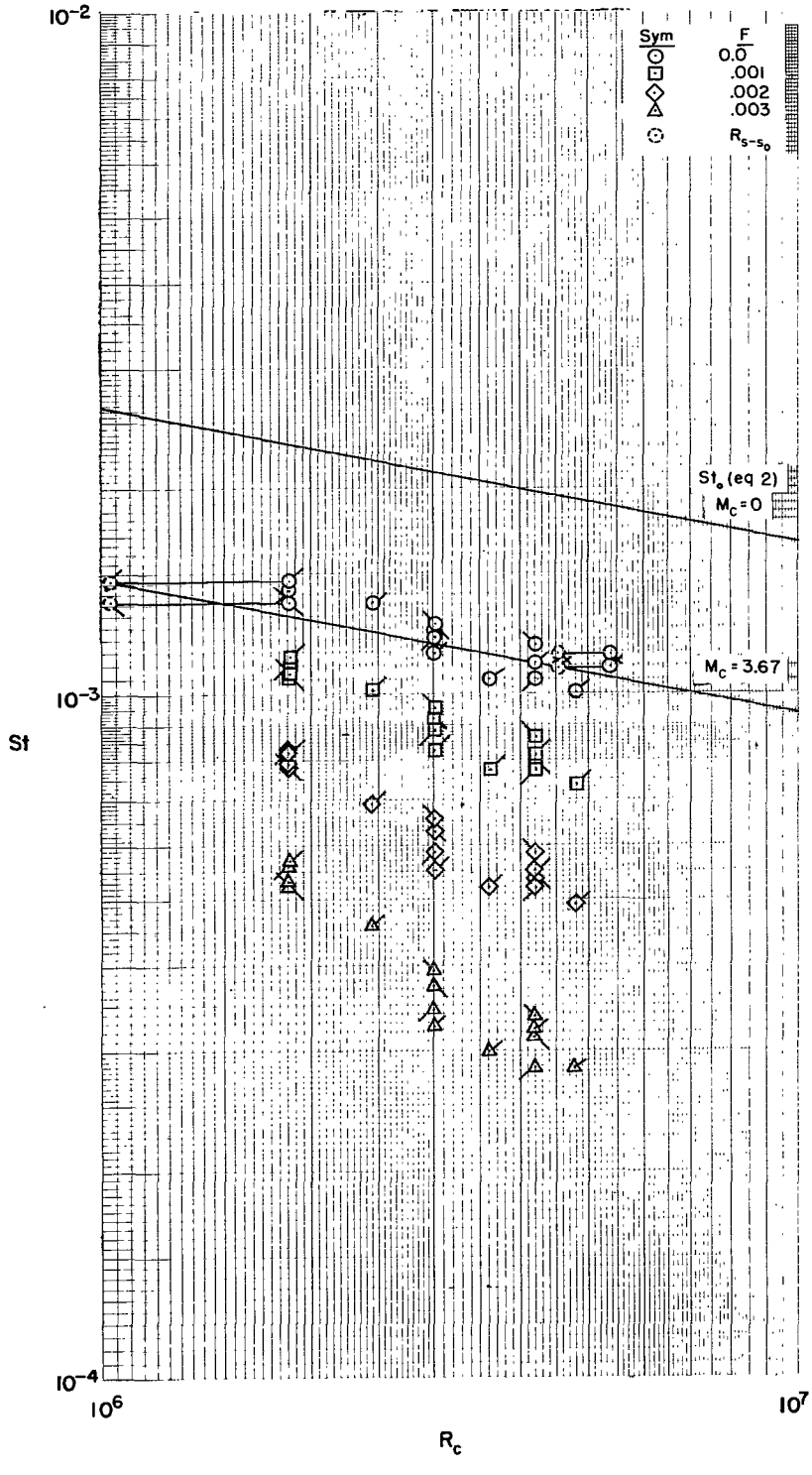

(c) Freon-12 injection, M_c = 3.67.

Figure 14.- Concluded.

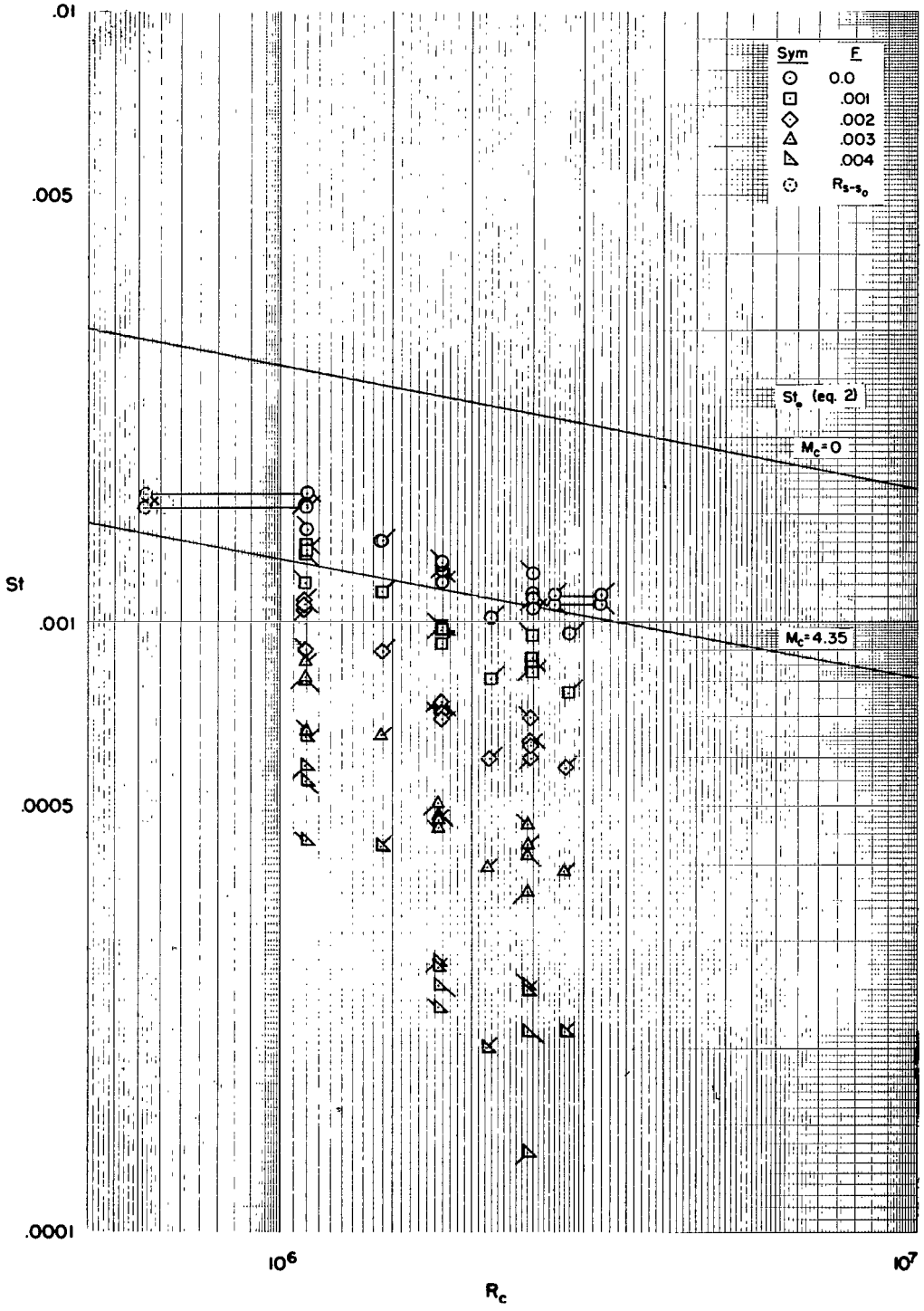

(a) Air injection, $M_c = 4.35$.

Figure 15.- Effect of Reynolds number on Stanton number.

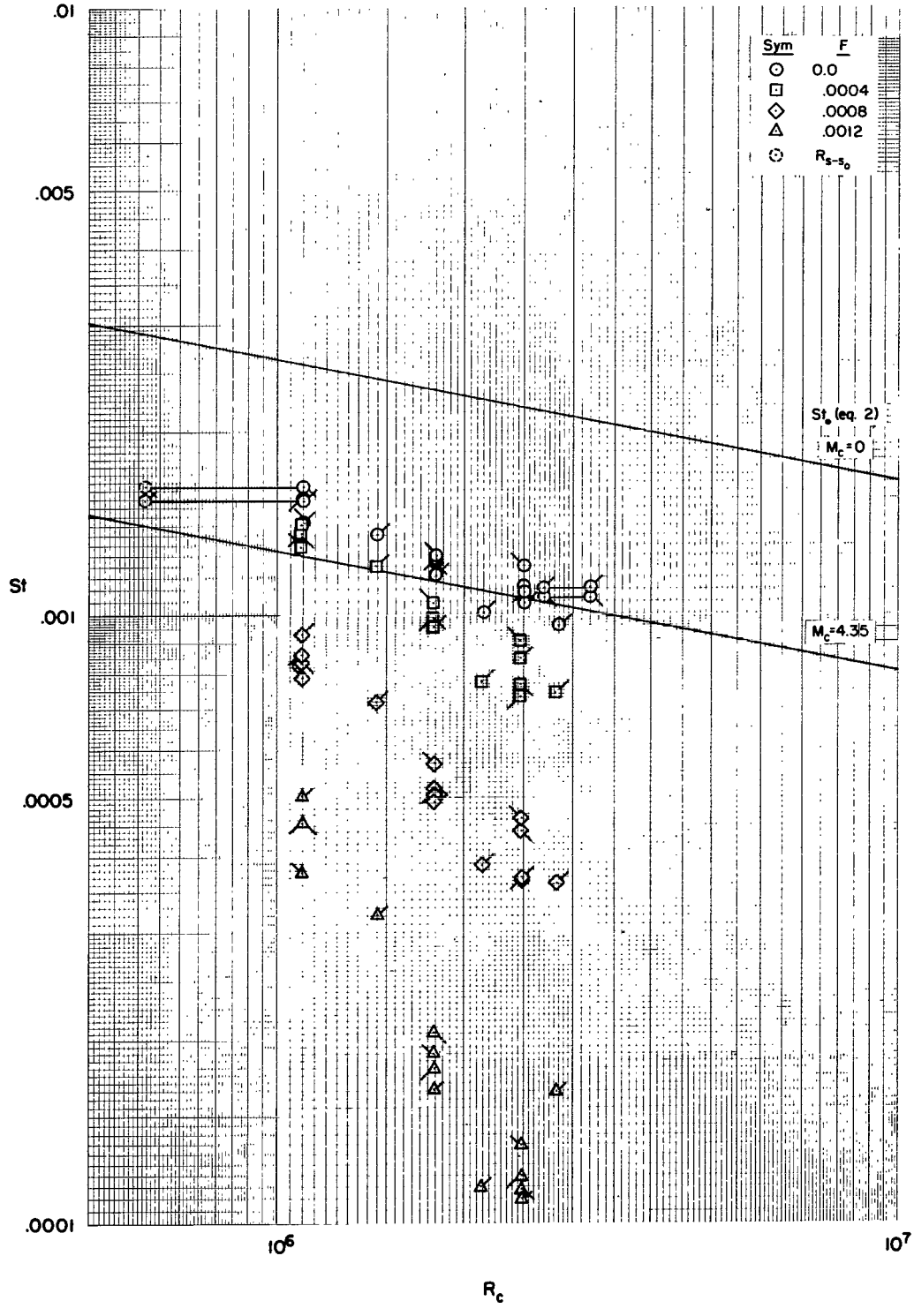

(b) Helium injection, $M_c = 4.35$.

Figure 15.- Continued.

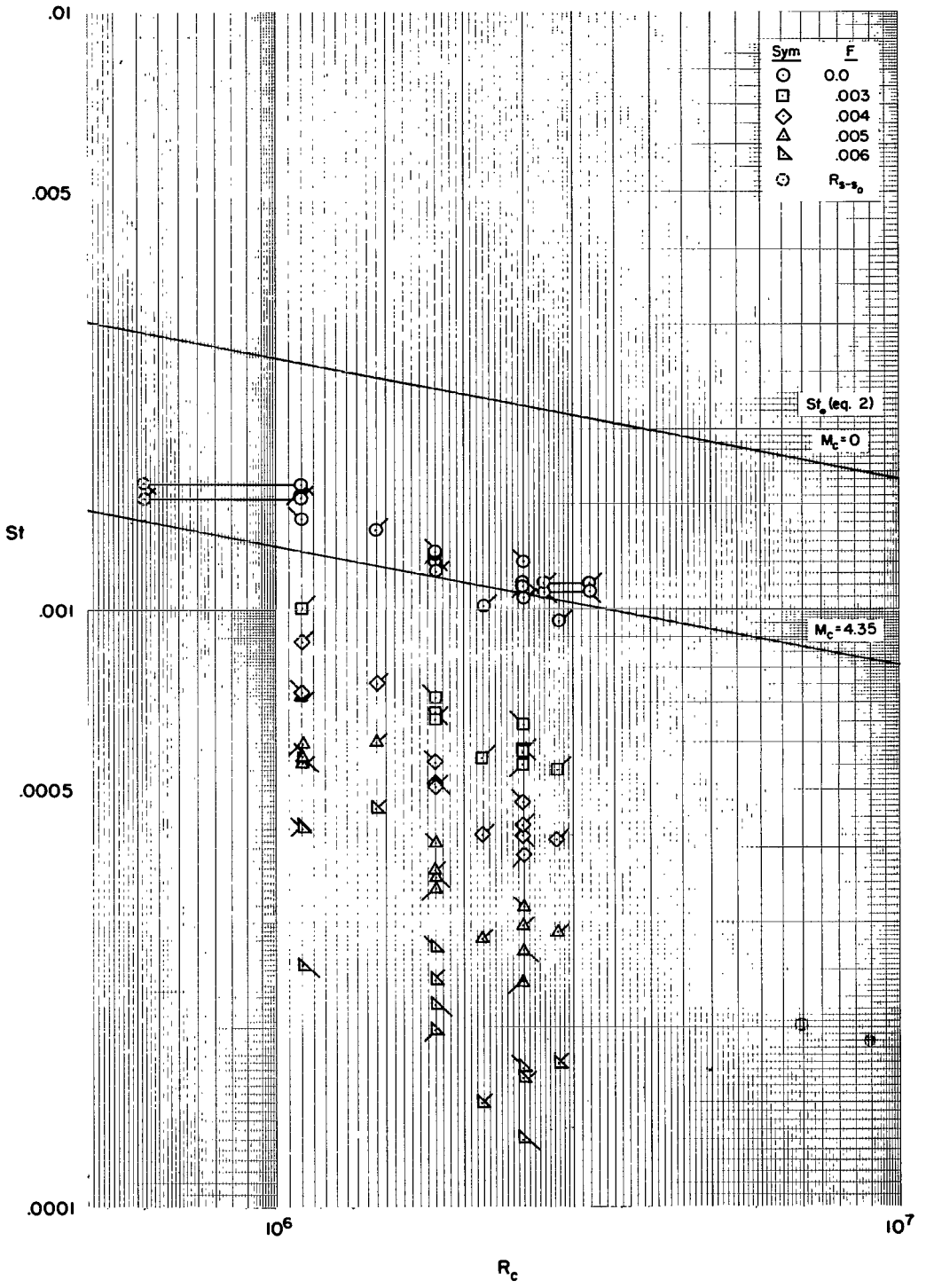

(c) Freon-12 injection, $M_c = 4.35$.

Figure 15.- Concluded.

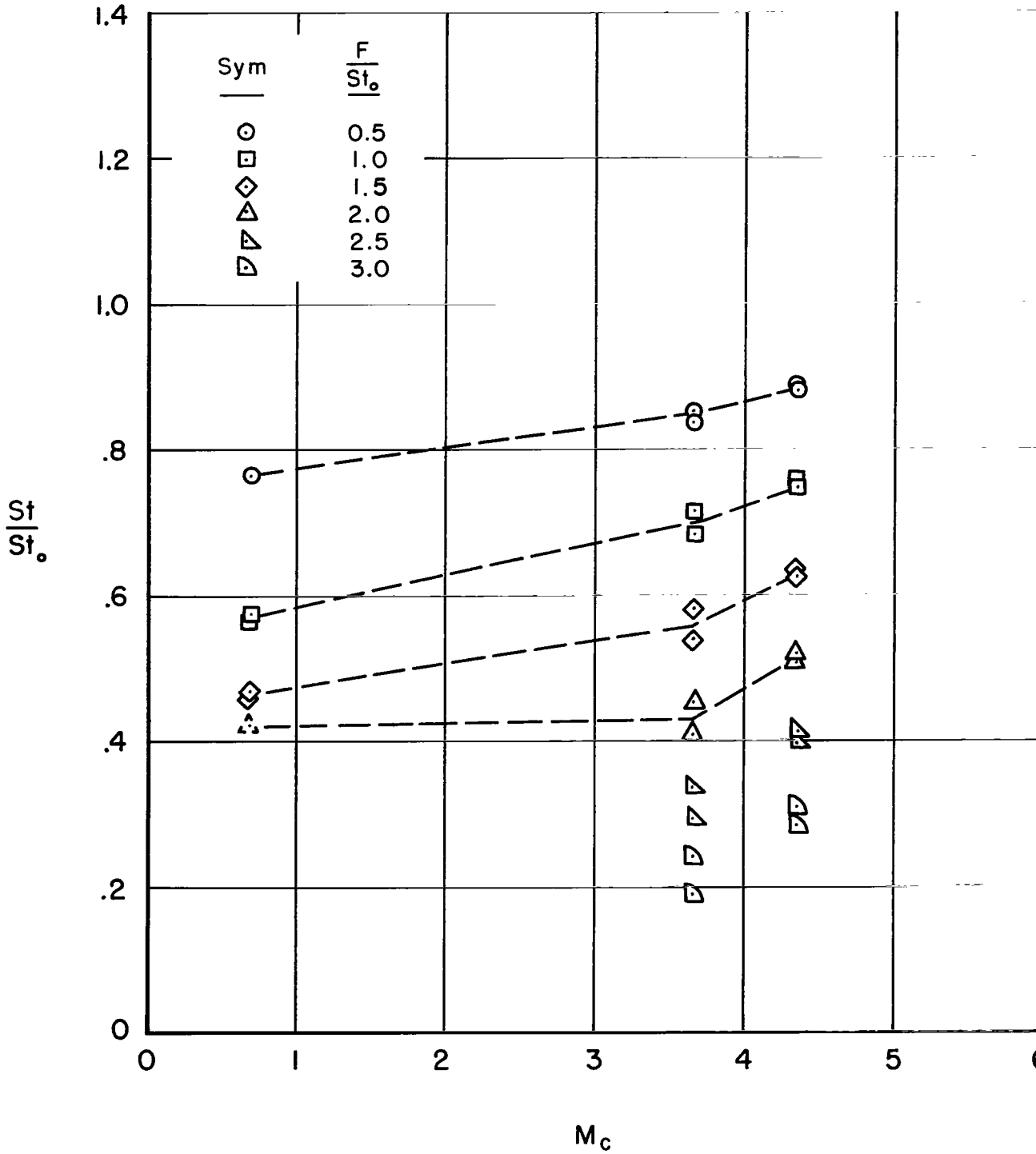

(a) Air injection.

Figure 16.- Effect of Mach number on the relative reduction in Stanton number.

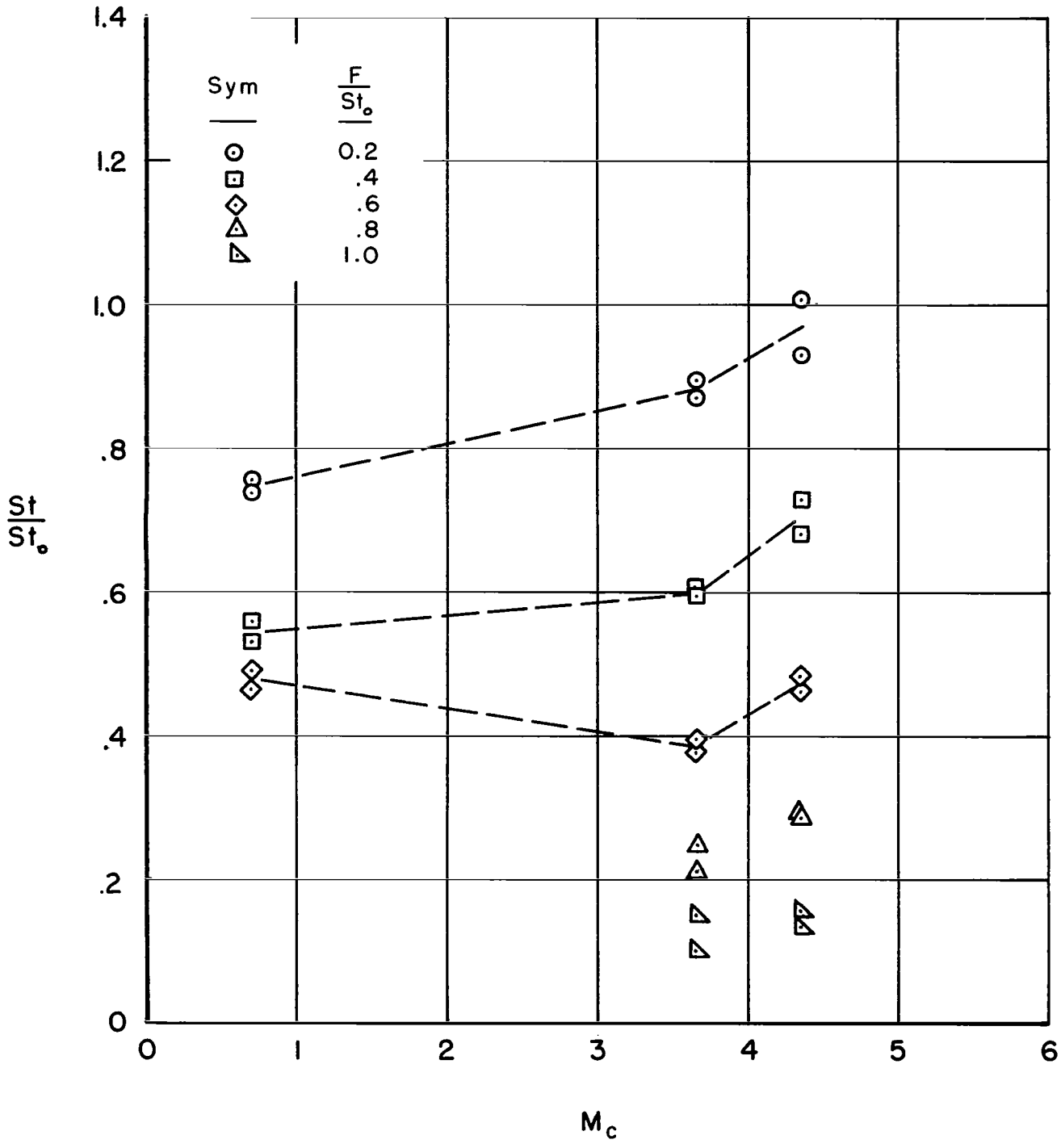

(b) Helium injection.

Figure 16.- Continued.

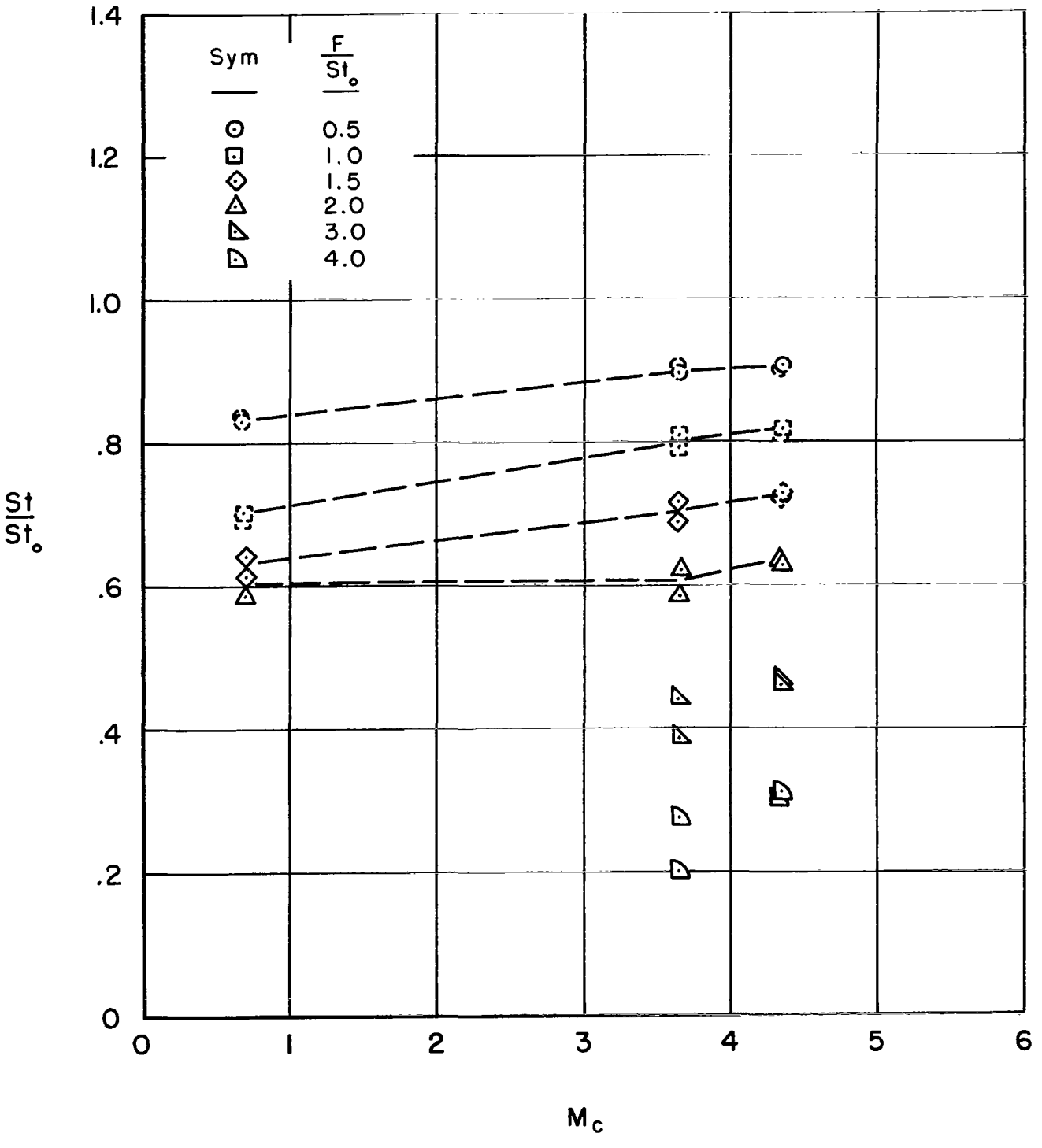

(c) Freon-12 injection.

Figure 16.- Concluded.

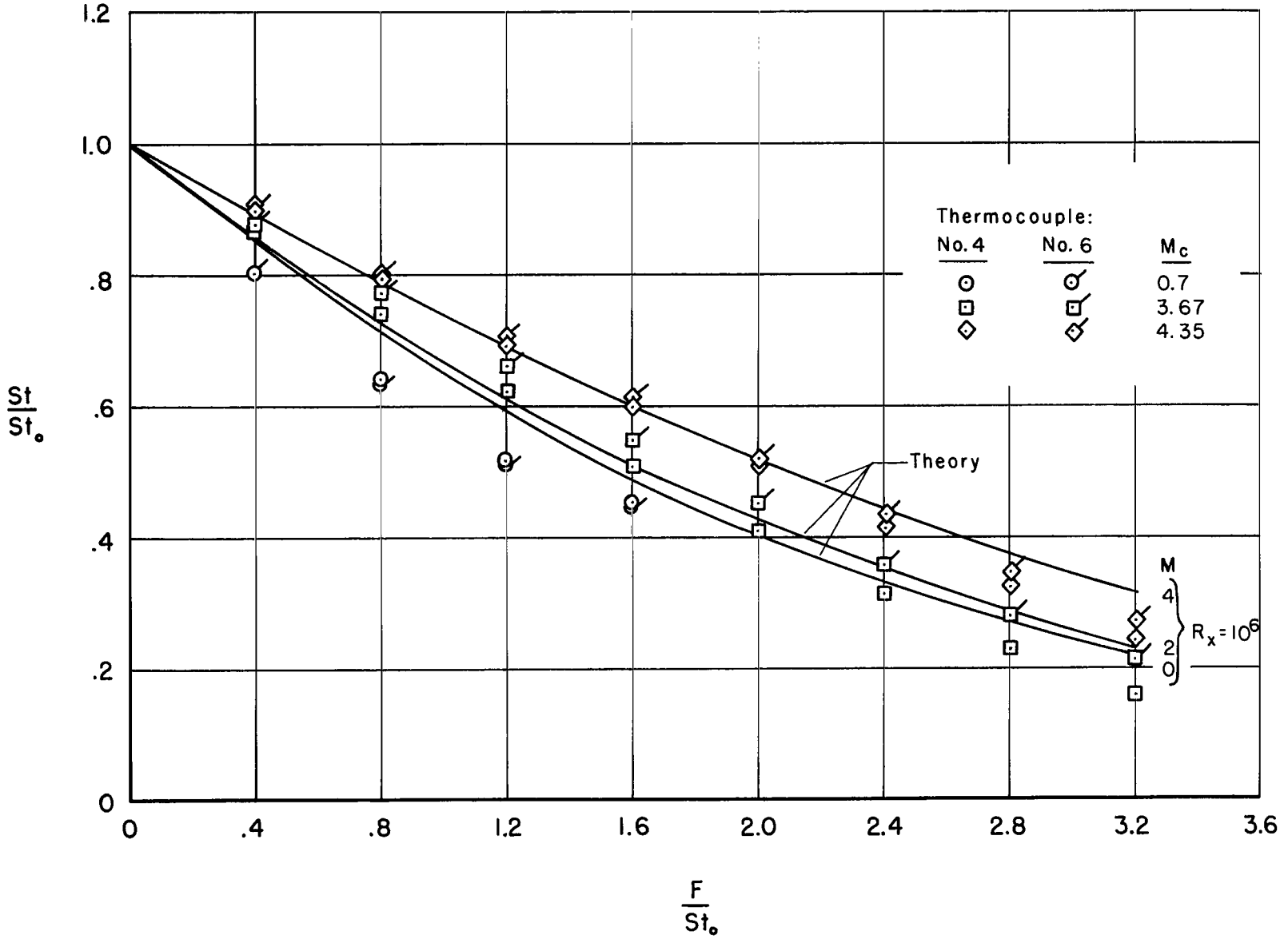

Figure 17.- Comparison of experiment with theory for air injection.

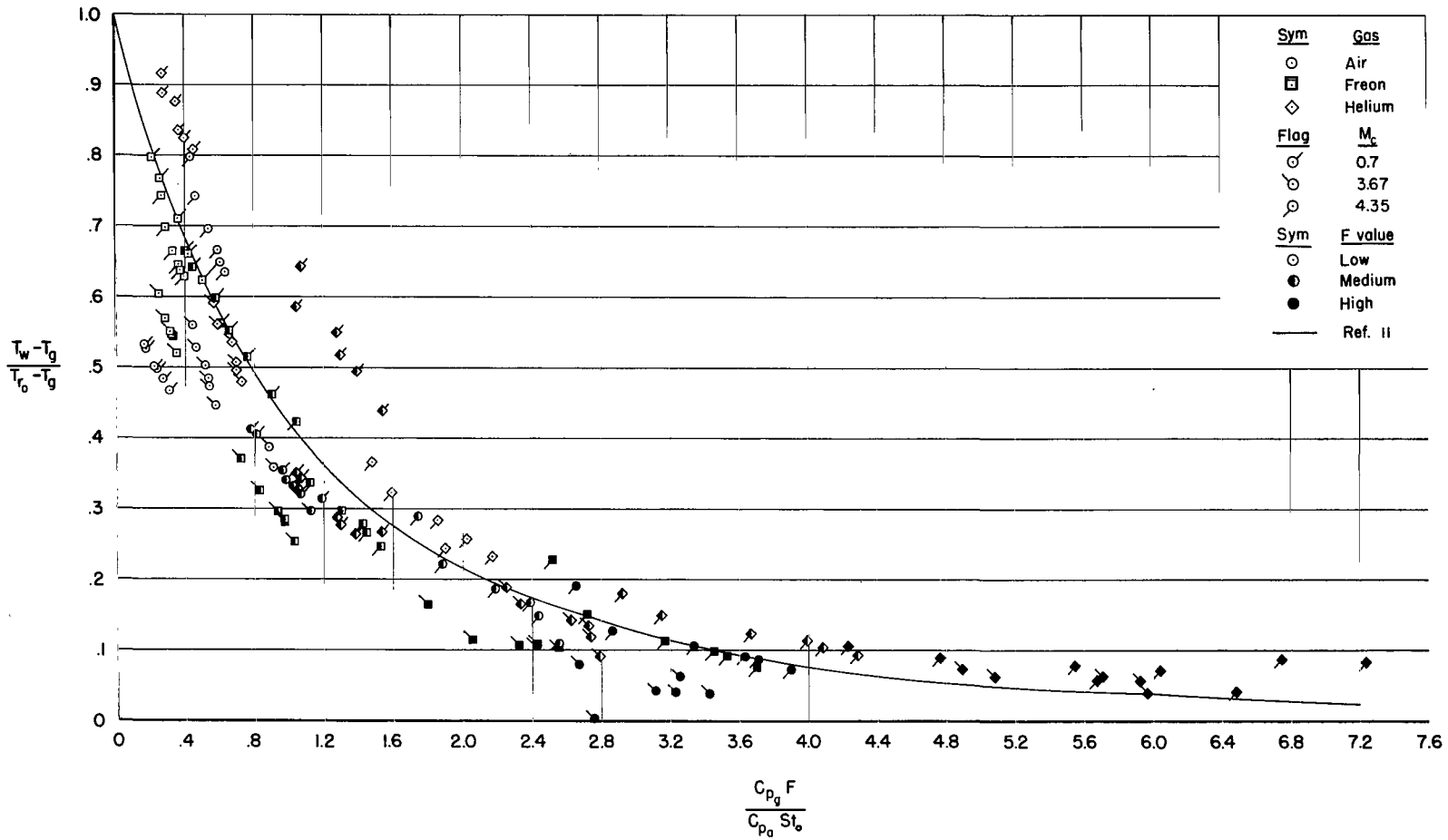

Figure 18.- Temperature effectiveness for a porous wall with gas injection.

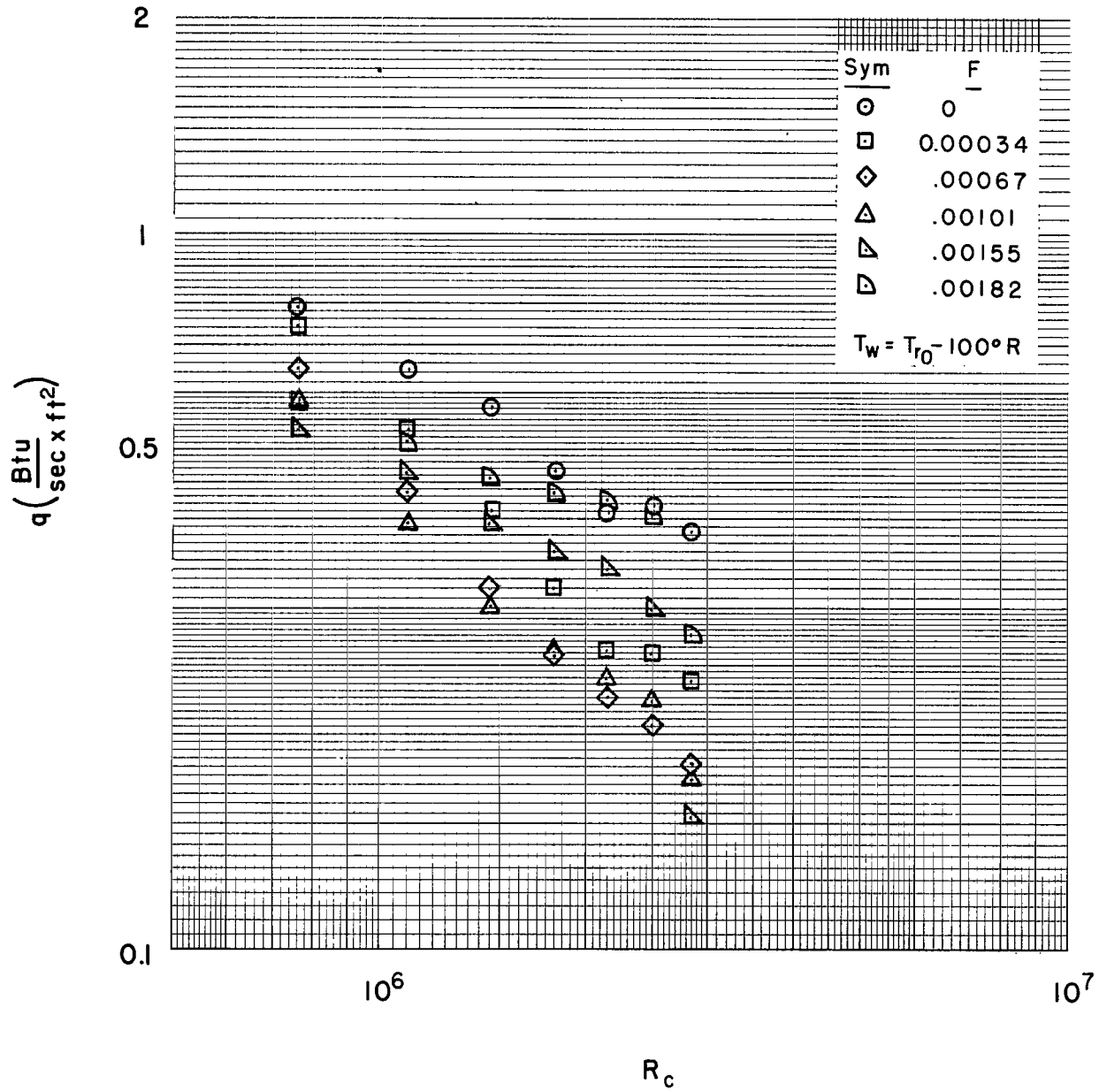

Figure 19.- Heat transfer to a porous wall at high rates of helium injection, $M_c = 4.35$.

"The National Aeronautics and Space Administration . . . shall . . . provide for the widest practical appropriate dissemination of information concerning its activities and the results thereof . . . objectives being the expansion of human knowledge of phenomena in the atmosphere and space."

—National Aeronautics and Space Act of 1958

NASA SCIENTIFIC AND TECHNICAL PUBLICATIONS

TECHNICAL REPORTS: Scientific and technical information considered important, complete, and a lasting contribution to existing knowledge.

TECHNICAL NOTES: Information less broad in scope but nevertheless of importance as a contribution to existing knowledge.

TECHNICAL MEMORANDUMS: Information receiving limited distribution because of preliminary data, security classification, or other reasons.

CONTRACTOR REPORTS: Technical information generated in connection with a NASA contract or grant and released under NASA auspices.

TECHNICAL TRANSLATIONS: Information published in a foreign language considered to merit NASA distribution in English.

TECHNICAL REPRINTS: Information derived from NASA activities and initially published in the form of journal articles or meeting papers.

SPECIAL PUBLICATIONS: Information derived from or of value to NASA activities but not necessarily reporting the results of individual NASA-programmed scientific efforts. Publications include conference proceedings, monographs, data compilations, handbooks, sourcebooks, and special bibliographies.

Details on the availability of these publications may be obtained from:

SCIENTIFIC AND TECHNICAL INFORMATION DIVISION

NATIONAL AERONAUTICS AND SPACE ADMINISTRATION

Washington, D.C. 20546